AD NUMBER
AD904907
LIMITATION CHANGES
TO: **Approved for public release; distribution is unlimited.**
FROM: **Distribution authorized to U.S. Gov't. agencies only; Test and Evaluation; 18 AUG 1972. Other requests shall be referred to Air Force Cambridge Research Laboratories, Attn: OPS, L. G. Hanscom Feild, Bedford, MA 01730.**
AUTHORITY
AFGL ltr, 15 Jan 1981

AFCRL-72-0053

INFRARED RADIOMETER EXPERIMENT

Gary C. Vliet

Lockheed Missiles & Space Company, Inc.
Lockheed Palo Alto Research Laboratory
3251 Hanover Street
Palo Alto, California 94304

Contract No. F19628-70-C-0012

Project No. 5130

FINAL REPORT

Period Covered: 1 August 1969 to 9 March 1972

Date of Report: 9 March 1972

Contract Monitor: John A. Sullivan
Optical Physics Laboratory

SPONSORED BY
DEFENSE ADVANCED RESEARCH PROJECTS AGENCY
ARPA ORDER NO. 1366

Monitored by
Air Force Cambridge Research Laboratories
Air Force Systems Command
United States Air Force
Bedford, Massachusetts 01730

MISSING PAGE
NUMBERS ARE BLANK
AND WERE NOT
FILMED

Program Code No.	1E50
Effective Date of Contract	1 Aug 1969
Contract Expiration Date	9 Mar 1972
Principal Investigator and Phone No. . . .	E. R. Streed/(415) 493-4411, Ext. 45867
AFCRL Project Scientist or Engineer and Phone No.	John A. Sullivan/(617) 861-4854

LOCKHEED PALO ALTO RESEARCH LABORATORY
LOCKHEED MISSILES & SPACE COMPANY
A GROUP DIVISION OF LOCKHEED AIRCRAFT CORPORATION

AFCRL-72-0053

INFRARED RADIOMETER EXPERIMENT

Gary C. Vliet

Lockheed Missiles & Space Company, Inc.
Lockheed Palo Alto Research Laboratory
3251 Hanover Street
Palo Alto, California 94304

Contract No. F19628-70-C-0012

Project No. 5130

FINAL REPORT

Period Covered: 1 August 1969 to 9 March 1972

Date of Report: 9 March 1972

Contract Monitor: John A. Sullivan
Optical Physics Laboratory

SPONSORED BY
DEFENSE ADVANCED RESEARCH PROJECTS AGENCY
ARPA ORDER NO. 1366

Monitored by
Air Force Cambridge Research Laboratories
Air Force Systems Command
United States Air Force
Bedford, Massachusetts 01730

ARPA Order No. – 1366

Program Code No. – 1E50

Name of Contractor – Lockheed Missiles & Space Co., Inc.

Effective Date of Contract – 1 Aug 1969

Contract No. – F19628-70-C-0012

Principal Investigator and Phone No. – E. R. Streed/ (415) 493-4411, Ext. 45867

AFCRL Project Scientist and Phone No. – John A. Sullivan/ (617) 861-4852

Contract Expiration Date – 9 Mar 1972

FOREWORD

This research was supported by the Defense Advanced Research Projects Agency of the Department of Defense and was monitored by Air Force Cambridge Research Laboratories under Contract No. F19628-70-C-0012.

The major portion of the work under the contract was performed in the Engineering Sciences Laboratory of the Lockheed Palo Alto Research Laboratories, Palo Alto, California. The principal investigator was Dr. G. C. Vliet. Several other persons contributed greatly to the contract technical effort. The original concept of the double-focused, refractive system was largely promoted by Dr. R. P. Caren. The optical train design was developed by Mr. C. Klug and the electronics design by Messrs. W. Fleenor and W. Currie. Messrs. T. Nast and W. Foster were responsible for the design and construction of the cryogenic equipment for the radiometer and frost-fog prevention system. The evaluation of the frost fog prevention system was conducted by Dr. C. K. Liu. The evaluation and calibration of the detector array were performed by Dr. S. R. Hawkins. Mr. A. Funai performed the scattering and transmittance measurements on the refractive materials and was involved in a significant portion of the radiometer evaluation. Mr. S. I. Ingham contributed significant to the fabrication and assembly of the radiometer. The many long hours spent by Mr. R. Kightlinger on the evaluation tests of the radiometer and flight hardware, and during the two balloon flights, are greatly appreciated.

The gondola fabrication, gimbal drive mechanism, and flight integration of the radiometer with the power supply, recording equipment, telemetry, and ground command were largely the work of personnel at the Denver Research Institute, University of Denver. In particular, the work of Dr. D. Murcray and Mr. J. Kosters is greatly appreciated.

The contract was monitored by Mr. J. Sullivan, under the direction of Mr. T. Condron of AFCRL. Mr. L. Marcotte was responsible for reduction of the flight data. The assistance of Mr. T. Condron during the contract is greatly appreciated. Mr. E. R. Streed contributed to the completion of the final report.

ABSTRACT

The design, fabrication, calibration, and flight of a double-focused refractive optical system employing a solid cryogen for operation at 22 °K on a balloon-supported platform are described. The inherent out-of-field energy rejection and the diffraction limited characteristics of a refractive system have been combined with a 4-element Ge:Hg detector array for an optimized radiometric measuring system for the 8- to 13-μm wavelength range. Additional features include an 8-position spectral filter wheel, a 2-position neutral density filter, a 4-decade logarithmic amplifier, and a frost prevention system. The system was developed to measure the atmospheric emittance as a function of elevation angle near the earth's horizon while at a nominal floating altitude of 90,000 ft.

The results of laboratory evaluation of the individual optical, detector, and electronic components, as well as the system performance for responsivity, optical resolution, out-of-field energy rejection, and field of-view, are presented. Simulated flight tests in an evacuated chamber were performed to verify the cryogenic and electro-optical design. Finally, the description and results of a successful balloon flight in June 1971 are summarized in Appendixes A, B, and C.

A follow-on contract (No. F19628-72-C-0033) effort is in progress to fabricate an attachable calibration source, modify some of the electronic and mechanism components, and perform a complete calibration, and to support two additional balloon flights in 1972.

CONTENTS

ILLUSTRATIONS

TABLES

Table

Section 1
INTRODUCTION AND BACKGROUND

This report describes the development, calibration, and initial performance data of an infrared radiometer capable of operation from a balloon platform. The objective of the balloon flight measurement program is to measure the atmospheric emission in the 8- to 13-μm wavelength range. Azimuthal scans are made at balloon-floating altitudes of about 90,000 ft to obtain the spatial and spectral variations for fixed elevation angles between the earth's limb and the vertical.

This unique radiometer has a solid-cryogen-cooled, double-focused, refractive optical system with excellent capability for out-of-field energy rejection and a relatively large field of view. By operating the optical system and the Ge:Hg detector array at a temperature of 22°K, the background radiation is minimized and an optical measuring system approaching the diffraction limit is possible.

The radiometer system was designed and fabricated by the LMSC Palo Alto Research Laboratory. Calibration was performed at the LMSC facility (Ref. 1) and at the Arnold Engineering Development Center by a team of AFCRL and LMSC personnel. Two balloon flights (Feb and Jun 1971) have been described in individual flight data reports. (See Refs. 2 and 3.)

Electronic modifications to the radiometer, complete recalibration including the use of an attachable source, and two additional balloon flights in 1972 are planned under Contract No. F19723-72-C-0033.

Section 2
RADIOMETER FUNCTIONAL DESCRIPTION

The double-focused (12.7-cm diam.) optical system permits the location of a vibrating reed type chopper, an 8-position spectral filter wheel, and a 2-position neutral density filter wheel at the first focal plane, and a 4-element detector array at the second focal plane. A MOSFET integrated circuit located on the detector mount provides impedance matching to four preamplifiers. The preamplifier outputs are synchronously filtered, demodulated, fed into individual logarithmic amplifiers, and rectified to provide outputs of 0 to 5 Vdc. A pickup on the chopper provides a synchronous signal which is phase-adjusted for optimum detector signal. The analog signal is recorded with an onboard tape recorder and/or telemetered down to the control station. The electronics also include a power supply and control circuitry to position stepper motors for the two filter wheels and provide a status signal for each wheel.

The system design includes an occulting shade, cooled by liquid-nitrogen (LN_2), located forward of the optical train. The shade and first optical element are covered by a motorized movable cover. The cover serves as protection for the optical system from condensation at low altitudes and as a low-temperature-calibration source during flight. The optical train and detectors are conductively and radiatively cooled by solid neon formed in a toroidal tank around an aluminum optical barrel. The entire optical assembly and neon tank are enclosed in a LN_2-jacketed, double-evacuated dewar. The main components of the radiometer system are shown in Fig. 2-1.

A frost-free optical system is ensured by purging the optical region with a mixture of neon vent gas and warm nitrogen gas at the shade aperture. A separate LN_2 tank, a heat exchanger, and a hot water tank are carried aloft with the balloon to provide the warm nitrogen gas for the frost-free system.

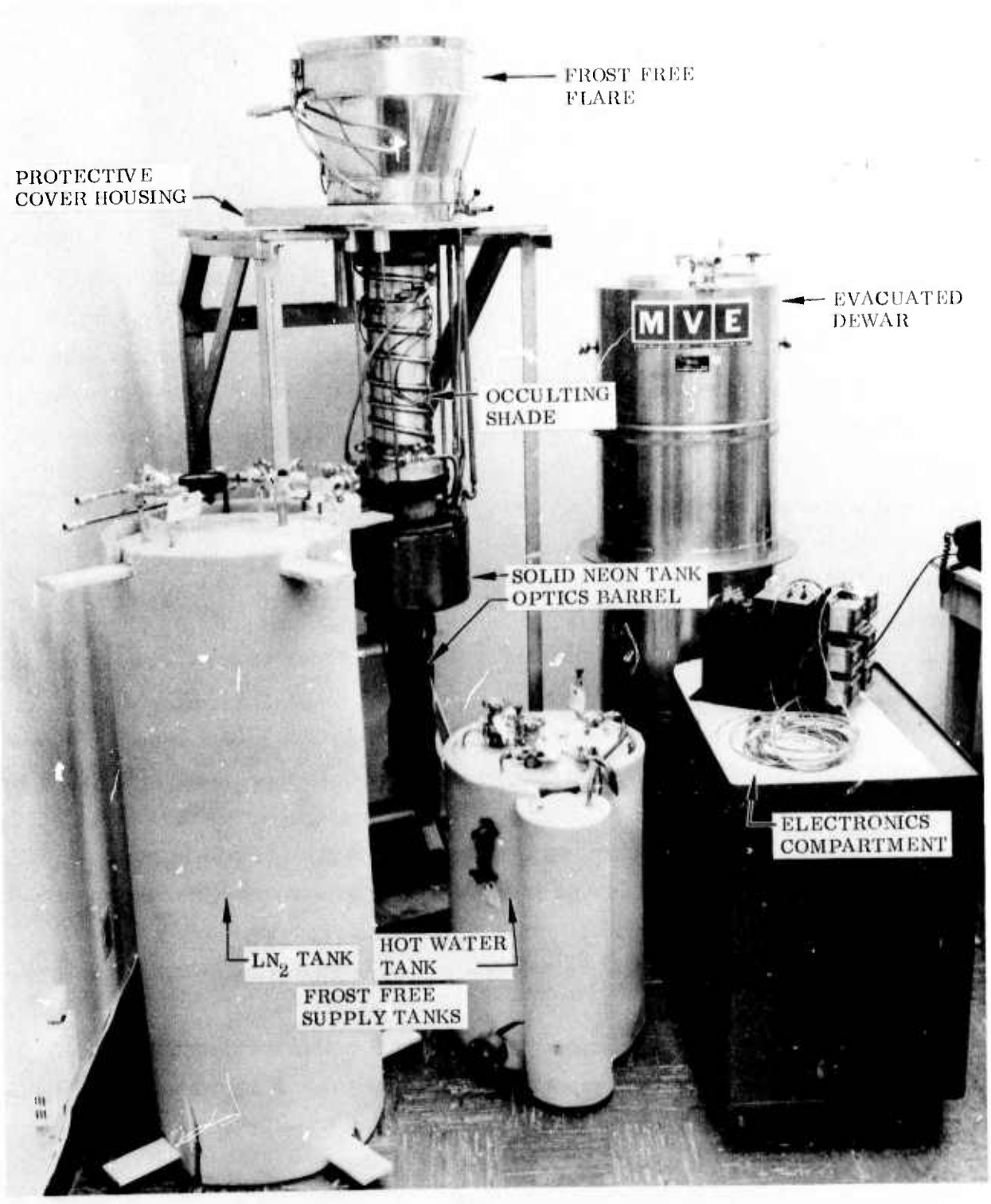

Fig. 2-1 Main Radiometer System Components

The radiometer and dewar assembly is mounted on a gimbal system which is operated as part of the balloon gondola equipment to enable viewing at angles of 90 deg (vertical), 45, 30, 15, 10, 5 deg, (horizontal) and -5 deg. The complete apparatus is shown in Fig. 2-2, as suspended from the launch vehicle just prior to the first launch.

2.1 OPTICAL DESIGN

The on-axis double-focusing optical design* is conceptually similar to the solar coronagraph but does not use an occulting disk. By using a cooled occulting shade forward of the optics and a cooled mask aperture at the first focal plane, the out-of-field energy rejection can theoretically reach 10^9 for radiation more than 0.5 deg out of the field of view (FOV).

The optical design, shown schematically in Fig. 2-3, consists of a 12.7-cm diam., 25.4-cm focal length germanium collecting element with one aspheric surface. A three-element array of transfer optics, with unit magnification, is comprised of two germanium elements and one TI-1173 glass element. The calculated first focal plane aberrations of the objective lens are shown in Fig. 2-4, as a function of off-axis angle. The aberration curves for the total optical system at the second focal plane are shown in Fig. 2-5 for operation at 65°K. Although the occulting shade allows an FOV of 8 deg, the present application is limited by the detector array to about 0.91 deg.

The choice of germanium and TI-1173 glass was based upon their excellent transmission in the 8- to 12-μm range, good low temperature stability, and large difference in refractive index.

All optical elements were antireflection-coated** to provide maximum transmission as shown in Figs. 2-6 and 2-7 for germanium and TI-1173 glass, respectively. Eight spectral filters and two neutral density filters have been considered for the measurement

*Developed by Optical Instruments Corporation, Buena Park, California
**By Optical Coating Laboratory, Santa Rosa, California

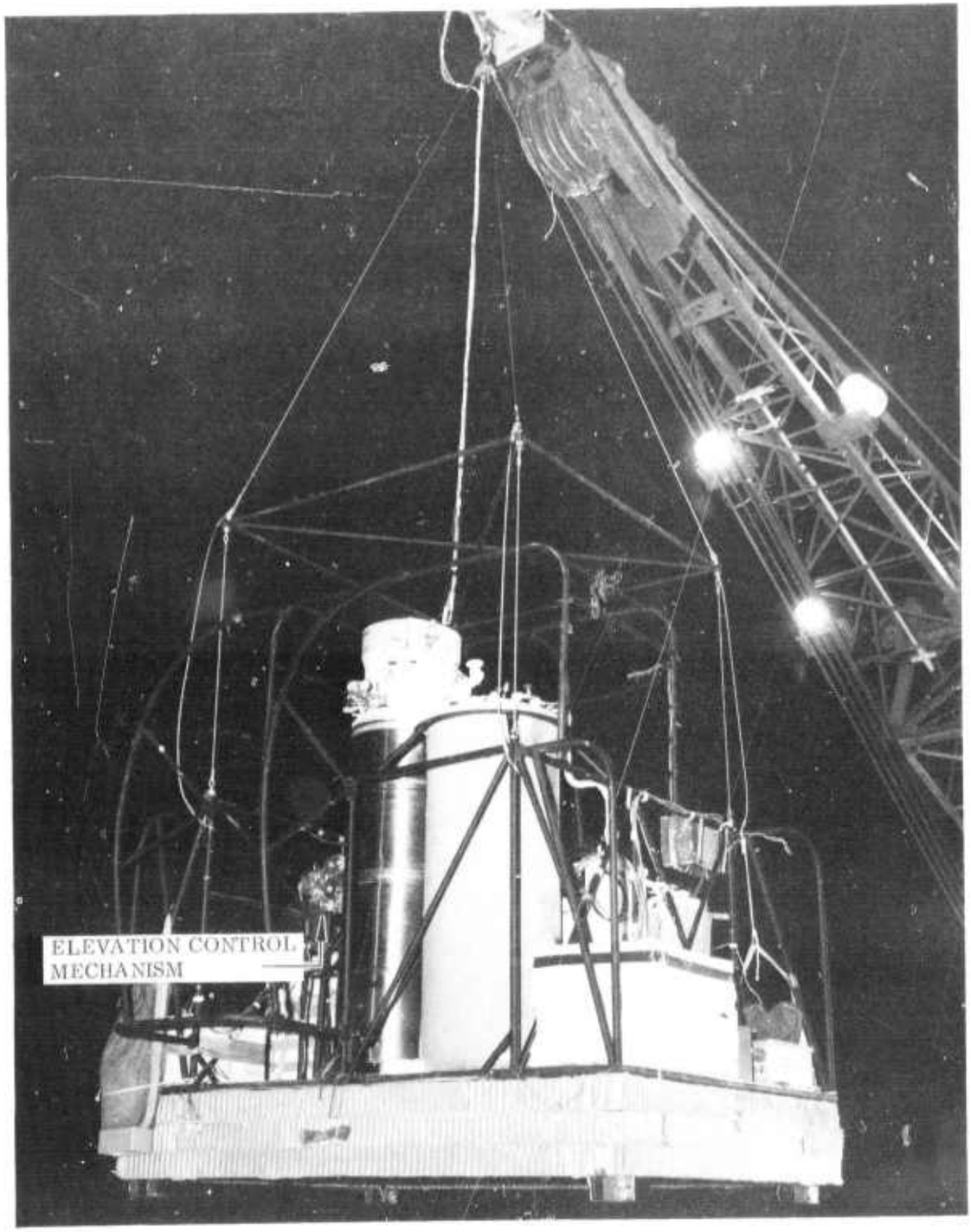

Fig. 2-2 Radiometer and Associated Equipment Mounted on Balloon Gondola Before Launch

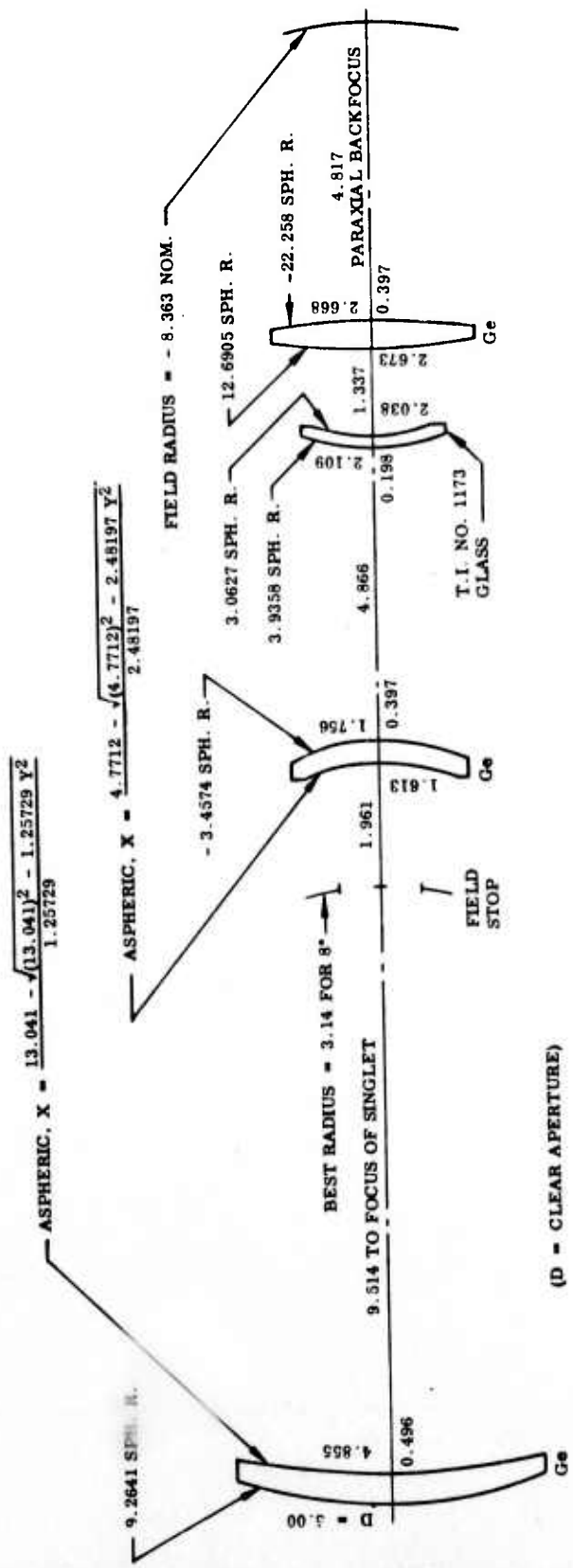

Fig. 2-3 Double-Focus Refractive Optical System

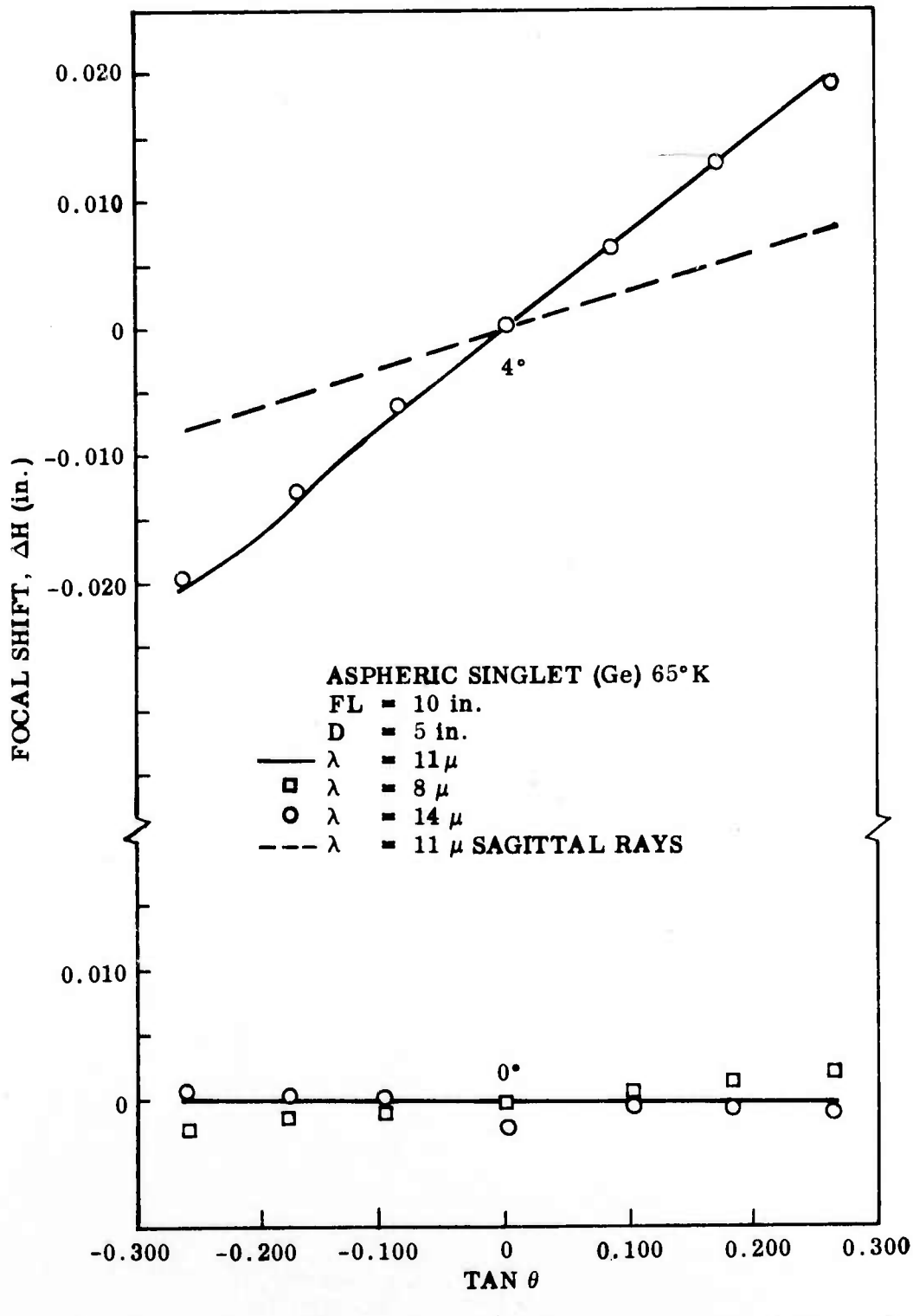

Fig. 2-4 Objective Lens Aberrations at the Center and Edge of the Field of View

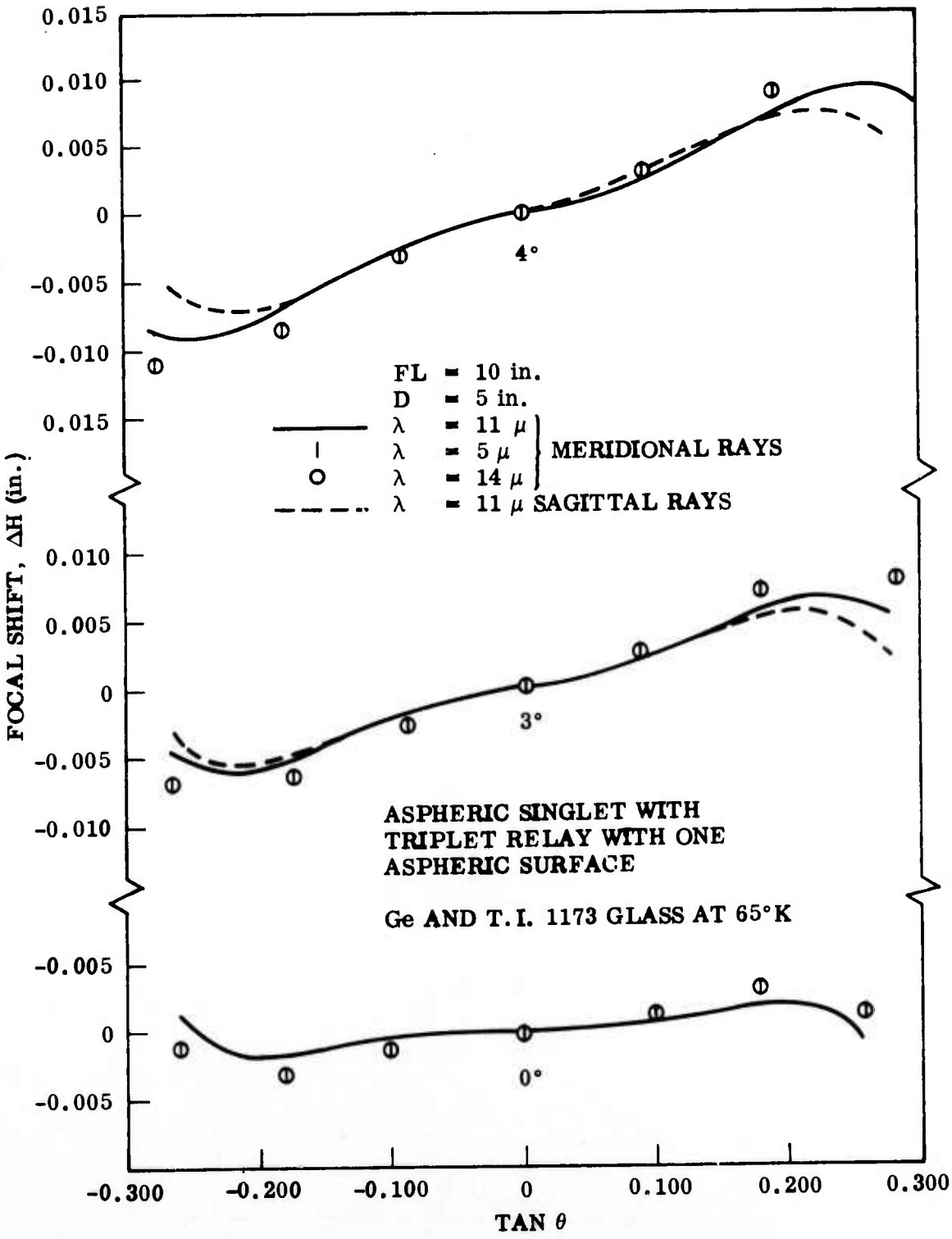

Fig. 2-5 Total Optical System Aberrations at Second Focal Plane

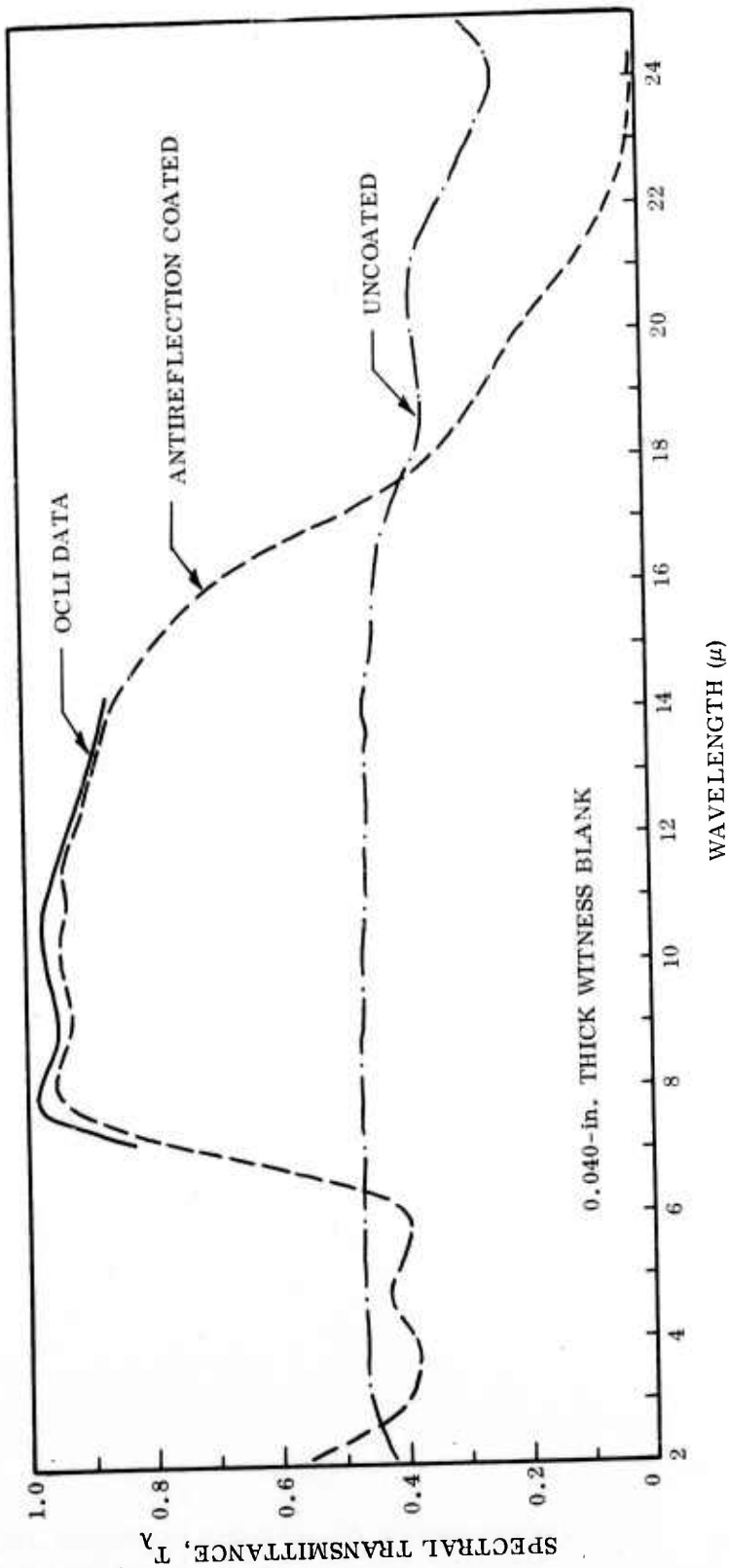

Fig. 2-6 Spectral Transmittance of Coated Germanium Witness Blanks

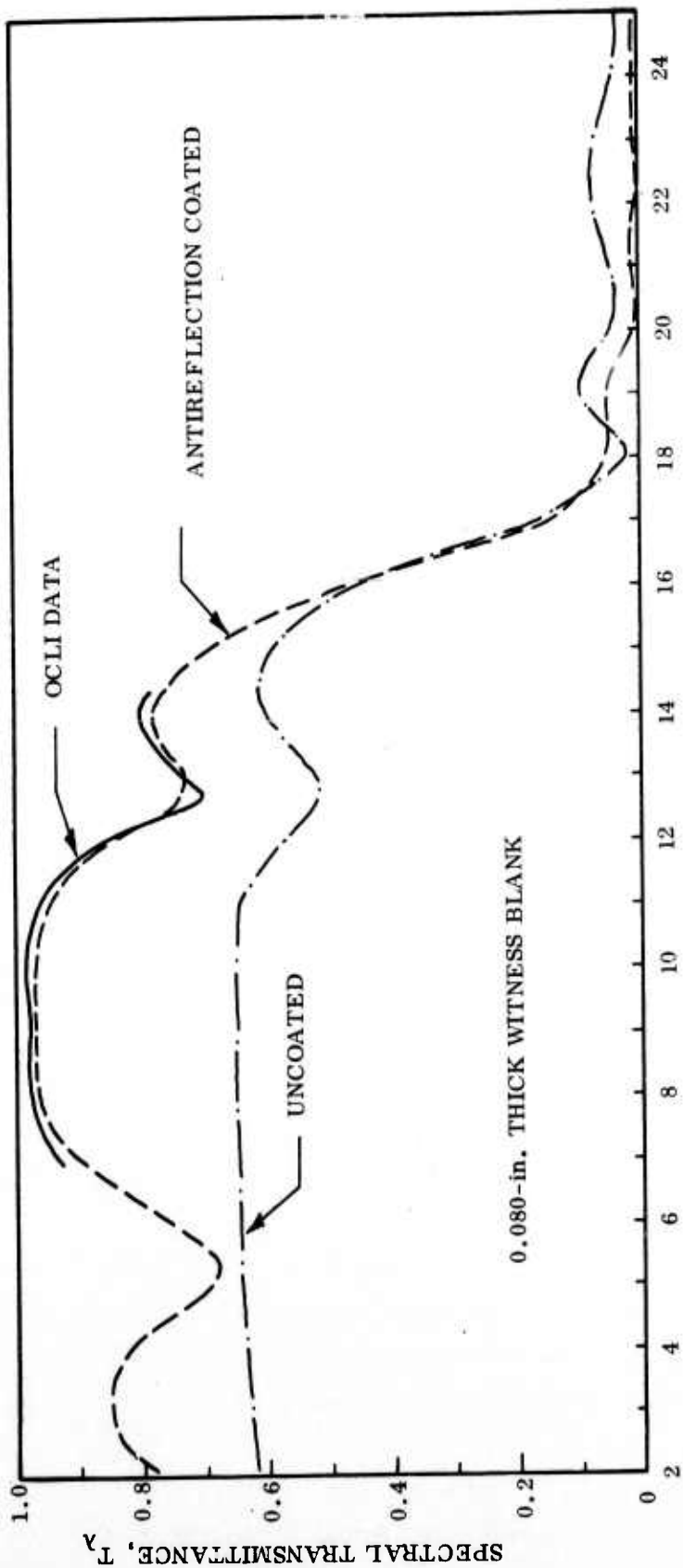

Fig. 2-7 Spectral Transmittance of Coated TI 1173 Class Witness Blanks

program as shown in Figs. 2-8, 2-9, and 2-10. Flight data have been obtained with spectral filter No. 6 and the 1.0-percent neutral density filter.

2.2 OPTICAL CONSTRUCTION

2.2.1 General

The optical elements were ground and polished* to the following specifications:

- Surface Quality: 80/50
- Contraction: 0.00011-cm – total indicated reading, maximum surface runout at edge of lens
- Test Plate Fit (Spherical Surfaces): Two fringes spherical, 1/4-fringe irregularity (6328 Å)
- Null Corrector (Aspherical Surfaces): Half fringe (6328 Å)

The barrel housing for the optical elements was machined in two pieces to permit ready access to the first focal plane. Thermally good-conducting 6061-T6 aluminum ensured good temperature uniformity. Machining tolerances and lens mounting techniques allowed for the contraction of the system when cooled to operating temperatures. Because of the large difference in expansion coefficient between germanium and aluminum, the germanium elements were mounted in molybdenum alloy (mo + 0.5 percent Ti) seats. Each seat is mounted,by means of three shoulder screws, to the aluminum barrel. The screws fit snugly in three radially slotted holes in the seat, 120 deg apart, to permit radial thermal expansion between the aluminum barrel and the seat to maintain concentricity. A typical Ge lens seat assembly is shown in Fig. 2-11.

The TI-1173 glass has a thermal expansion coefficient, similar to aluminum, which allows the lens to be mounted directly in the barrel with spring loading against two hard stops. Belleville type washers were used to maintain spring pressure to the lens holder screws as the optical system was cooled.

*By Optical Instruments Corporation, Buena Park, California

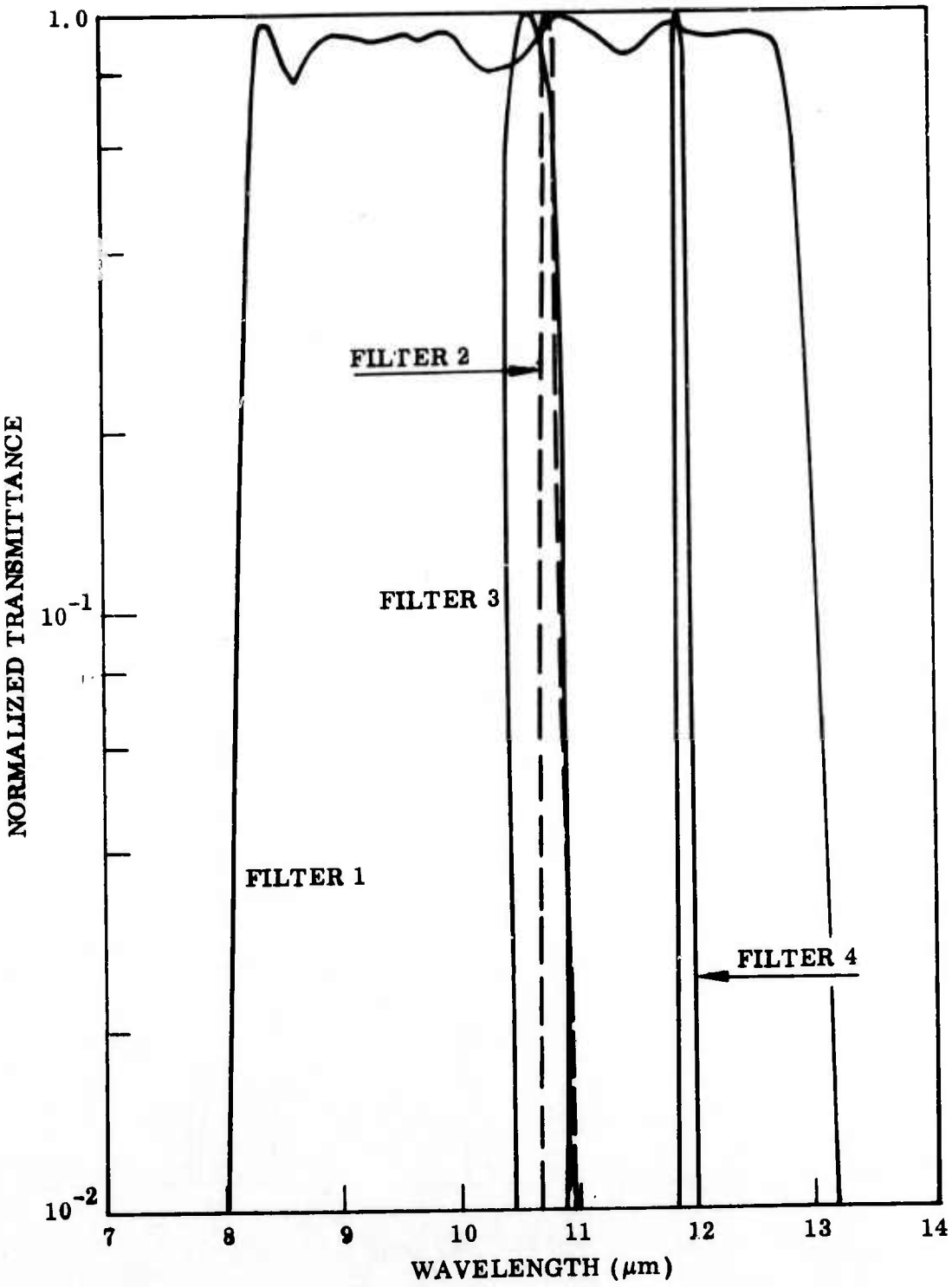

Fig. 2-8 Spectral Transmittance of Filters 1 Through 4

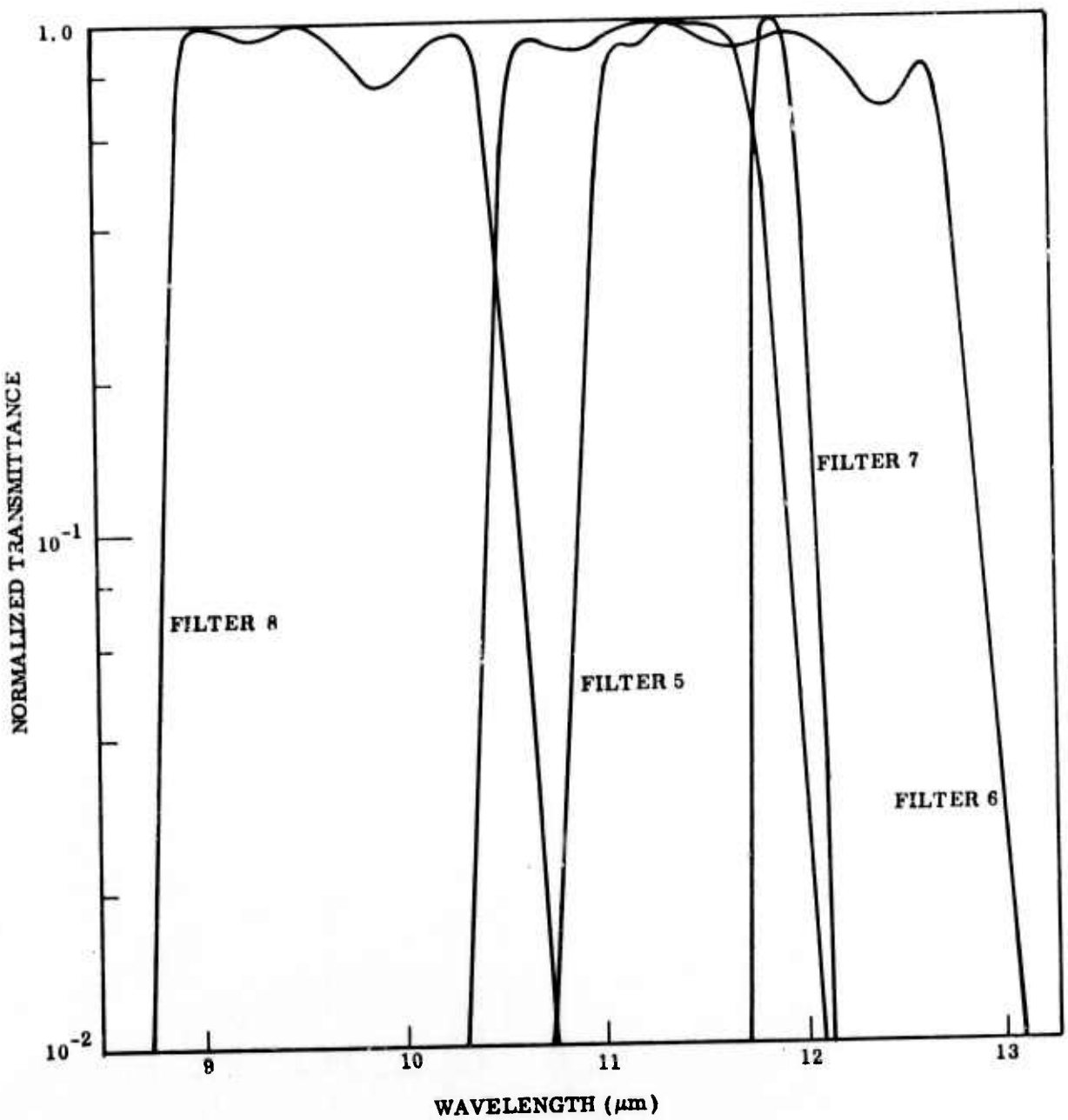

Fig. 2-9 Spectral Transmittance of Filters 5, 6, 7, and 8

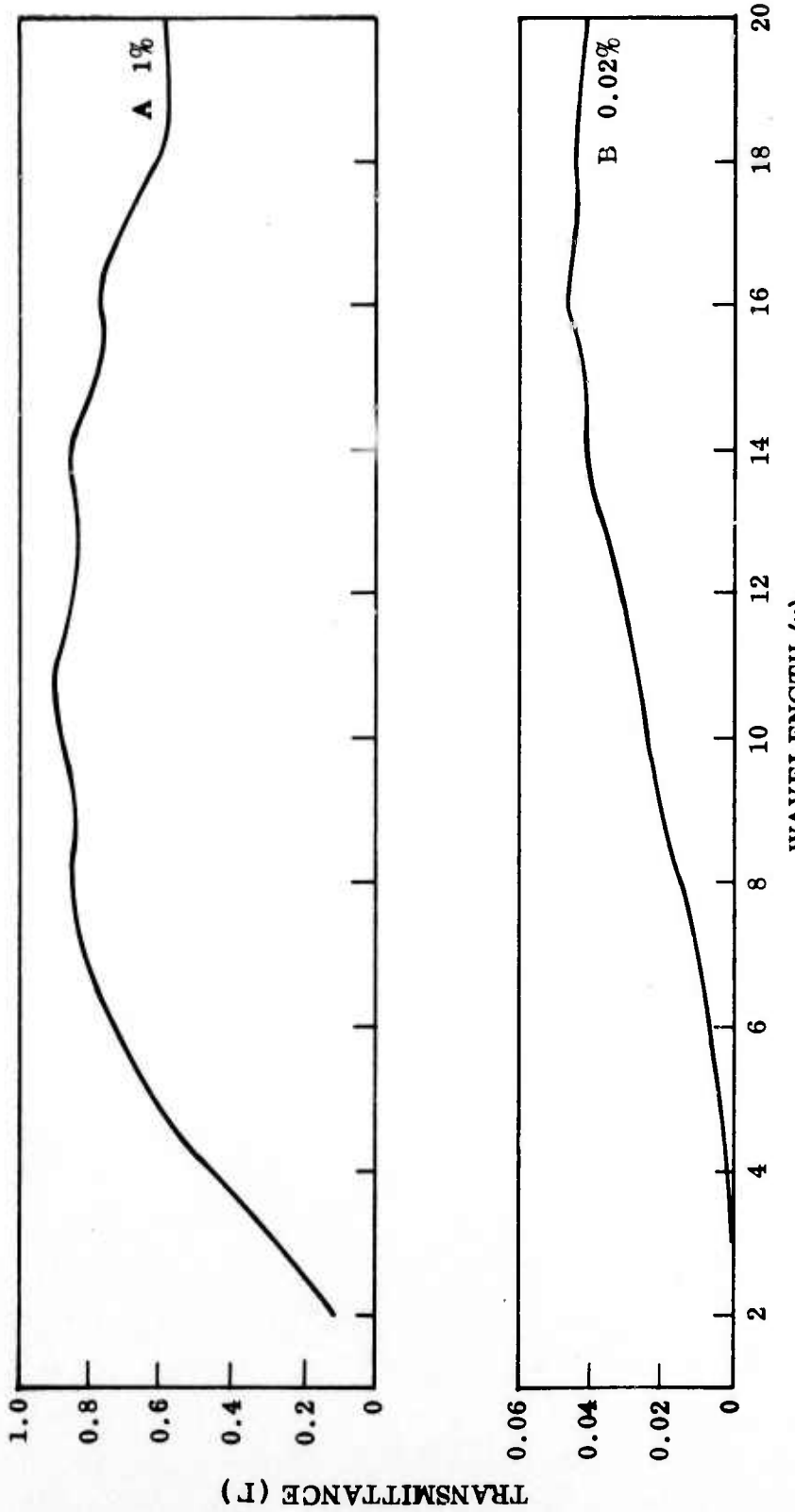

Fig. 2-10 Spectral Transmittance of the 1-Percent and 0.02-Percent Neutral Density Filter

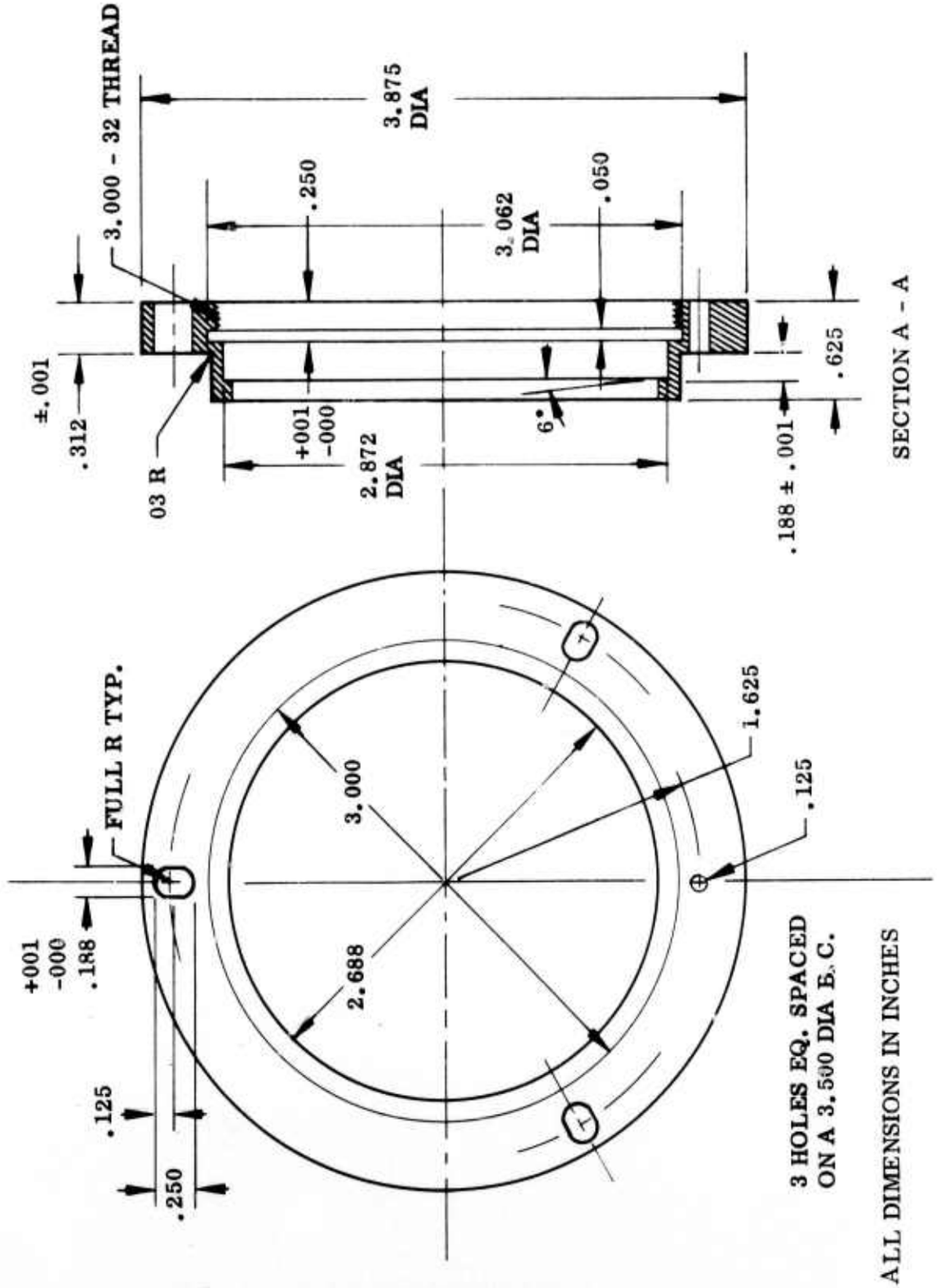

Fig. 2-11 Aft Germanium Lens Seat

A field stop with the same configuration as the detector array was mounted at the first focal plane radiation cone as detailed in Fig. 2-12. The array and dimensions of the mask and appropriate detectors are shown in Fig. 2-13. The mask and appropriate detectors are shown in Fig. 2-13. The mask image was determined by scanning the second focal plane with a thermistor bolometer detector with the optical system cold. The mask is black-anodized to minimize signals reflected from the chopper surface.

2.2.2 Chopper and Filter Wheels

The optical chopping is accomplished with a vibrating reed chopper* located just aft of the field stop. The nominal 200-Hz chopping frequency is controlled by an electronic oscillator located in the electronic chassis. Because of the lower resistance in the drive coil at operating temperature, the control circuit was modified by adding variable resistors in series with the pickup and driver coils. The chopper is mounted with the blade vignetting about half of the FOV of each detector in the null position and oscillates with an amplitude of about 2 mm. A pickup coil mounted adjacent to the driver coil is used to provide the synchronous signal for the main amplifier and filter. A status voltage is monitored during flight to verify proper performance of the chopper.

The spectral and neutral density filter wheels are located aft of the chopper and actuated by individual stepper motors and associated gearing. The spectral filter wheel will accommodate eight filters (1.58 cm diam. × 1.5 mm thickness), equally spaced 45 deg apart, as shown in Fig. 2-14. The four-position (90-deg per step) stepper motors** are mounted to the underside of the dewar cover to permit maintenance of their temperatures above -70°C and to ensure operation in the radiometer cooled condition. An 0.5-in.-diam. shaft with flexible couplings at each end connects the motor drive to the geared filter wheel with a 2:1 reduction. The control circuit located in the electronics package is energized by individual commands transmitted by a telemetry channel. The status (position number) of the filter wheel is indicated by the magnitude of the motor-winding voltage determined by the motor polarity and a microswitch actuated by the filter wheel.

---

*American Time Products, Model L 43.5 CA
**Servonetics, Inc., Model M1161C

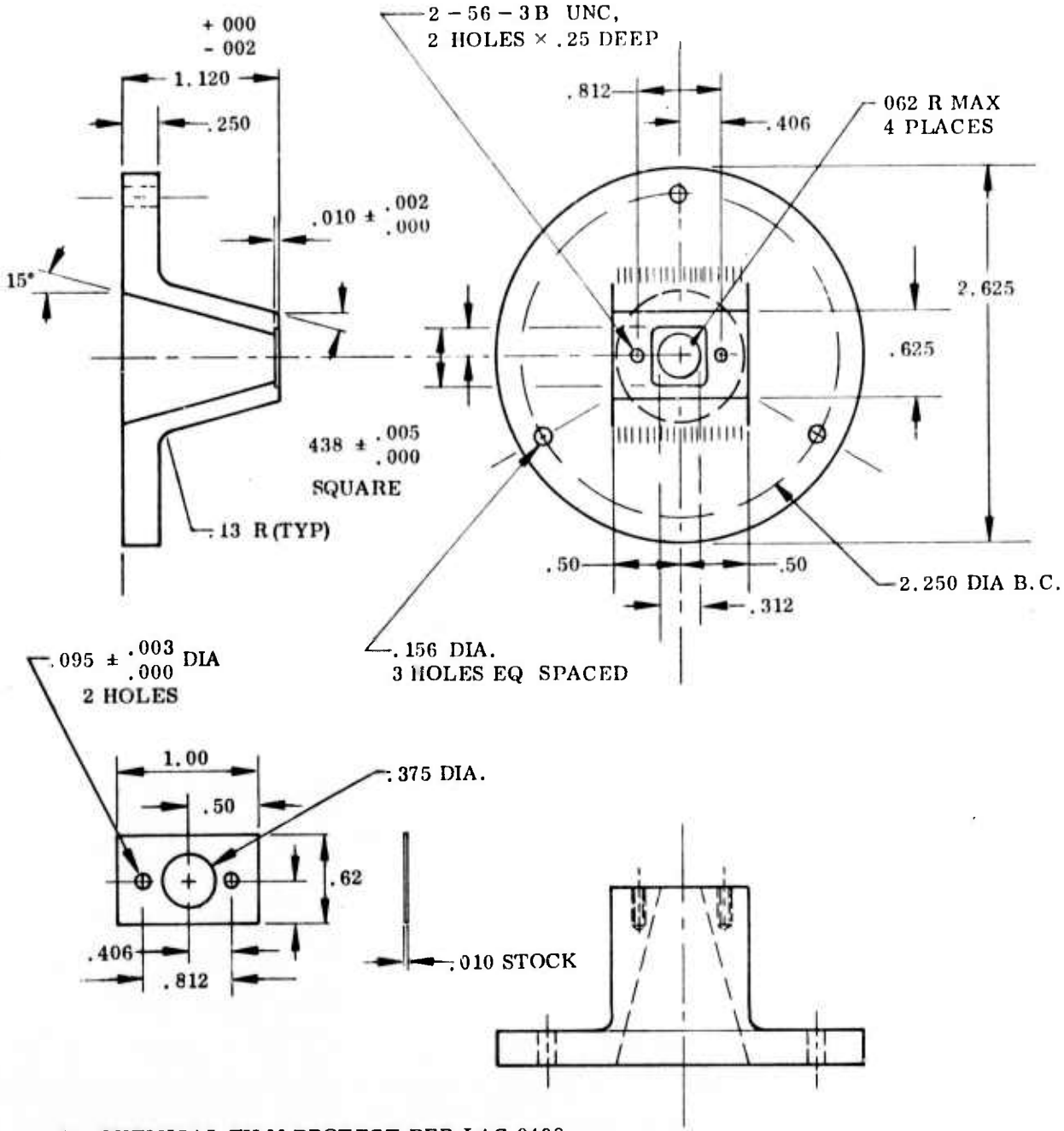

4. CHEMICAL FILM PROTECT PER LAC 0498
3. SOLUTION ANNEAL BEFORE FINAL MACHINING
2. IDENTIFY PER LAC 3575, METHOD A, TYPE I
1. MACHINE TO PROCESS SPEC LAC 3601

1.120 +.000 -.002
-.010 +.000 -.002
+.002 +.0005 -.0005
1.112 +.0005 -.0045

Fig. 2-12 First Focal Plane Radiation Cone and Aperture Mask Mount (All Dimensions in Inches)

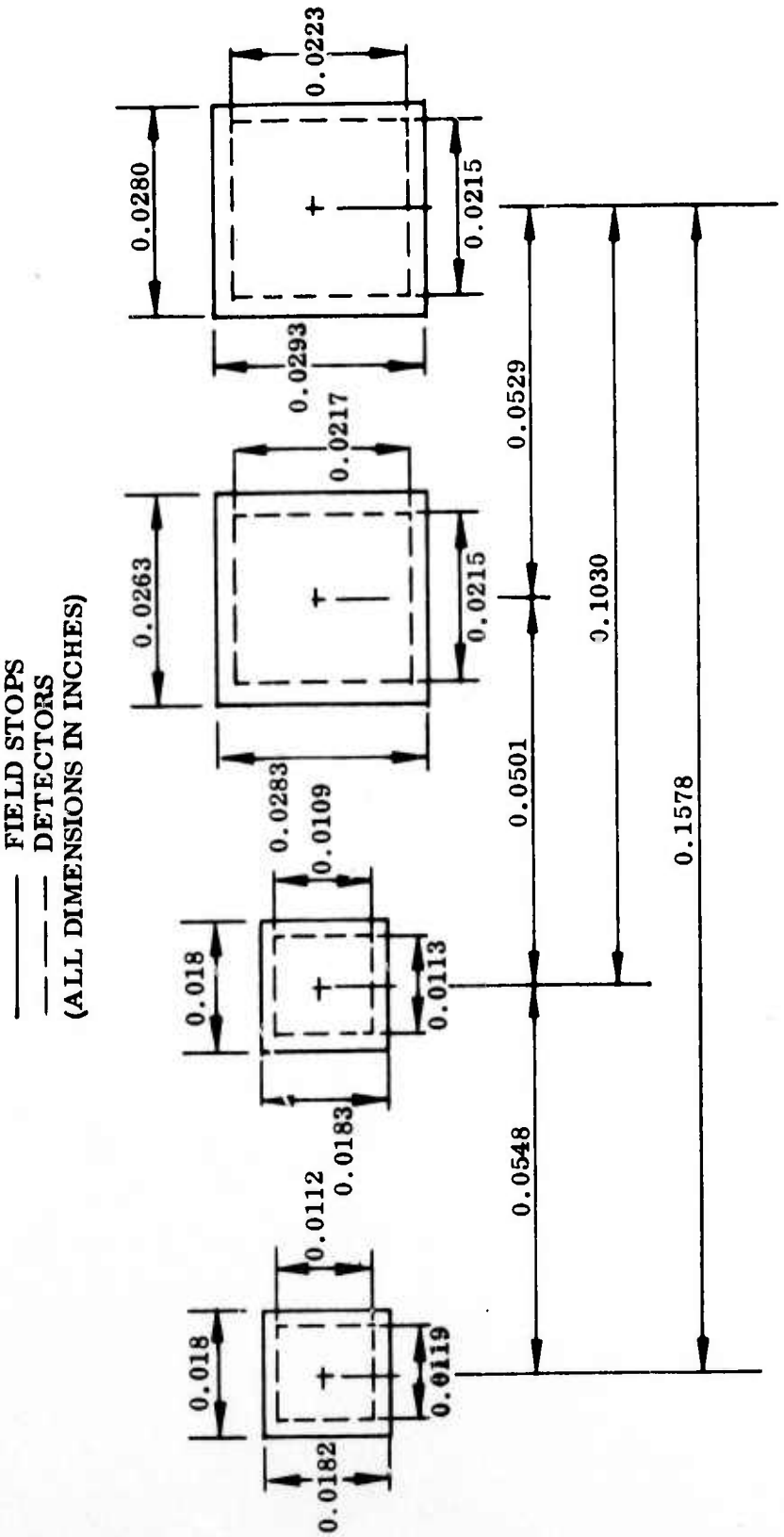

Fig. 2-13 Size and Relative Location of Detector Array and Four-Hole Field Stop

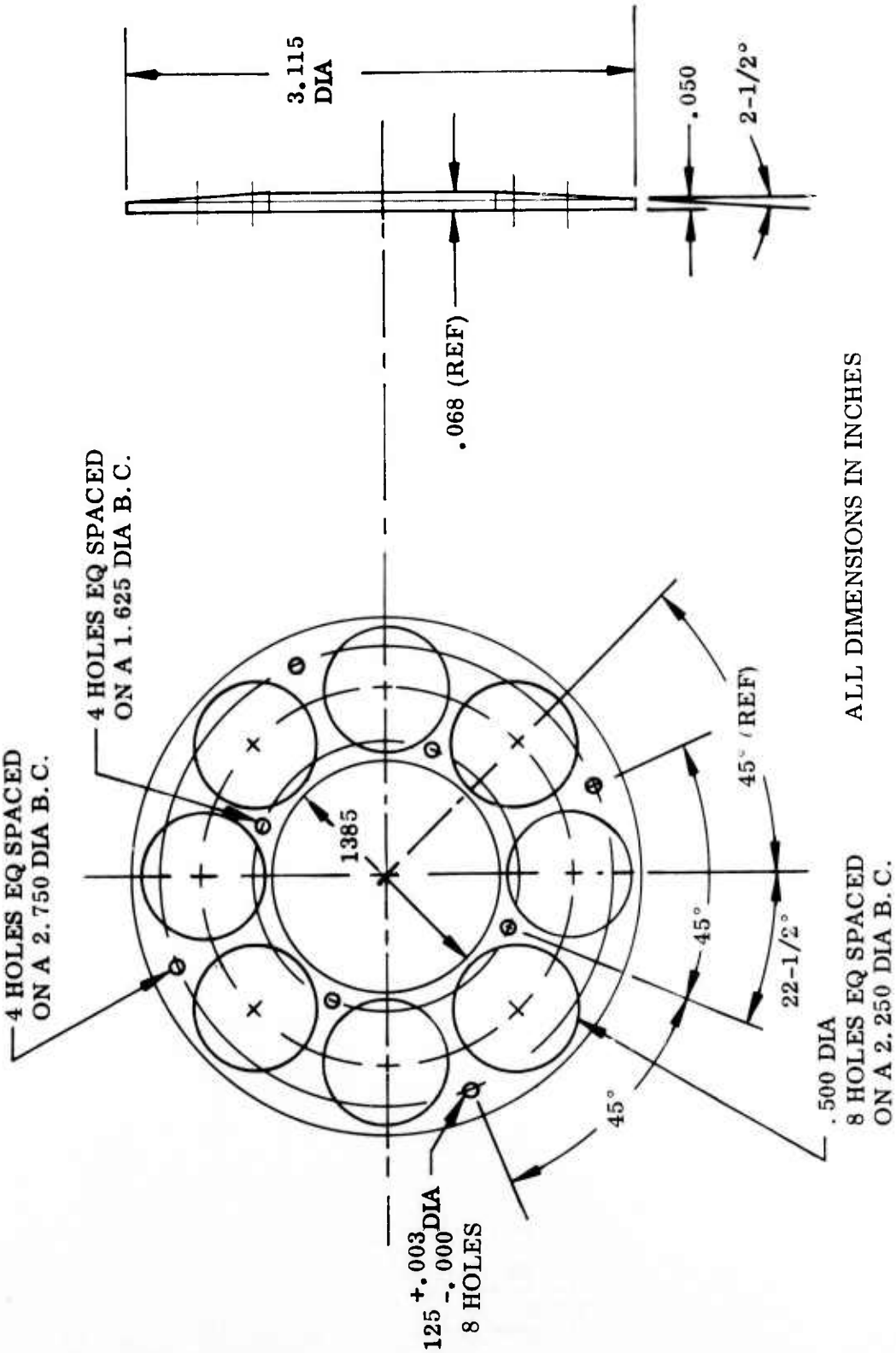

Fig. 2-14 Spectral Filter Wheel Retainer

The motor-winding position, voltage, and corresponding status voltage are listed in Table 2-1.

Table 2-1

SPECTRAL FILTER WHEEL WINDING AND STATUS VOLTAGES

E_o (Status) J2-T	Microswitch Input J1-T (V)	Winding A		Winding B		Connector and Pin – Master Winding Condition (i.e., Current Flow)
		A1 J1-R (V)	A2 J1-S (V)	B1 J1-P (V)	B2 J1-N (V)	
0.05	0	2.0	27.0	1.0	1.0	A2 to A1
0.54	0	1.0	1.0	2.0	27.0	B2 to B1
0.97	0	27.0	2.0	1.0	1.0	A1 to A2
1.47	0	1.0	1.0	27.0	2.0	B1 to B2
2.32	28	2.0	27.0	1.0	1.0	A2 to A1
2.77	28	1.0	1.0	2.0	27.0	B2 to B1
3.19	28	27.0	2.0	1.0	1.0	A1 to A2
3.73	28	1.0	1.0	27.0	2.0	B1 to B2

The netural density filter utilizes two positions, "In" and "Out," which may be manually or automatically changed. The In position puts an 1.0-percent transmission filter in the optical beam. In the Out position there is no added attenuation in the optical path. The automatic mode provides for the introduction of the neutral density filter when the output signals of each detector channel reach 4 V. If the signal decreases below 0.5 V in any one of the detector channels, the filter is automatically removed from the optical path. Selection of the automatic or normal mode and the manual filter position is also remotely controlled from the ground. The neutral density filter motor winding and status voltages are listed in Table 2-2.

2.3 DETECTOR ARRAY

The detector array consists of four Ge:Hg elements* aligned horizontally at the second focal plane. The array consists of two large (0.433-mm square) and two small

*Santa Barbara Research Center

Table 2-2

NEUTRAL DENSITY FILTER WHEEL STATUS (MOTOR VOLTAGE: 28V APPLIED TO NDF MOTOR)

Sequence	Mode – Controlled by Input Command	E_o (V) J2-6	Signal Level (V)	Winding Polarity (V)		
				J1-a	J1-b	J1-$\bar{c}$
1	NDF Out-Man	0.80	NA	0	28	28
2	NDF In-Man	1.55	NA	28	0	28
3	NDF Out-Auto	2.37	$\lesssim 0.06$	0	28	28
	NDF In-Auto	3.37	$\gtrsim 4.9$	28	0	28

(0.279-mm square) detectors spaced about 1.27 mm between centers. As indicated in Fig. 2-15, this extrinsic photoconductive detector resistance and response are not achieved until cooling to a temperature of 28°K or less occurs. Relative quantum efficiency and spectral response curves shown in Figs. 2-16 and 2-17, respectively, illustrate the characteristics of typical Ge:Hg material for the 2- to 15-μm wavelength range. The resistance of each detector size as a function of background photon flux is shown in Fig. 2-18. Because of the variation in responsivity and spectral response with the temperature, the detector and background levels are maintained at their operating level during calibration.

The detectors are mounted on a copper heat sink which, in turn, is mounted to an aluminum end plate at the aft end of the optical barrel. A platinum resistance thermometer is attached to the neon tank to monitor the temperature during flight.

Separate bias supplies are provided for the two sizes of detectors; +10 Vdc for the large size and +5 Vdc for the small size. A schematic of the MOSFET source follower and electrical circuitry for the detector system is shown in Fig. 2-19. The rms noise voltage as a function of the background photon flux for the MOSFET source follower is shown in Fig. 2-20.

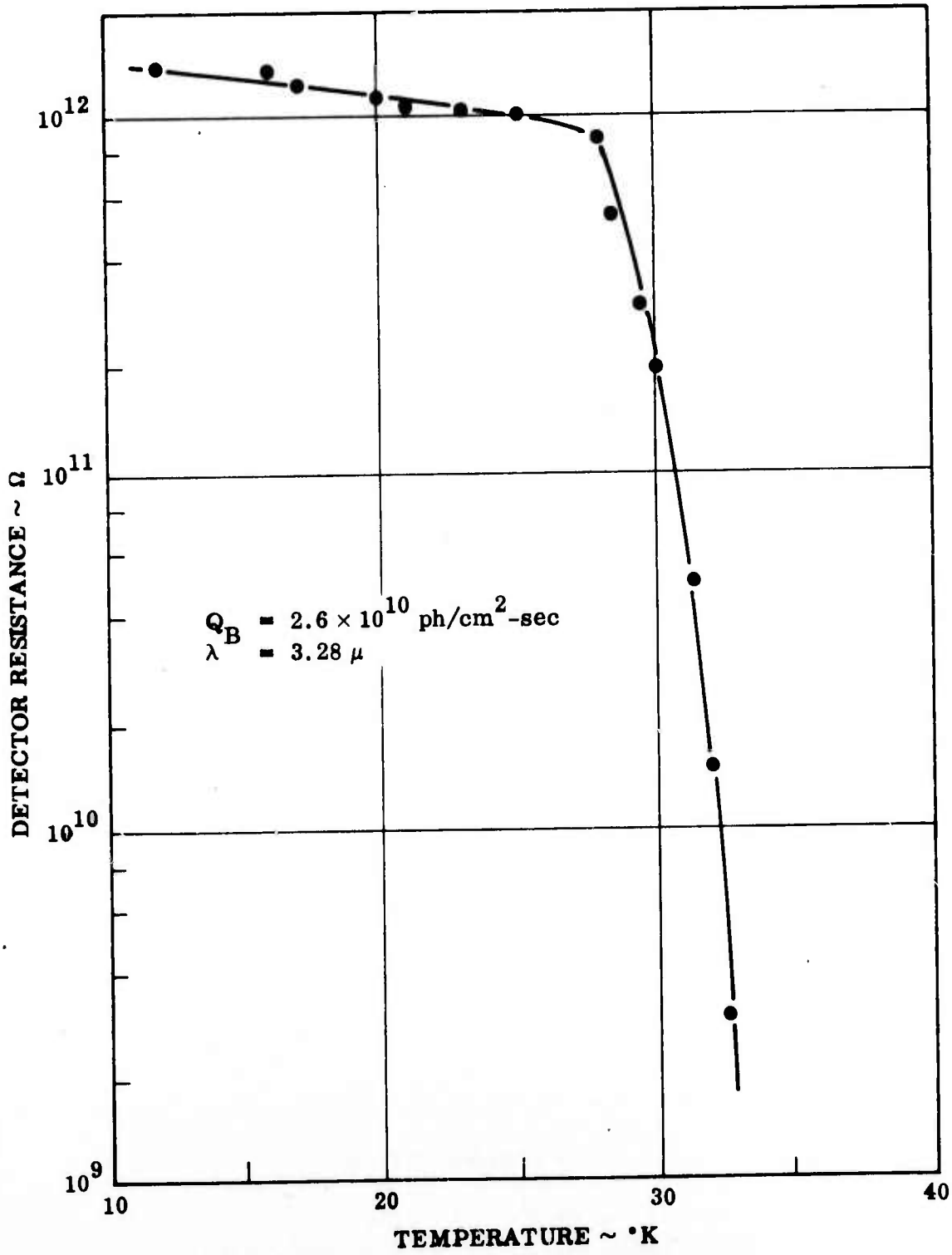

Fig. 2-15 Ge:Hg Detector Resistance As a Function of Temperature

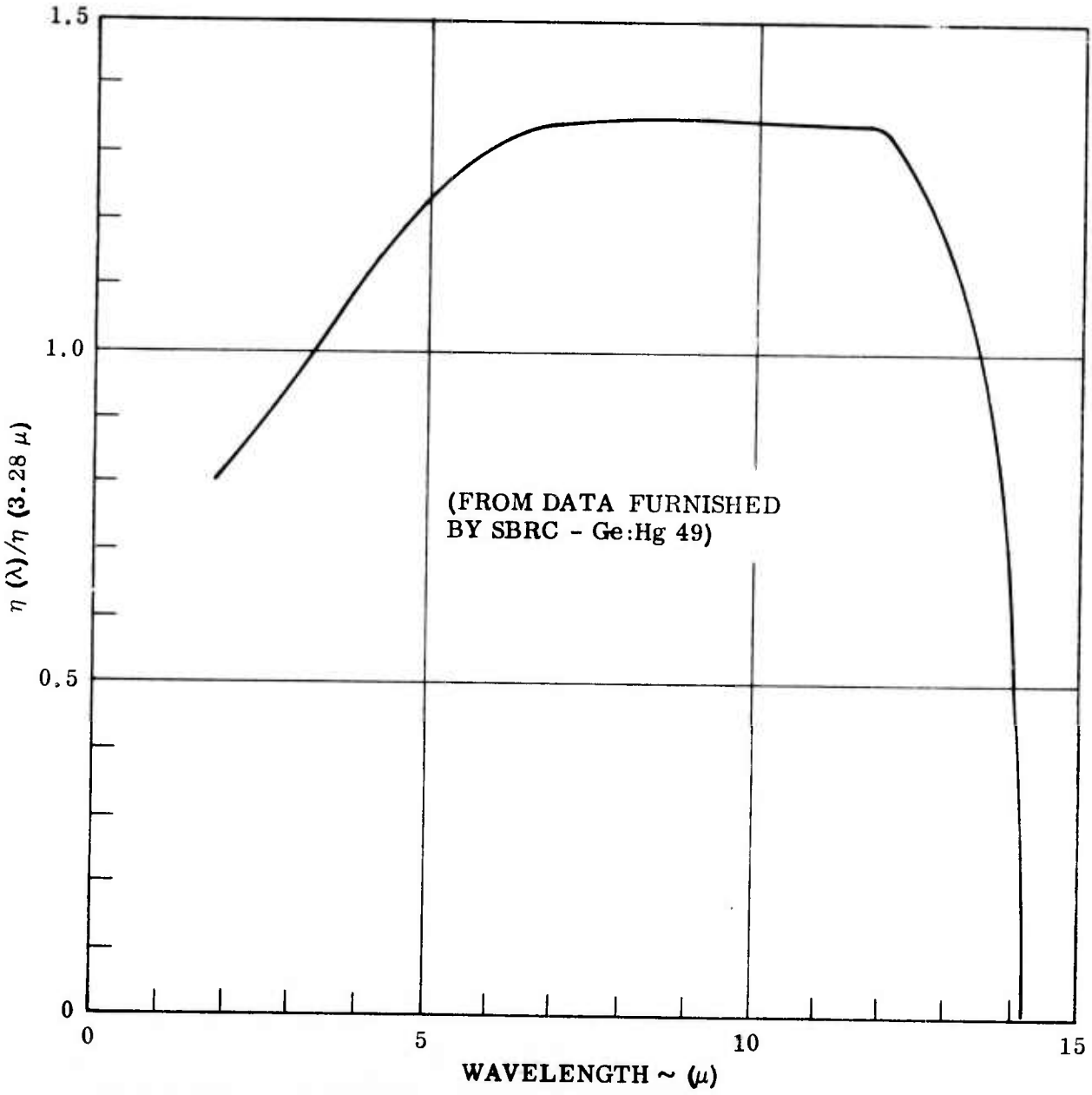

Fig. 2-16 Ge:Hg Spectral Quantum Efficiency Based Upon 3.28-μm Radiation Measurements

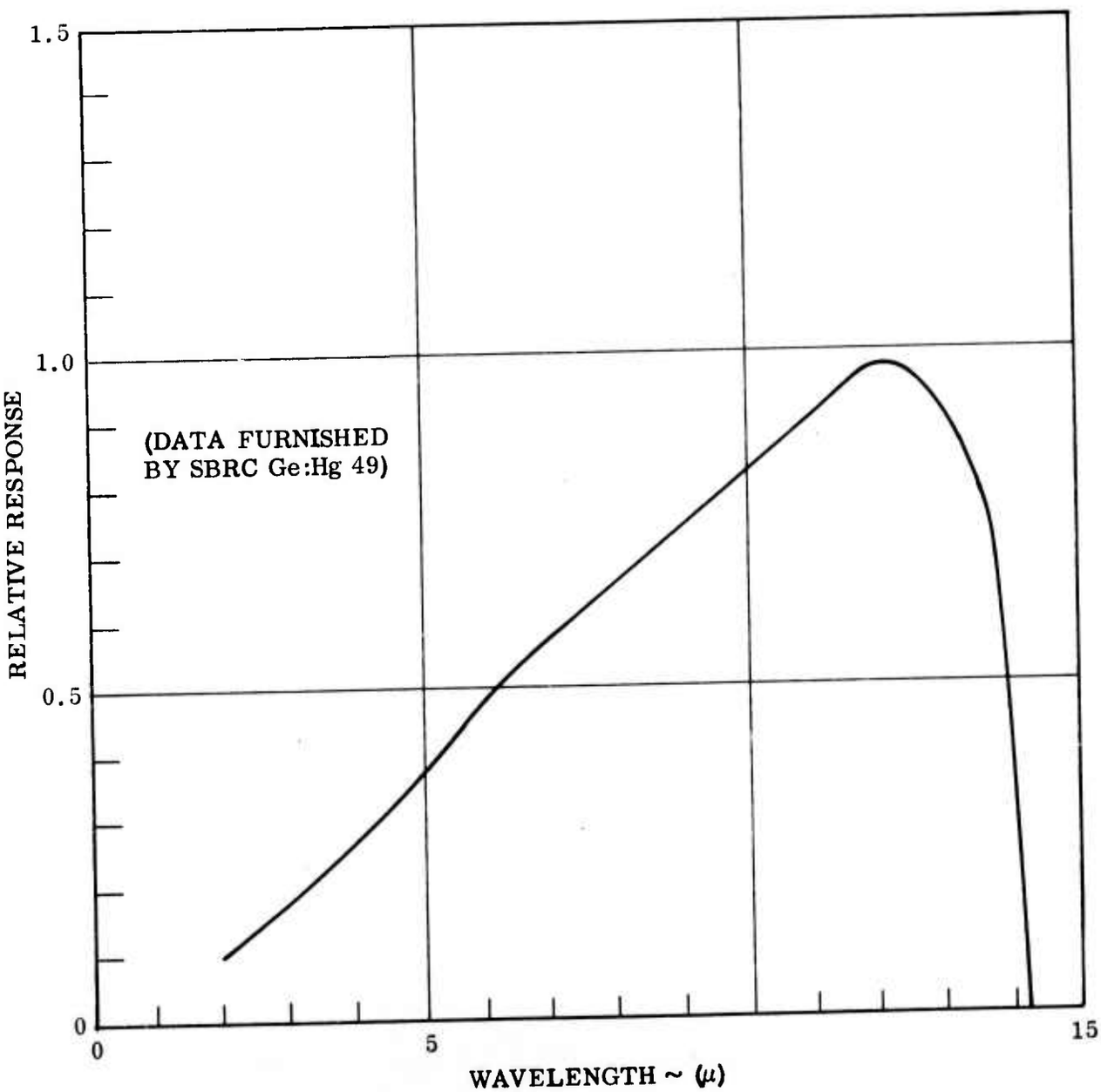

Fig. 2-17 Ge:Hg Relative Spectral Response (SBRC Ingot No. 49)

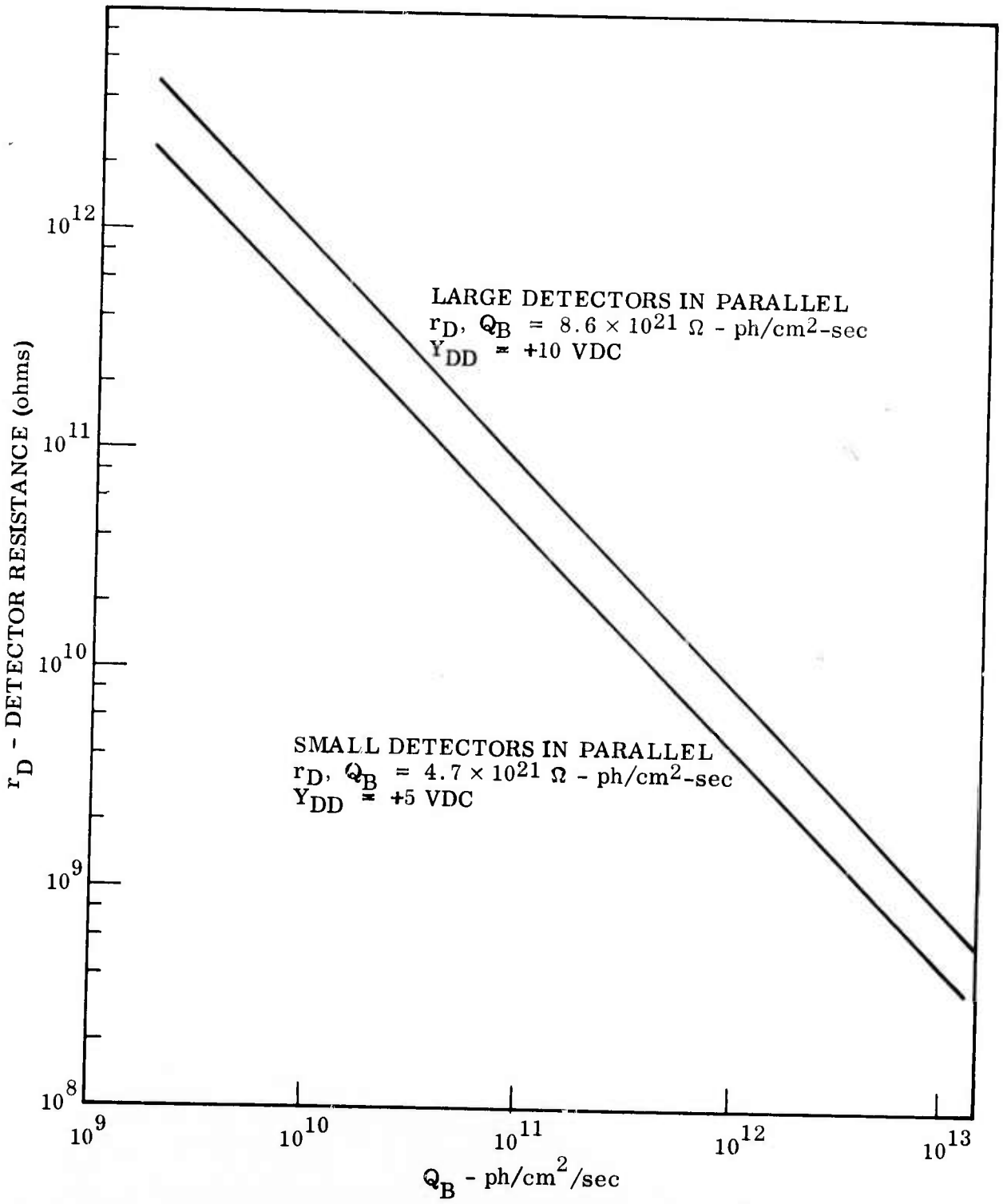

Fig. 2-18 Resistance of Small and Large Detectors As a Function of background Photon Flux Density

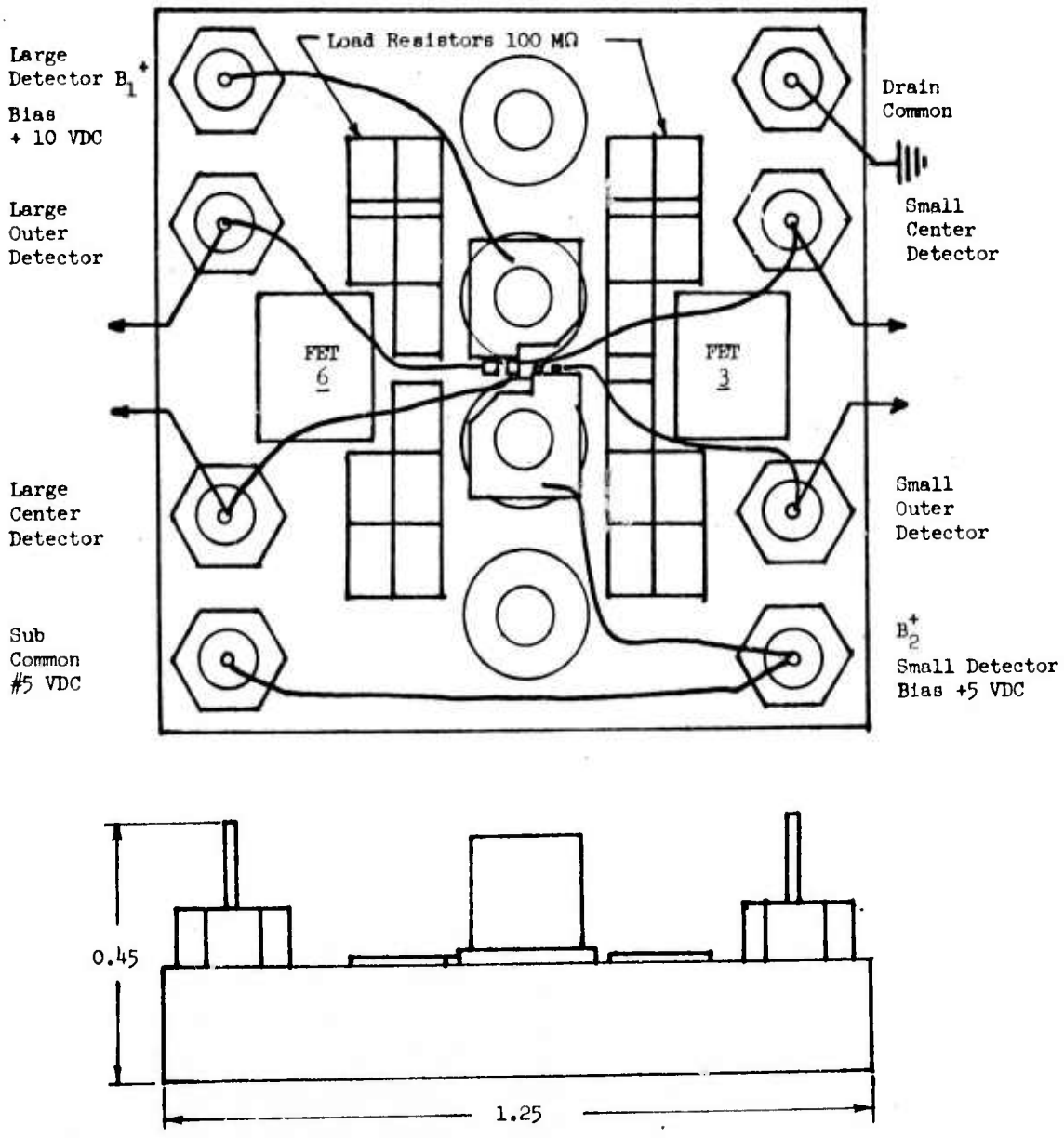

Fig. 2-19 Detector MOSFET Circuitry – Schematic

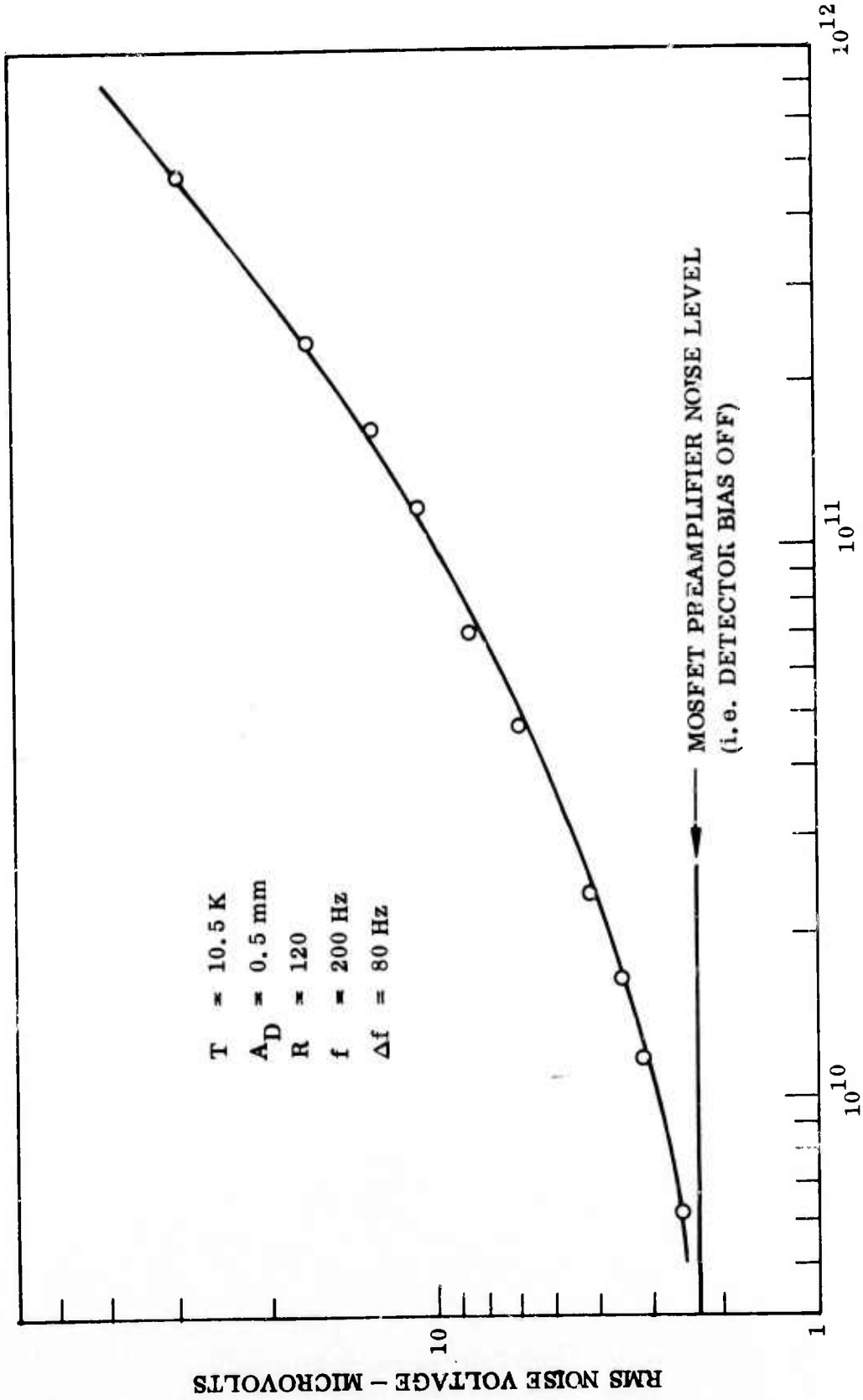

Fig. 2-20 Photon Flux Noise Voltage As a Function of Background

2.4 ELECTRONICS

The transistorized electronic system is powered by a 28-V battery capable of providing up to 87 W. The electronic package consists of the following units:

- Signal conditioning electronics
- Chopper oscillator, synchronous generator, and phase-shifting network
- Neutral density and spectral filter switching and status electronics
- Special power supplies for the foregoing units
- Temperature sensor signal conditioner
- Relay for calibration of signal channels
- Relay and hatch cover drive mechanism
- Thermostat and heater for electronic housing temperature control

A description and circuit diagram of the main electronic components are presented in the Appendix. The system electronic block diagram is depicted in Fig. 2-21.

Temperatures at six locations are monitored to enable evaluation of system performance before and during flight. These locations include the neon container, aft shade, shade front, hatch cover, flare section, and electronics housing. Platinum resistance thermometers* and associated bridge circuits and 0- to 5-Vdc transmitters** are used as the temperature transducers. The temperature measurement circuit schematic is shown in Fig. 2-22.

The electronics housing is temperature-controlled about 305°K ± 5°K using two 7-Ω flexible heater blankets,† a thermostat,‡ 0.44-cm thick flexible foam insulation inside, and 1.27-cm rigid foam insulation outside. The inside of the electronics housing is painted black to increase radiative heat transfer, and the exterior is painted white to minimize heating if exposed to solar radiation.

---

*Rosemont Engineering Co. Model 104 ME4A
**Model 441 RC
† Montgomery Co. Model PH-100
‡ Stemco Controls Type 414-3

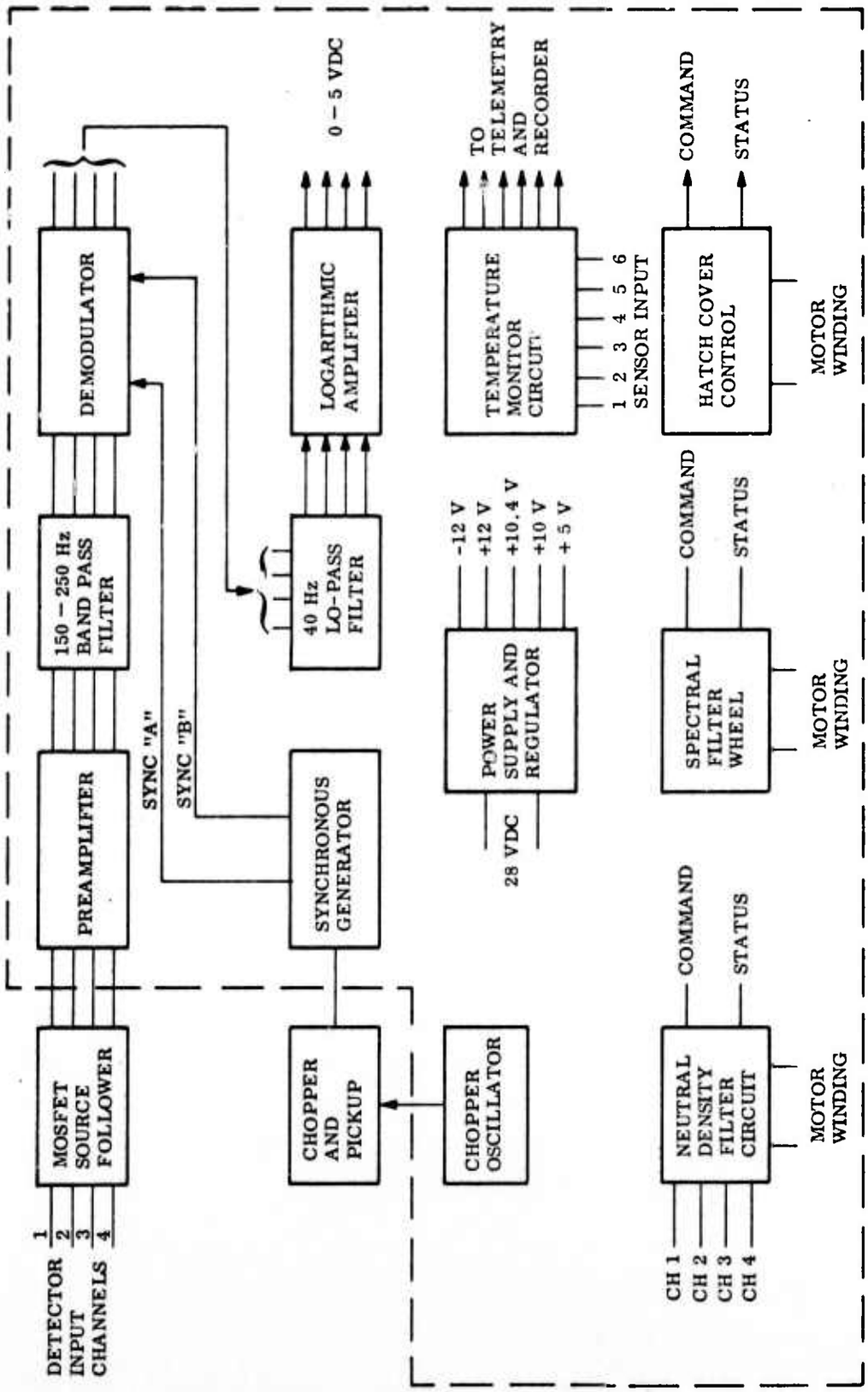

Fig. 2-21 System Electronics — Block Diagram

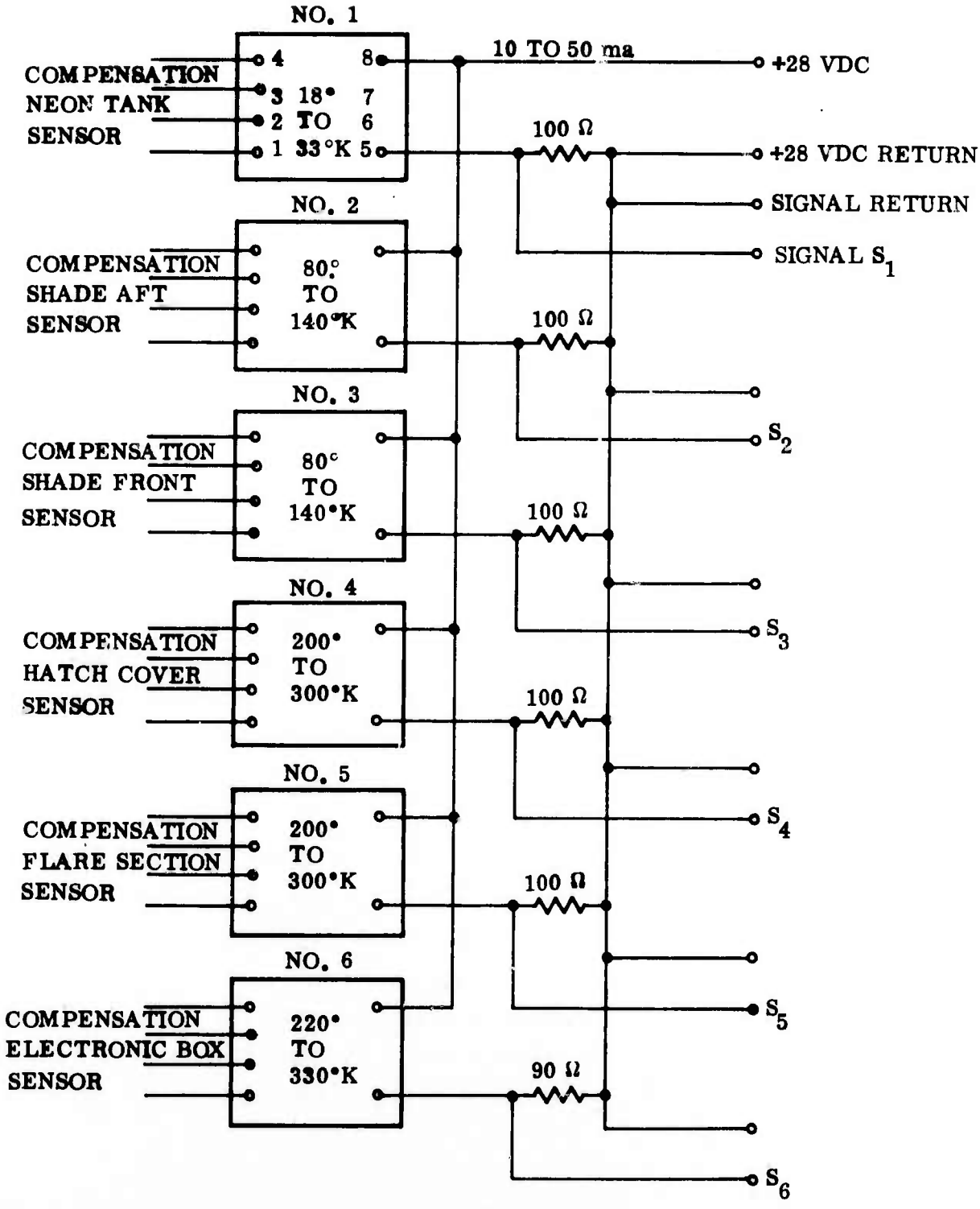

Fig. 2-22 Temperature Measurement System — Schematic

Inflight check of the four signal channels is provided by 0-, 2.5-, and 4.9-Vdc calibration signals. These signals are automatically fed to each channel by the use of microswitches and a switching relay when the hatch cover closes or opens. A double-pole magnetic relay is closed upon ground command to actuate the hatch cover.

2.5 RADIOMETER COOLING

As indicated in Section 2.3, the operation of an infrared radiometer is very dependent upon low-temperature operation. Although satisfactory background attenuation could be achieved by operating the optical elements and housing at 65° K, the Ge:Hg detectors required a temperature of 28° K or lower to function. Thermal isolation of the detector from the optics while maintaining a good alignment would have resulted in additional design complexities. Therefore, the entire optical, chopping, filtering, and detection system was conductively and radiatively coupled to the solid-cryogen container. Neon, with a triple point at 24.8° K, was selected as the cryogen because the other two potentially usable gases (helium and hydrogen) present disadvantages; i.e., safety requirements for handling hydrogen and the low heat of vaporization of helium overshadow the additional cost of using neon. Neon can be maintained at 22° K in the solid-state at 10 mm hg (the approximate pressure at operating altitude), thus alleviating the problem of handling a liquid when changing radiometer orientation.

The cylindrical copper neon tank contains copper baffles to keep the gradient between the solid neon and the tank wall to temperature of about 1° K. Internal coolant lines are provided to permit subcooling and freezing of the neon with liquid helium. One fill and two vent ports are used to service the tank and to direct gaseous neon boiloff into the frost-prevention system. The 5.25-liter tank has a hold time of about 10 hr after termination of the helium cooling. A platinum resistance thermometer located on the tank and a special amplifier are used to provide a 1- to 5-Vdc output signal for the 18° to 33° K temperature range.

An occulting shade forward of the optical train is cooled with LN_2 to minimize the background radiation on the first objective element and to reduce scattered radiation. The

shade is attached to the dewar cover and to the optical barrel with fibre glass transition adapters for thermal isolation. A 2-in.-thick layer of open-cell polyurethane foam is wrapped around the shade section for additional insulation. The complete assembly is then housed in a double evacuated dewar* with flexible copper thermal links extending down into the LN_2 dewar reservoir. A removable hatch cover is located over the sensor entrance aperture to seal the system completely during cooldown or when it is not in use. A schematic of the cooling plumbing and insulation is shown in Fig. 2-23.

2.6 FROST FOG PREVENTION SYSTEM

The exposure of cold optical elements to the balloon launch and flight environment can cause potential problems of condensation on the optics and the formation of fog within the FOV. The adopted concept employs a cold "dry"-gas stream to maintain the front optical element and the occulting baffle near the necessary 77° K and a secondary warm dry-gas stream to mix with and warm the cold stream to ambient temperature before it is exposed to the wet exterior environment. The cold stream is introduced through peripheral jets immediately forward of the front optical element, and the warm stream is introduced at the forward end of the shade through jets and a 9-in. section of porous wall as indicated in Fig. 2-24. The outer section of the shade is flared to an angle of about 10 deg to place it beyond the direct FOV of the optical system.

A model of the system was fabricated and tested in the space simulation chamber at conditions simulating pressure conditions for altitudes from 45,000 to 100,000 ft. Although the ambient temperature used was about 300° K, instead of the flight condition of 220° K, the partial pressure of water was increased accordingly to provide similar dewpoint conditions. An external air cross flow was created with a fan blowing across the end of the flared section at a velocity of 8.3 ft/sec. Recommended flow rates of 0.6 lb/hr of cold jet GN_2 and 6.1 lb/hr each of warm jet and porous wall GN_2 were determined as required to maintain a frost- and fog-free system despite significant fluctuation in flow rates and environmental conditions.

---

*Minnesota Valley Engineering Company, Model HLSM, 130CT

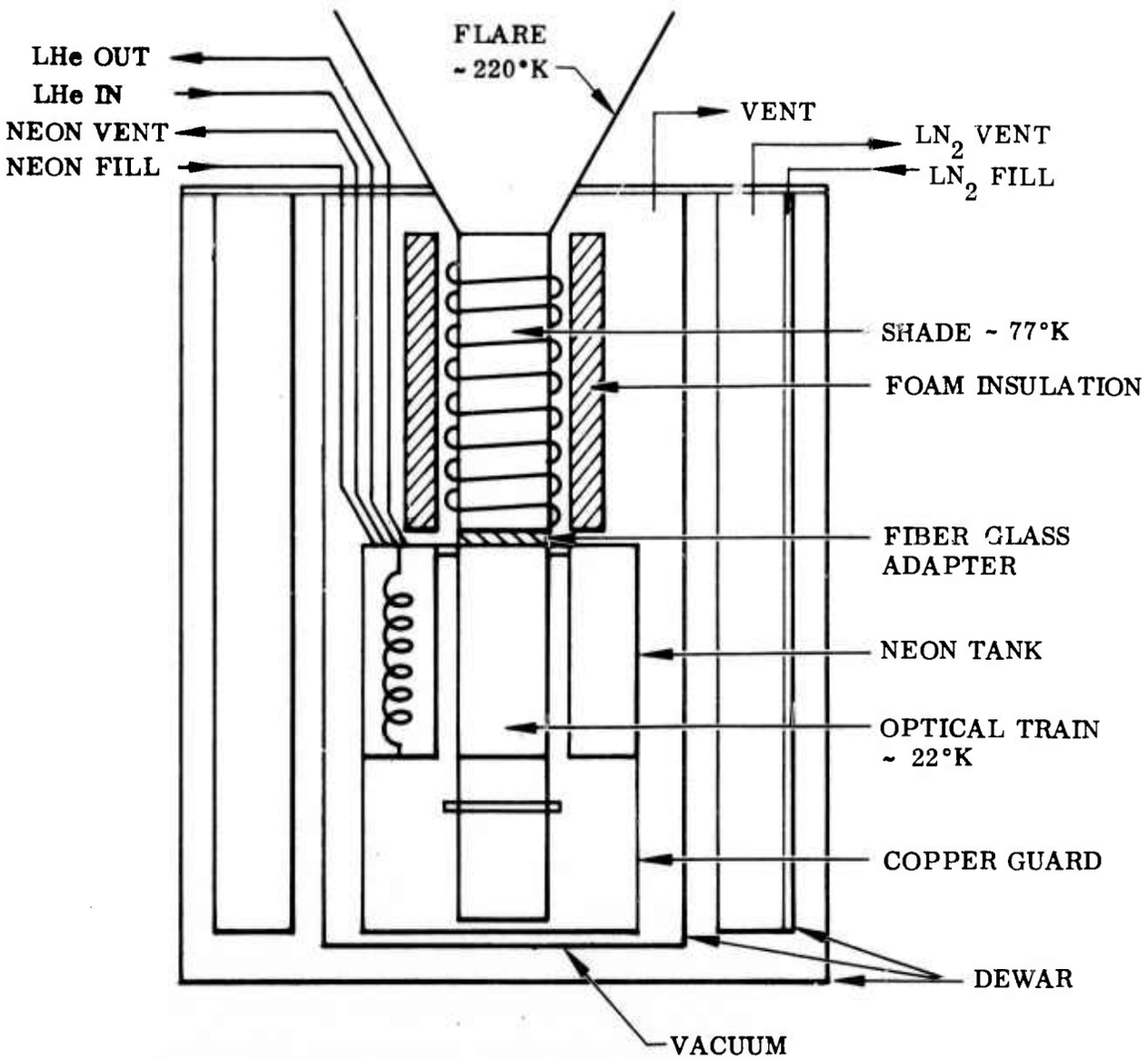

Fig. 2-23 Cooling System Plumbing and Thermal Protection

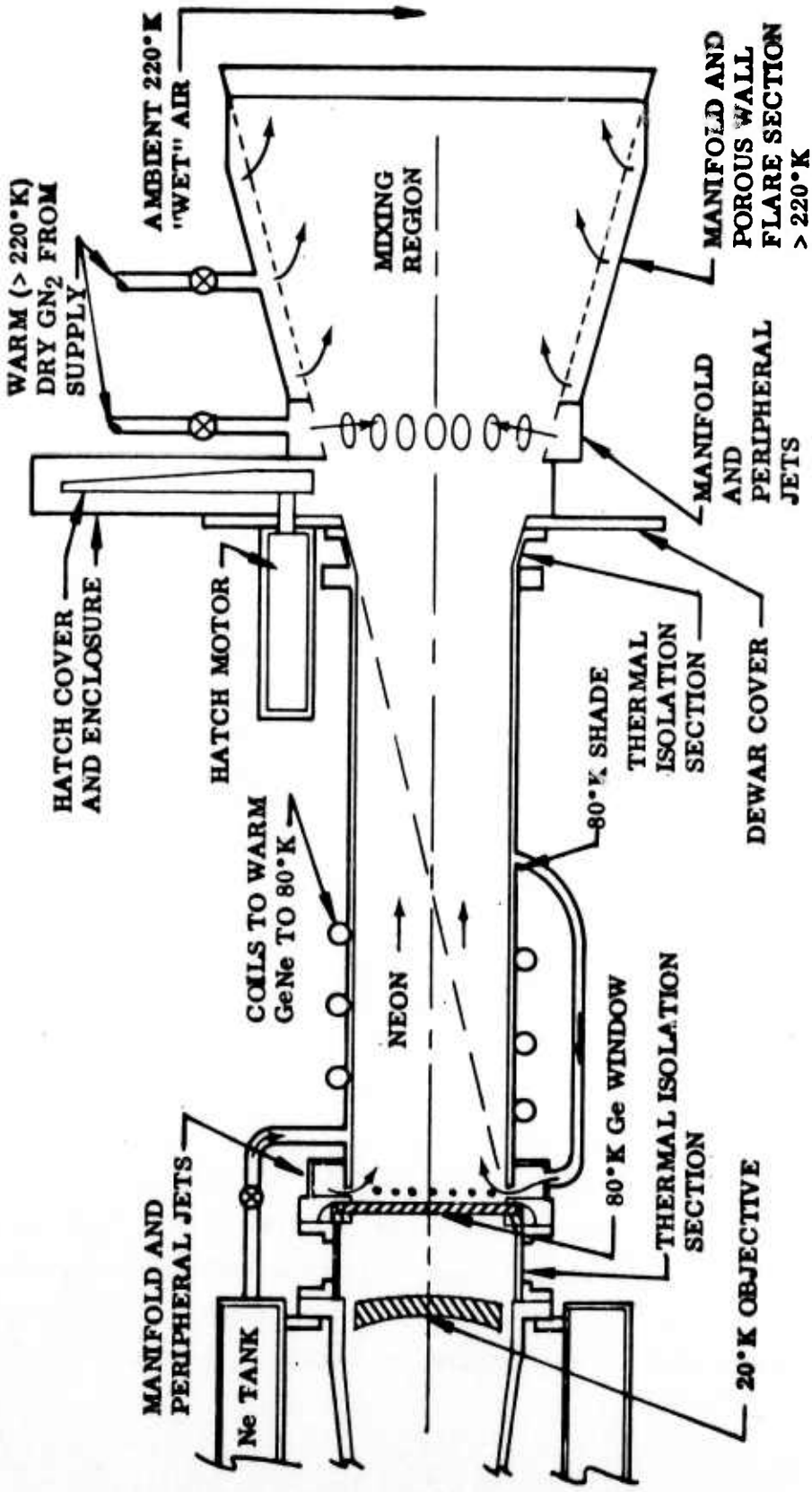

Fig. 2-24 Frost-Fog Prevention System – Schematic

The cold gas used to purge the shade area is available from the boiloff of the solid neon. The warm dry nitrogen is supplied from an onboard LN_2 supply which is vaporized and heated with the hot water system.

The germanium objective lens used as the first optical element is cooled to about 22° K and could condense oxygen or nitrogen on its exterior surface. A flat germanium window is therefore mounted at the aft end of the shade and cooled to the shade temperature to protect the cold optics. The window does not require an absolute vacuum seal because of the relatively small pressure differential.

Additional environmental and physical protection for the optical system is provided by a movable hatch cover before launch, during flight, and in the ascent phase. The 7.5-in.-diam. cover is lifted and rotated by a cam mechanism driven by a planetary-gear-reduced d-c motor.* Sequencing cams actuate microswitches automatically by means of the radiometer tilt mechanism for opening or closing of the hatch cover during ascent or descent and upon command for calibration. The inside surface of the hatch cover is anodized black (emittance = 0.85) to serve as a gray body calibration source when closed. A cross-sectional view of the hatch cover assembly and a list of the components are presented in Fig. 2-25.

The temperatures of the shade front and rear and the center of the hatch cover are monitored during flight with platinum resistance thermometers.

2.7 RADIOMETER FLIGHT PACKAGE

The radiometer/dewar assembly, electronics box, LN_2 storage vessel, and hot water tank are mounted on the flight gondola as shown in Fig. 2-26. The basic gondola platform (60 × 65 in.) has outriggers to support the command electronic package, tape recorders, electronic control panel, and a 28-V battery pack. The components are located to provide convenient integration and to balance the gondola for horizontal flight position.

---

*Type SS, 70-oz-in. torque (Globe Industries, Inc., Dayton, O.)

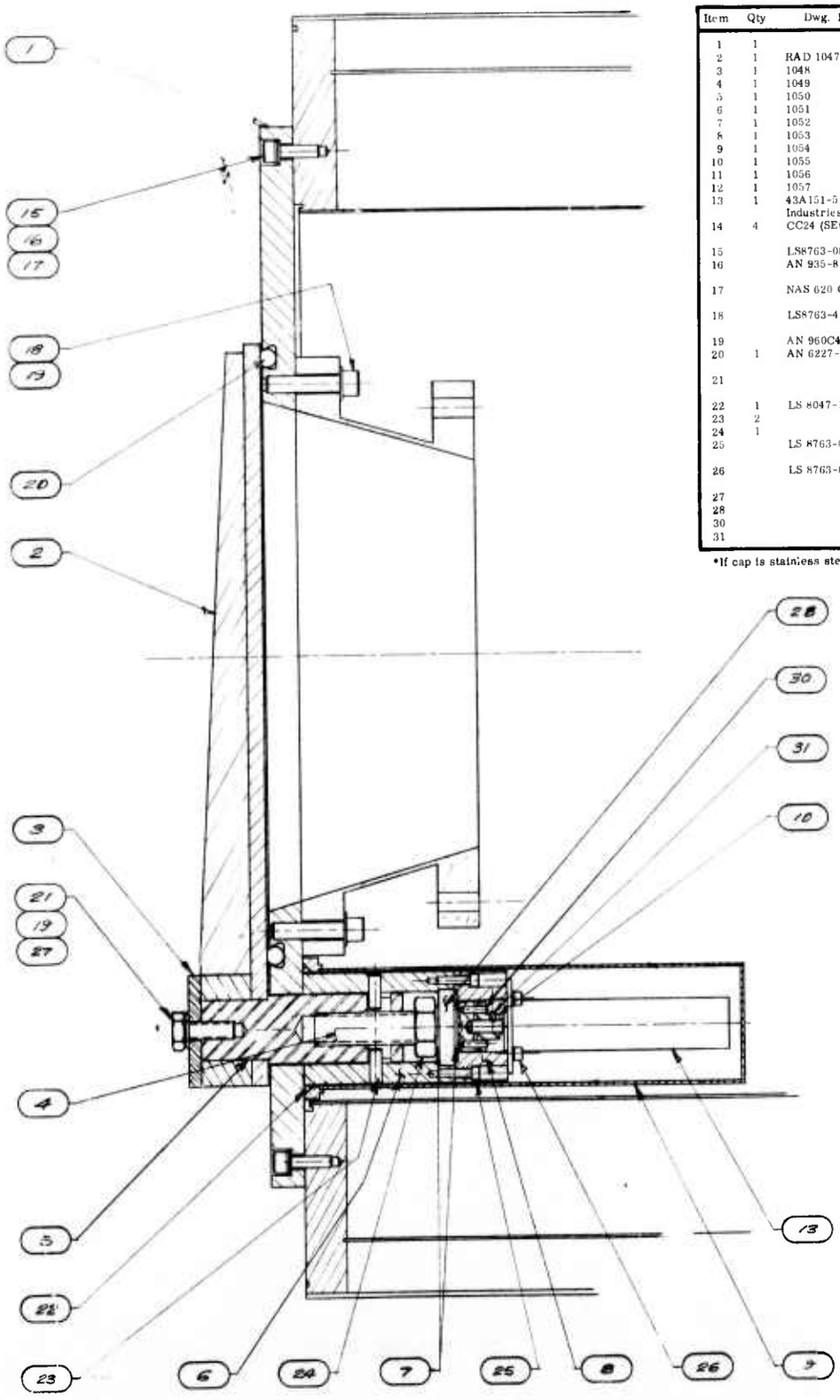

Item	Qty	Dwg. No.	Description
1	1		Mounting Plate
2	1	RAD 1047	Cover, Hatch
3	1	1048	Washer, Hatch
4	1	1049	Screw, Hatch
5	1	1050	Cam, Hatch Drive
6	1	1051	Bushing, Hatch Drive
7	1	1052	Spacer, Hatch Drive
8	1	1053	Motor-Mount, Hatch Drive
9	1	1054	Housing, Hatch Drive
10	1	1055	Coupling, Hatch Drive
11	1	1056	Bracket, Closure Switch
12	1	1057	Bracket, Closure Switch
13	1	43A151-5 (Globe Industries)	Type S5 Planetary Gear Reduced DC Motor
14	4	CC24 (SEGS)	Component Mounting Clamp (Alum.) Screw SOC HD Cap*
15		LS8763-08-10	8-32NF-3AX 5/8
16		AN 935-8L	Lock Washer, Spring Light Series (for No. 8 Screw)
17		NAS 620 C-8	Washer, Flat Reduced OD (for No. 8 Screw)
18		LS8763-4-16	Screw, 50 C HD Cap 1/4-28NF-3AX 1
19		AN 960C416L	Washer, Flat (for 1/4 screw)
20	1	AN 6227-73	O-Ring Packing (0.475 ID × 0.275 In.)*
21			Screw, HEX Hd 1/4-28NF-3A × 3/4
22	1	LS 8047-130	O-Ring (1.613 ID × 0.103W)
23	2		Pin (0.18801D × 0.500), Hardened
24	1		Nut, 1/2 13 NC
25		LS 8763-04-8	Screw, SOC Hd Cap, 4-40 NC - 3A - 1/2
26		LS 8763-04-6	Screw, SOC Hd Cap 4-40 NC - 3A - 3/8
27			Washer (for 1/4 screw)
28			Bushing Seat
30			Aligning Pin
31			Set Screw

*If cap is stainless steel, P/N is CE20.

SECTION A-A

Fig. 2-25 Hatch-Cover Assembly and Components List

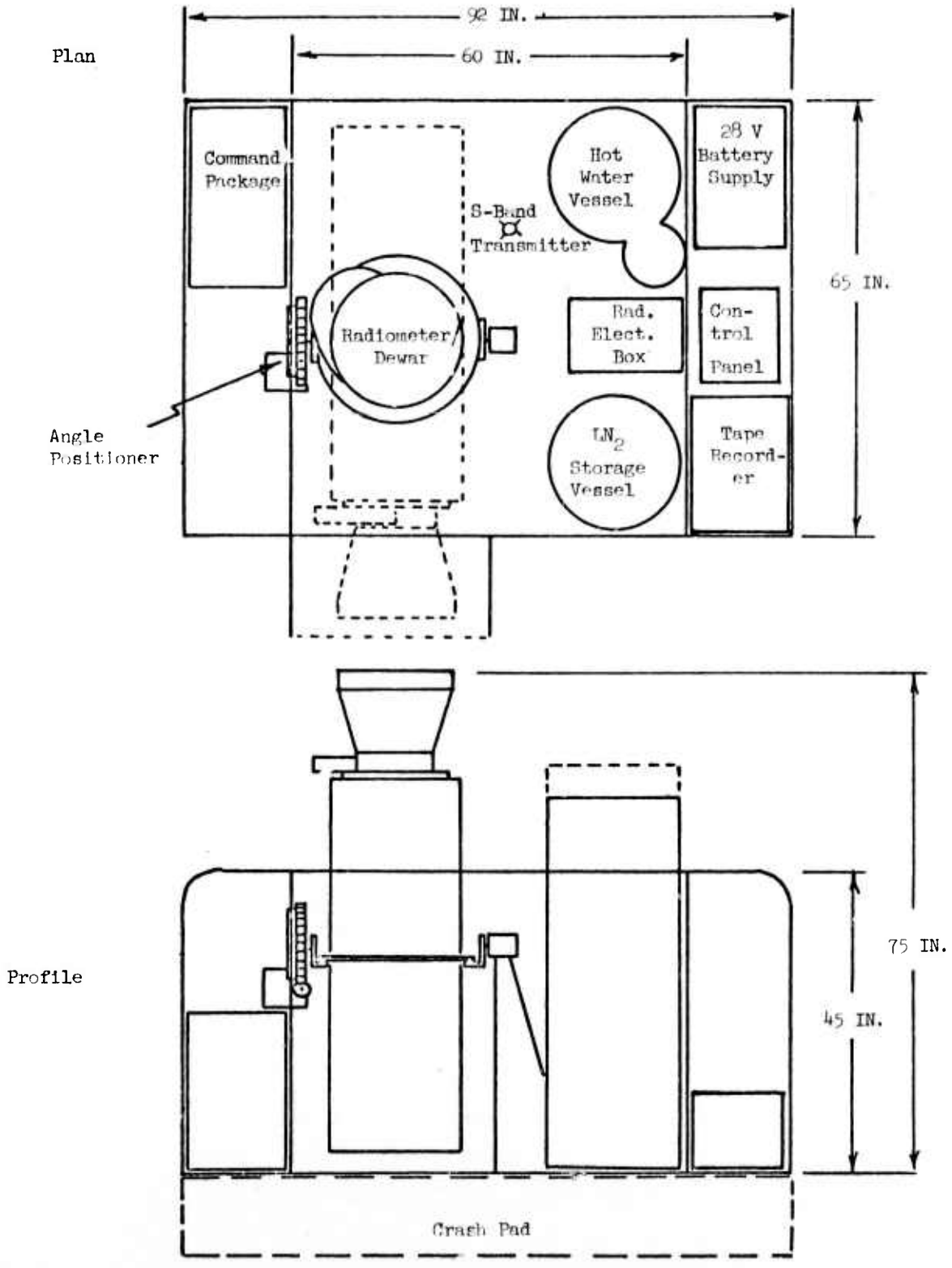

Fig. 2-26 Location and Profile of the Radiometer Flight Package

The radiometer dewar is oriented in a vertical position at launch. The worm-gear-driven gimbal system supports and positions the radiometer optical axis to each of seven successive angles upon ground command. The radiometer dewar is mounted near its center of gravity for ease of rotation. When fully rotated to the horizontal position, the overhanging portion is protected by an extended guard railing.

The power to both the elevation angle positioner and the hatch cover is turned on before reaching float elevation by ground command and backed up with an aneroid switch. The electrical interconnections for the main instrumentation and power circuits are shown in Fig. 2-27.

A 14-channel tape recorder* is used as the primary onboard instrument. Frequency-modulated telemetry (0 to 5 Vdc) is available, using both S-band (2250 MHz) and P-band (240 MHz). Two flux-gate magnetometers are installed on the gondola to provide azimuth position during the flight. A central control panel, provided as part of the gondola, electrically integrates the radiometer with the power supply, tape recorder, the AFCRL-supplied command package, and the telemetry. The control panel is used for preflight checkout of each measurement channel. A breakdown of the electrical power requirements of various parts of the system is shown in Table 2-3. A list of the major flight component and cryogen weights and the nominal gondola total weight is presented in Table 2-4.

*Precision Instruments Company, Long Island, New York, N.Y.

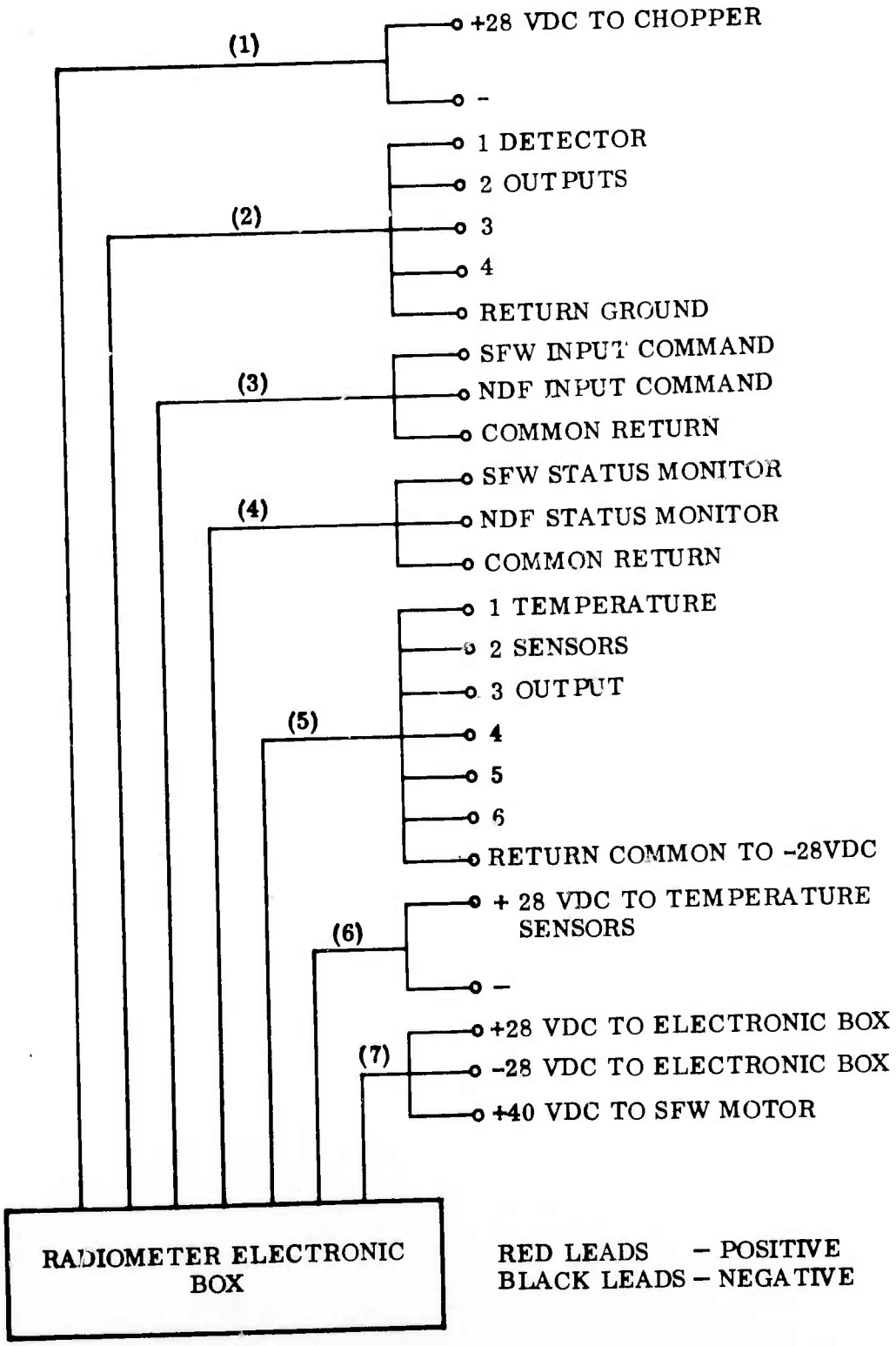

Fig. 2-27 Electrical Interface Between Radiometer and Gondola Control Panel

Table 2-3

POWER REQUIREMENTS FOR RADIOMETER EXPERIMENT

Item	Power (W)	Voltage (V)
Signal Electronics	10	
Phase-Adjust Circuitry	2	28
Temperature-Sensor Circuitry	6	
Chopper	Negligible	20
Spectral Filter Motor	4.5	40
Neutral Density Filter Motor	2.2	
Hatch Cover Drive Motor (5-W, max.) Intermittent, 20-Percent Duty Cycle	1	28
Subtotal	26	
Electronic Box Heater	56	28
Neon Container Heater	~ 5	28
Total	87	

Table 2-4

SUMMARY OF FLIGHT SYSTEM WEIGHTS

Component	Weight (Tare) (lb_m)	Normal Cryogens, Etc. (lb_{in})	Gross Weight (lb_m)
Radiometer/Dewar	420		
Liquid Neon (14 lb_m, max.)		14	
Liquid Nitrogen (59 lb_m, max.)		59	
LN_2 Storage Vessel	128		
Liquid Nitrogen (200-lb_m, max.)		100	
Water Tank	86		
Water (100-lb_m, max.)		75	
Electronics	40		
Subtotal	674	248	922
Gondola Weight[b]			248
Total[c]			1,170

(a) lb_m denotes weight just before lau
(b) Weighed 6 Jun 1971 (Second Flight)
(c) Includes all LMSC and Denver University hardware including two tape recorders, control panel, battery pack, crash pad, etc., but does not include AF equipment (i.e., ballast, command telemetry package, and parachute or balloon, etc.)

Section 3
RADIOMETER ASSEMBLY AND CALIBRATION

Assembly and calibration of the radiometer were conducted in several phases to provide an evaluation and data for the major components as well as the system. The detector array was calibrated in terms of frequency response, responsivity, and noise before integration with the optical system. The characteristics of the second optical focal plane were mapped to determine its exact position in the cold condition. Following installation of the detector array, the optoelectronic system was used to measure the field-of-view (FOV) and absolute responsivity of each detector, the optical transmission, and the noise equivalent flux density. Subsequent to these measurements, the radiometer was integrated with the flight control system, and further tests were conducted under simulated balloon flight conditions. These tests enabled recalibration of detector responsivity, using the hatch cover and verification of the performance of the frost-fog prevention system.

Additional field-of-view and system responsivity measurements were made 12 January 1971 at the Mark VII Infrared Test Facility of the Arnold Engineering Development Center. A complete system integration with the gondola at the University of Denver was performed before shipment of the apparatus to Holloman Air Force Base, New Mexico, for the first flight in February 1971.

Following the first flight, the radiometer was returned to LMSC for a postflight check and minor modifications; it was then prepared for the next flight in June 1971. Following the second flight, the radiometer was returned to LMSC and recalibrated.

3.1 OPTICAL SYSTEM EVALUATION

The optical system was evaluated with respect to spectral transmittance, out-of-field energy rejection, optical resolution, and focal plane mapping.

3.1.1 Optical System Spectral Transmittance

The total optical system includes the flat germanium window and four refractive lenses. The spectral transmittance was calculated from spectral absorptance data for the germanium (Ge) and TI 1173 [illegible]s and from specular transmittance measurements of witness blanks simultaneously [illegible]oated with the antireflection surfaces on the actual optical elements. The predicted spectral transmittance for the 8 to 13 μm wavelength range is shown in Fig. 3-1. From 8 to 11 μm, a transmittance of about 80 percent is achieved, but absorption by both Ge and TI-1173 resulted in a decrease down to 20 percent at 13 μm for the lense thicknesses used.

Spectral measurements of the cold optical system were made, using an extended black body, 0.1 μm band pass filters at 1.0 μm wavelength intervals, and the detector array as the sensing element. The measured spectral transmittance, also plotted on Fig. 3-1, exhibits the same spectral features as the predicted curve but is only about half the predicted value. The unknown angular transmission characteristics of the lense coatings, diffraction, scattering, alignment, and chopping efficiency could all contribute to the loss actually measured.

3.1.2 Out-of-Field Energy Rejection

The inherently good out-of-field energy rejection capability of the system required abnormally large distances during evaluation to minimize the reflection and scattering from surrounding walls. It was not possible, therefore, to perform these measurements with the system cold in the vacuum chamber.

The room temperature test was performed without the occulting shade, and a thermistor bolometer replaced the detector array. The optical apparatus and arrangement are shown in Fig. 3-2. The 0.254-cm diameter beam of a 3-W unpolarized CO_2 laser was expanded with a convex mirror to appear as a point source when viewed by the sensor. Neutral density filters were used to increase the dynamic range of the detector synchronous-amplifier (80 Hz) measurement system. The detector was mounted on a three-axis

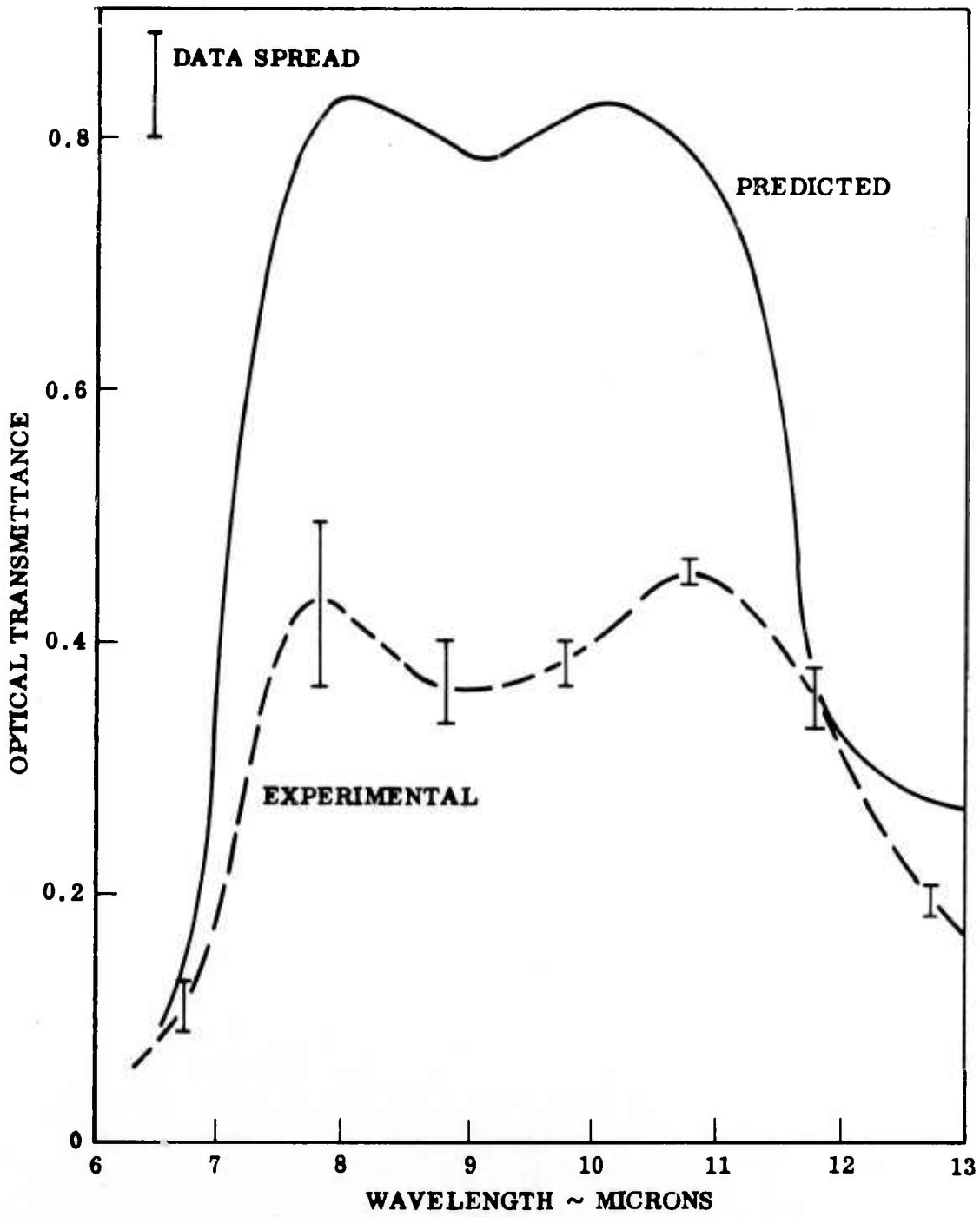

Fig. 3-1 Predicted and Measured Optical System Spectral Transmittance

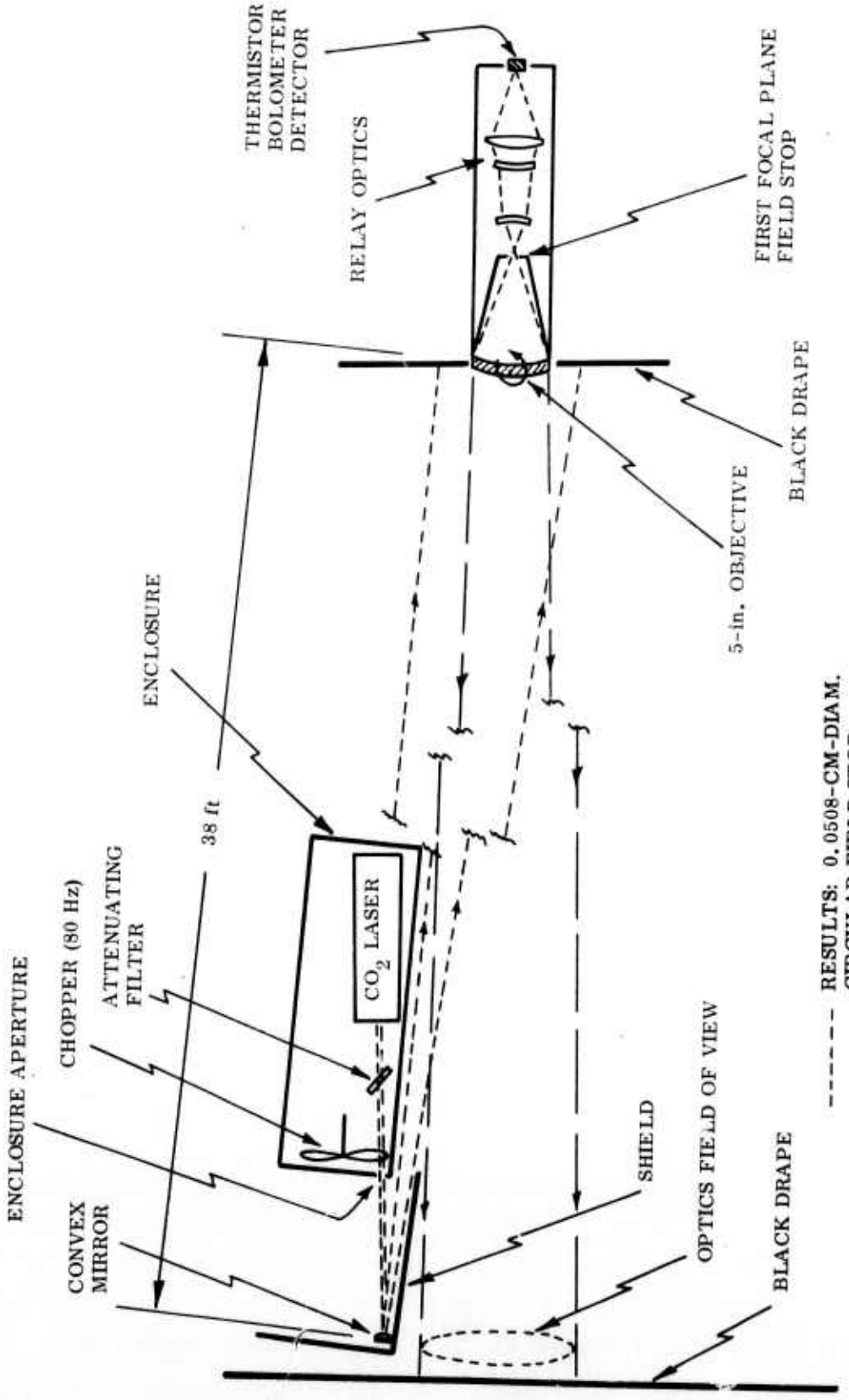

Fig. 3-2 Arrangement for Out-of-Field Energy Rejection Measurements

servo-controlled and digital-counter monitored traverse system to position the detector within 0.025 mm in each axis.

The measurements were made by rotating the optics-detector system about the front objective lens. Three different field stop configurations were used during these measurements, as follows:

- 0.0508-cm-diam. (0.11-deg FOV) circular
- 3.175 × 0.0508-cm (7-deg × 0.11-deg FOV) rectangle
- 3.175-cm-diam. (7-deg FOV) circular

Several cases for each configuration were measured with the detector at the center or the edge of the FOV and with two orientations of the rectangularly-shaped field stop. Typical plots of normalized response versus angle are shown in Figs. 3-3 and 3-4 which compare horizontal and vertical rectangularly-shaped field stops. As a comparison, the results for the 0.508-cm-diam. circular field stop are shown as dashed lines on Figs. 3-3 and 3-4.

A summary of the rejection measurements for the double-focused refractive optical system is presented in Table 3-1. Considering that rejection of energy relative to the edge of the instrument FOV is most significant, conservative rejection values of 8×10^6 at 0.25 deg, 10^6 at 0.5 deg, 2.5×10^7 at 1 deg, and 10^8 at 5 deg are indicated.

3.1.3 Optical Resolution Measurements

The diffraction limit for the refractive optical system at 10 μm is 0.2 mr, and state-of-the-art optical systems can achieve the limit within a factor of 2. Measurements of the optical system were made with the optics cooled with liquid nitrogen to about 84° K. A single detector with a 10-μ-diam. aperture mounted directly in front of it was located at the second focal plane and attached to the three-axis traverse mechanism. An 870° K blackbody with a 0.015-cm-diam. aperture was used as the source for a 20.3-cm-diam., 101-cm focal length, off-axis, parabolic mirror. The collimating system was mounted, as schematically shown in Fig. 3-5, on a two-axis rotary table in a vacuum chamber.

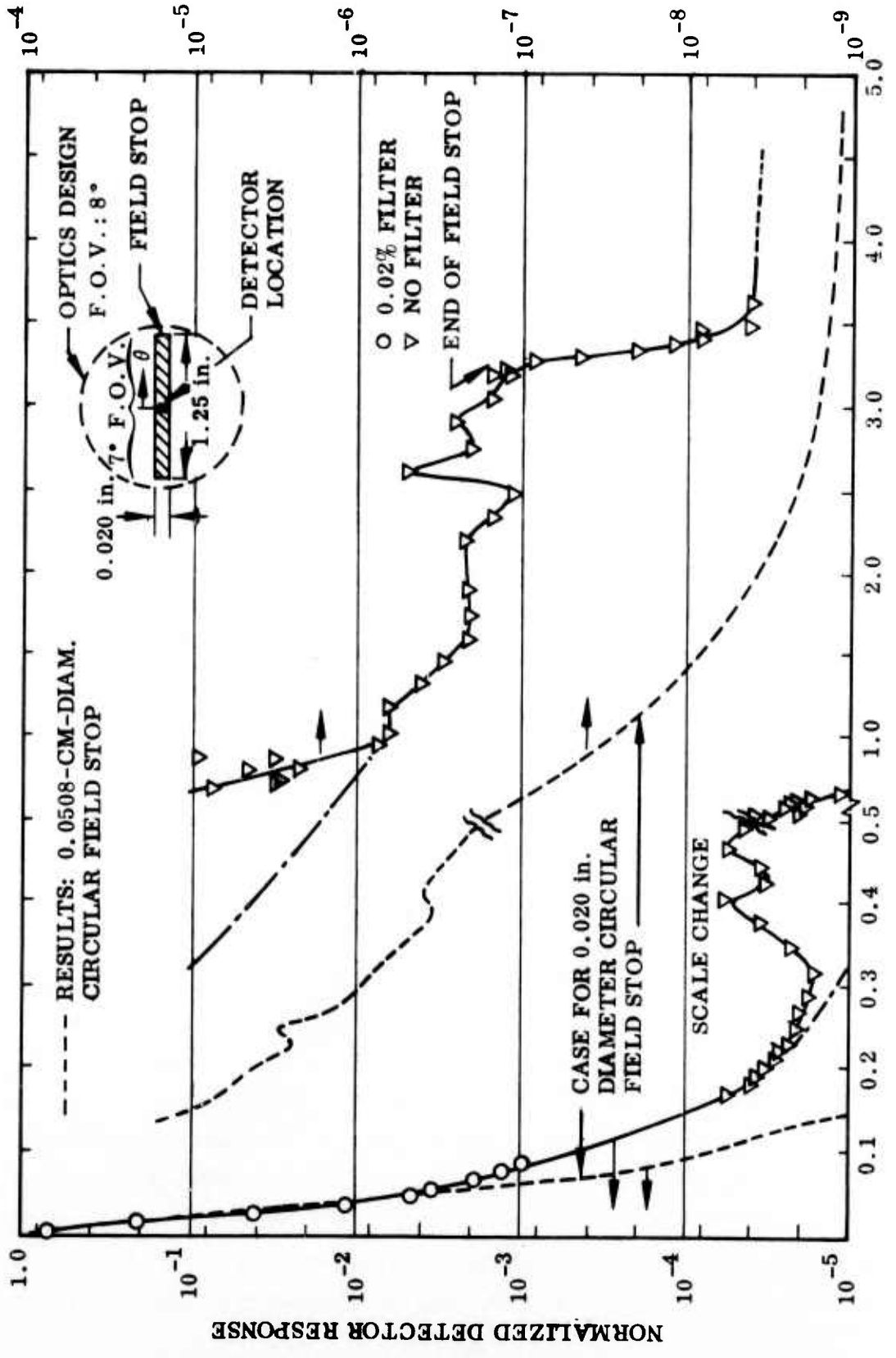

Fig. 3-3 Normalized Detector Response As a Function of Out-of-Field Radiation for a Horizontal Rectangular Field Stop

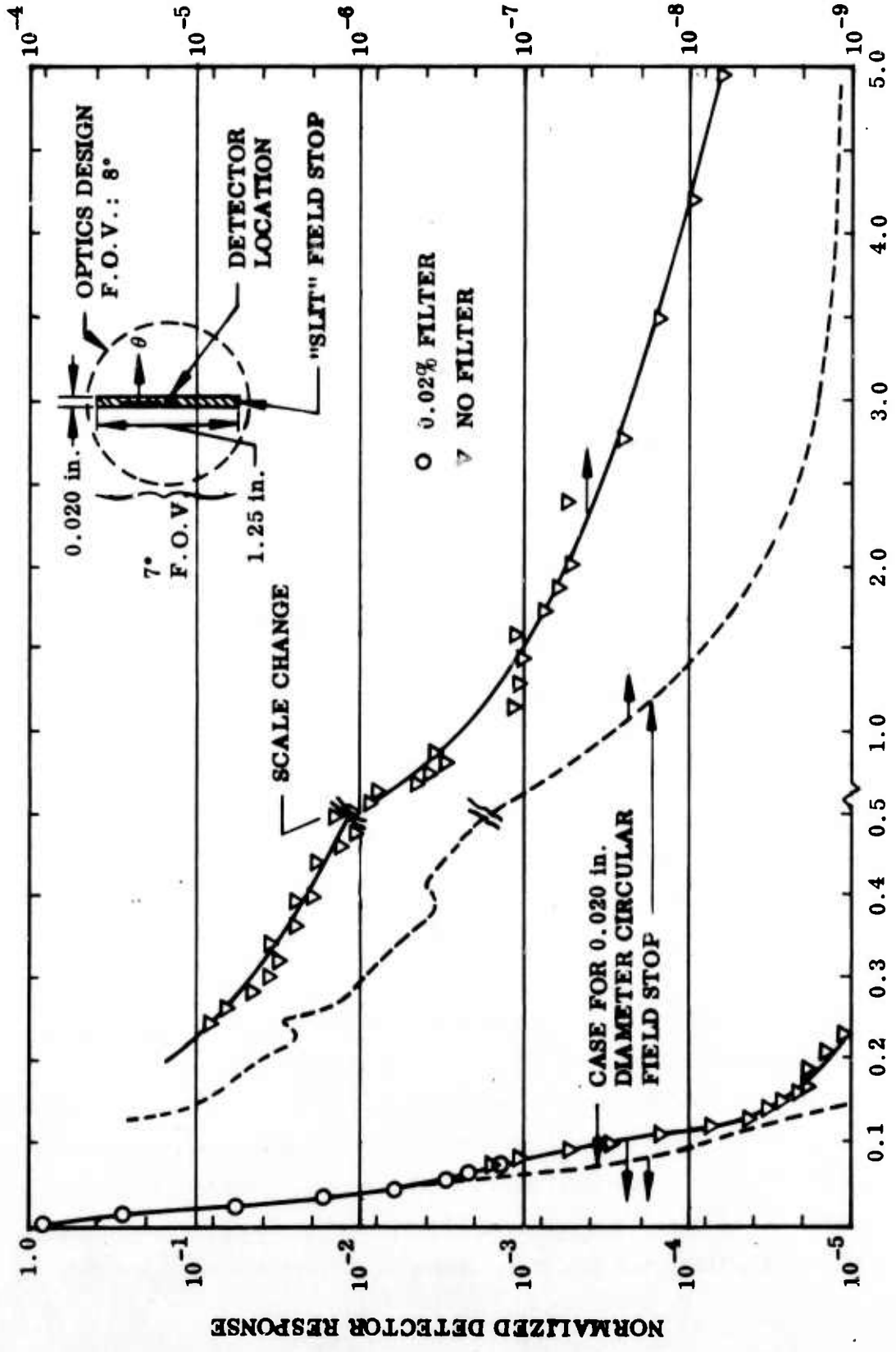

Fig. 3-4 Normalized Detector Response As a Function of Field Radiation for a Vertical Rectangular Field Stop

Table 3-1

SUMMARY OF OUT-OF-FIELD ENERGY REJECTION MEASUREMENTS

Field Stop Configuration and Detector Location	Energy Rejection (deg)			
	0.25	0.5	1	6
0.02-In.-Diam. Detector at Center	2×10^6	2×10^7	3×10^8	$\sim 10^9$
Rectangular Slit Detector at Center Source, Perpendicular to Slit	8×10^6	10^6	2.5×10^7	7×10^9
Rectangular Slit Detector at Slit End Source Along Slit	3×10^6	3×10^7	8×10^3	4×10^9
7-Deg FOV Circle Detector at Center Source Extending Radially Outward	5×10^5		10^6	10^8
Rectangular Slit Detector at Center Source, Along Slit	2×10^5		7×10^7	4×10^9

Measurements of the detector response were made for the following three locations within the 8-deg field-of-view:

- Approximately on axis
- 1.7 deg off axis
- 3.4 deg off axis

The source was located at each of these positions with the rotary table and the detector initially located at the corresponding point in the focal plane with the three-axis traverse. Profile measurements were taken by traversing the detector in the x, y, and z directions as indicated in Figs. 3-6 and 3-7. From these data, the deviation from the diffraction limited case was determined by a comparison of the effective image diameter to that of an Airy disc diameter (containing 84 percent of the energy). The energy distribution for each of the sets of x and y traverses was integrated with respect to their respective

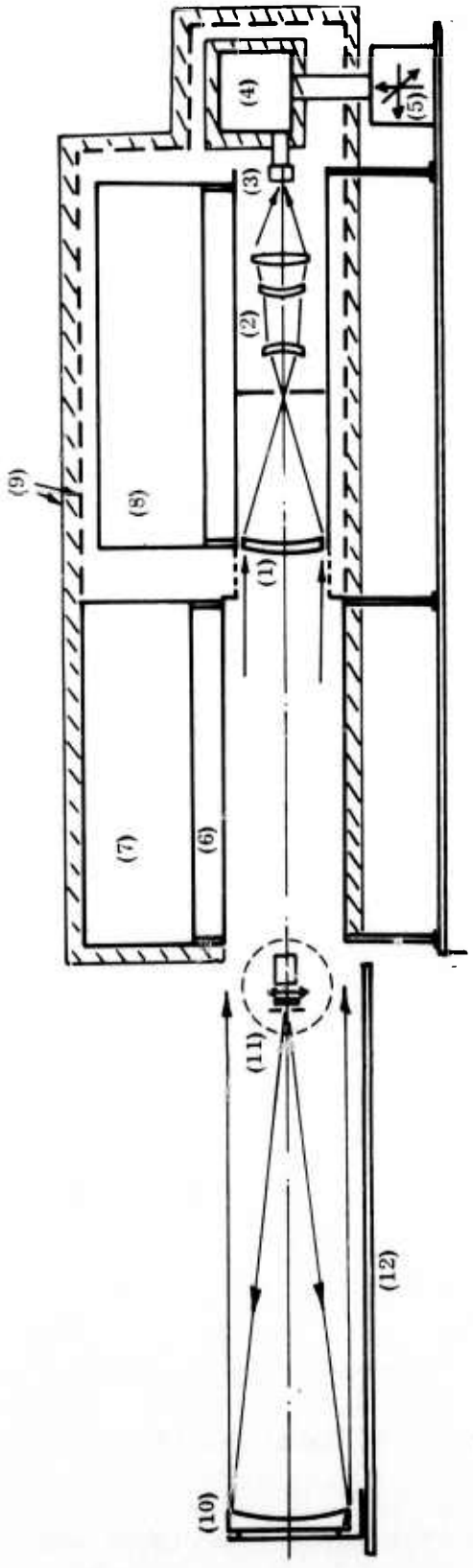

1. 5-in.-diam Ge lens (10-in. focal length)
2. Relay optics
3. GeHg Det. (with 10-μ aperture)
4. LHe for detector cooling
5. Three-axis traverse for detector
6. Shade
7. LN_2 for shade cooling
8. LN_2 for optics cooling
9. Shield and insulation
10. 8-in., 40-in. focal length off-axis collimating mirror
11. Aperture (6 mil), filter (8 to 13 μ), chopper and blackbody assembly
12. Collimator two-axis rotary table

Fig. 3-5 Experimental Setup for Optical Resolution Measurements

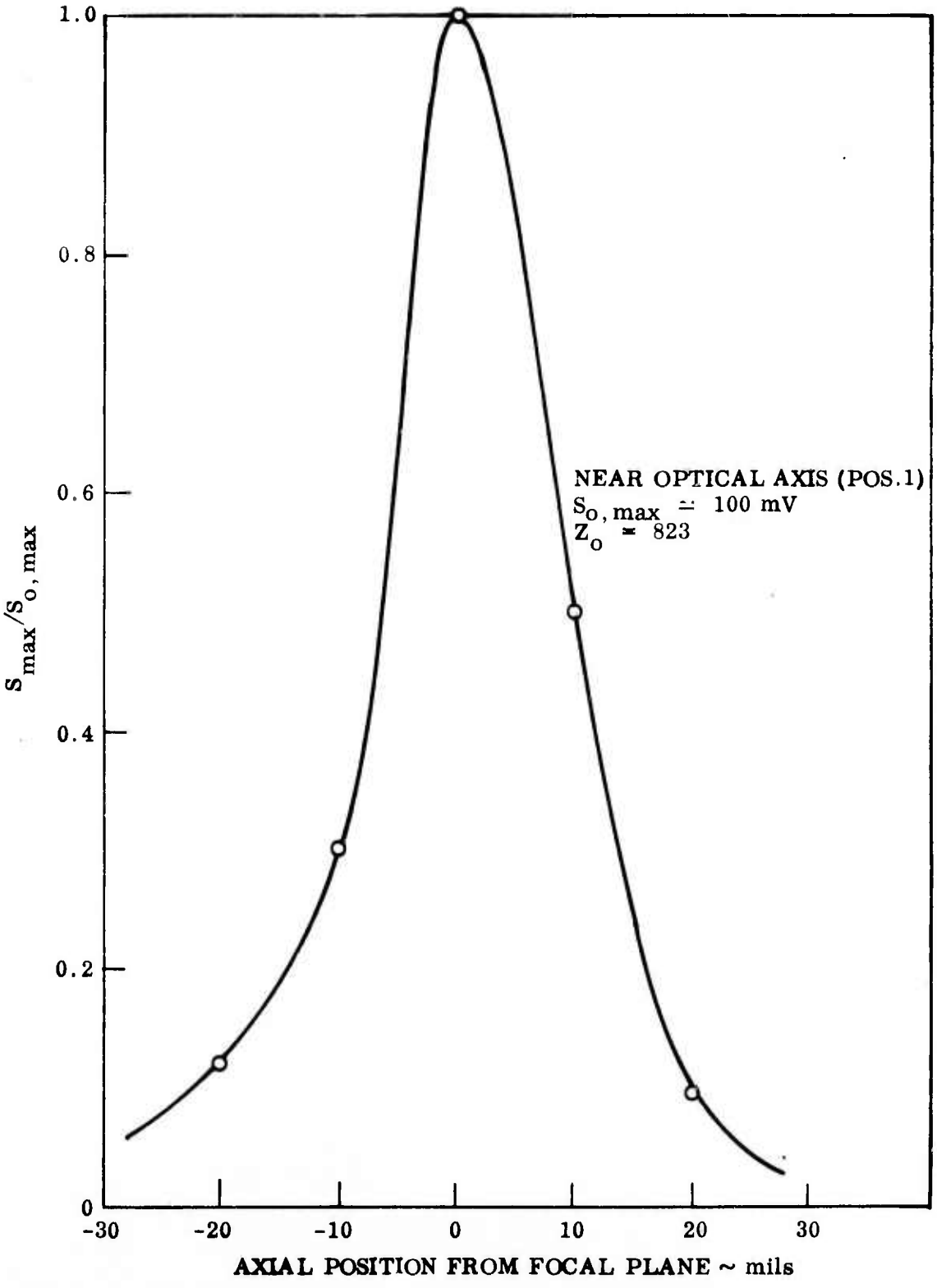

Fig. 3-6 Normalized Peak Signal Along Optical Axis

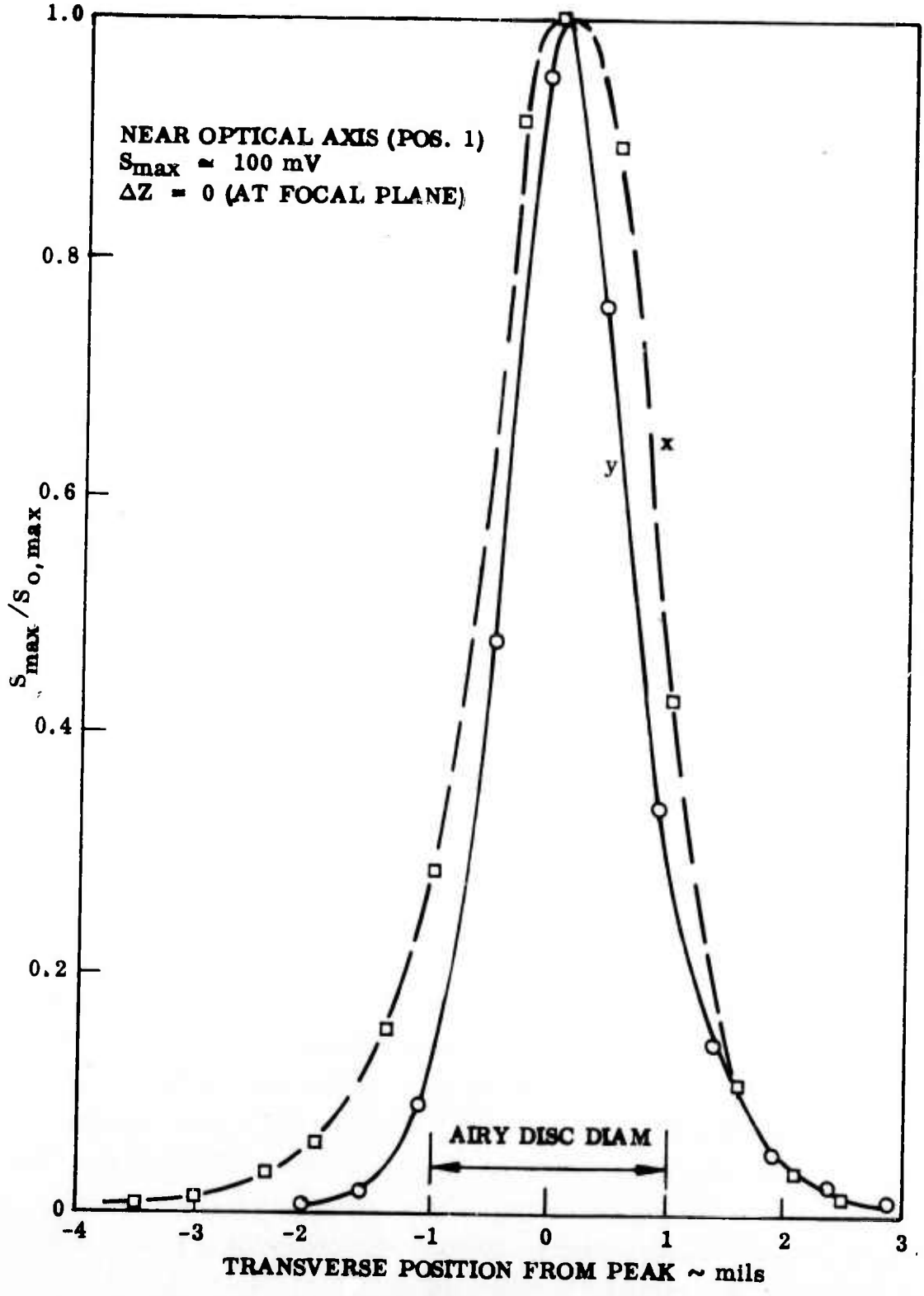

Fig. 3-7 Normalized Signal Response As a Function of Vertical and Horizontal Directions in Focal Plane

radii, and an effective radius containing 84 percent of the energy was determined. The results of this analysis in terms of multiples of the diffraction limit for the three FOV locations are shown in Table 3-2. The values shown in Table 3-2 can be further modified because the source used subtends an angle of 0.15 mr (3/4 of the diffraction limit) and for radiation near the outer edge of the field the system, is about 1.5 times the diffraction limit.

Table 3-2
OPTICAL RESOLUTION AS A FUNCTION OF OFF-AXIS RADIATION

Location in Field	Multiples of Diffraction Limit
On Optical Axis	1.7
1.7 deg Off Optical Axis	1.9
3.4 deg Off Optical Axis	2.3

3.1.4 Focal Plane Mapping

The image of the first focal plane field stop was mapped in the second focal plane to determine the location of the detector array. As shown previously in Fig. 2-13, the field stop is similar in configuration to the detector array but about 0.02 cm larger in each dimension to keep from masking the FOV.

The mapping was performed with the radiometer cold (nominal 20° K) and mounted in a vacuum chamber. At 870° K blackbody with a 0.8-mm-diam. aperture was located at the focal point of the 20-cm-diam., 101-cm focal length, off-axis collimator. The thermistor bolometer mounted on the three-axis traverse was scanned in steps along the optical axis in both the horizontal and vertical directions. The bolometer location was referenced to the optical barrel by two referencing systems located on the side of the detector mount. The four-element detector was mechanically located at the center of the optical axis as determined by this mapping.

3.1.5 Angular Response

The system angular response measurements were performed with an externally chopped source in a warm vacuum chamber. The detector signals were amplified with a synchonously rectified lock-in amplifier* to provide a dynamic range of four. The response of each detector as a function of elevation scan angle β is shown in Fig. 3-8 for detectors 1 and 2 and Fig. 3-9 for detectors 3 and 4. The responses for azimuth scan angle α are shown in Fig. 3-10. The effective solid angles for each detector in milliradians and the solid angle in steradians are presented in Table 3-3.

Table 3-3
DETECTOR ARRAY EFFECTIVE SOLID ANGLE

Detector No.	$\Delta\alpha$ (mr)	$\Delta\beta$ (mr)	Ω_{eff} (sr $\times 10^{-6}$)
1	2.23	1.97	4.39
2	2.18	2.01	4.38
3	1.36	1.06	1.44
4	1.26	1.15	1.45

3.2 RADIOMETRIC TRANSFER FUNCTION

Normalized transfer function relationships were established for each detector to simplify the calculation of radiometric quantities because of the nonlinear response of the electro-optical system. Assuming a relationship of

$$P = \text{const} \times V + P_o$$

*Model HR-8, Princeton Applied Research, Cambridge, Mass.

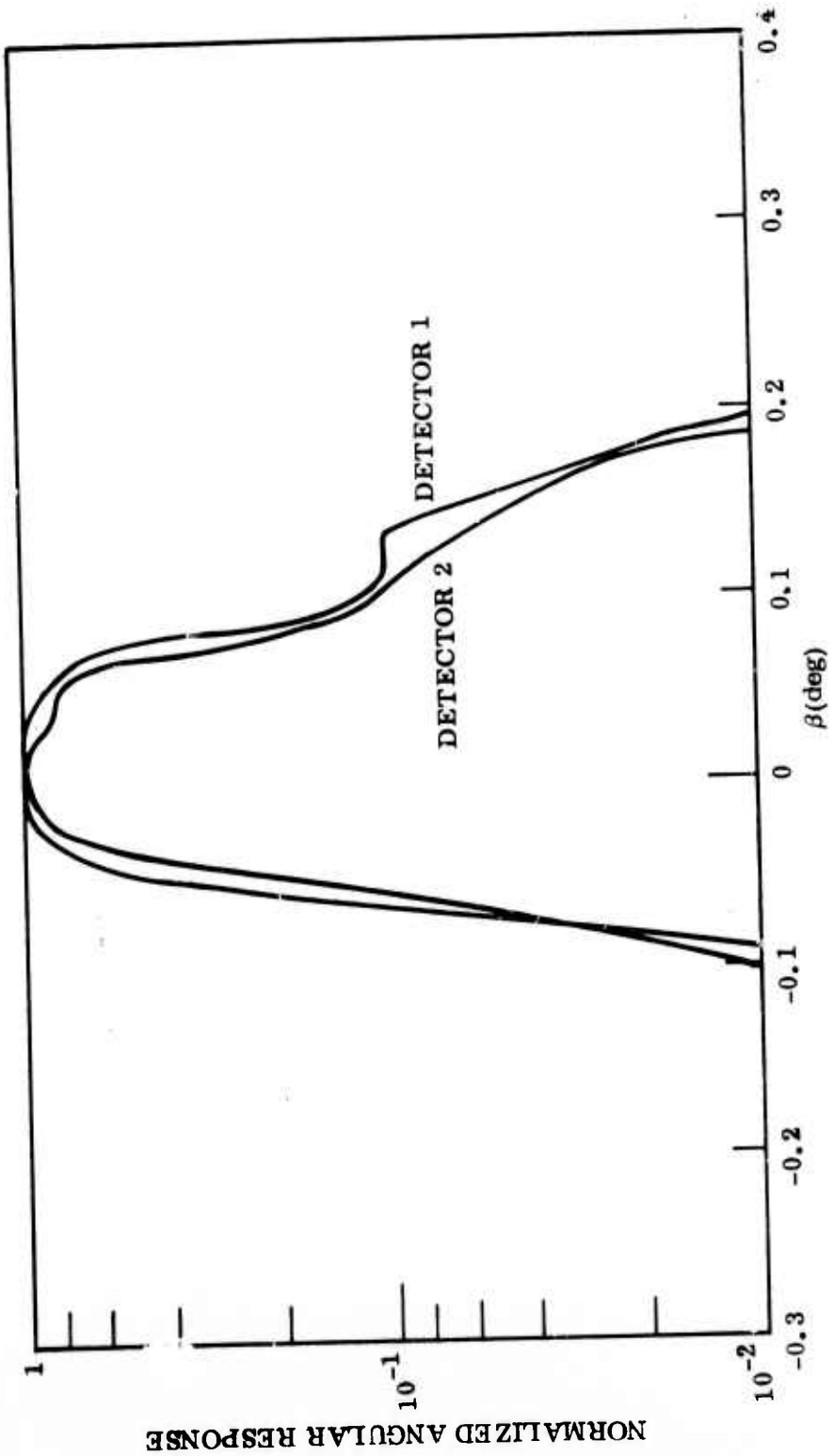

Fig. 3-8 Normalized Angular Response for Elevation Scan of Detectors 1 and 2

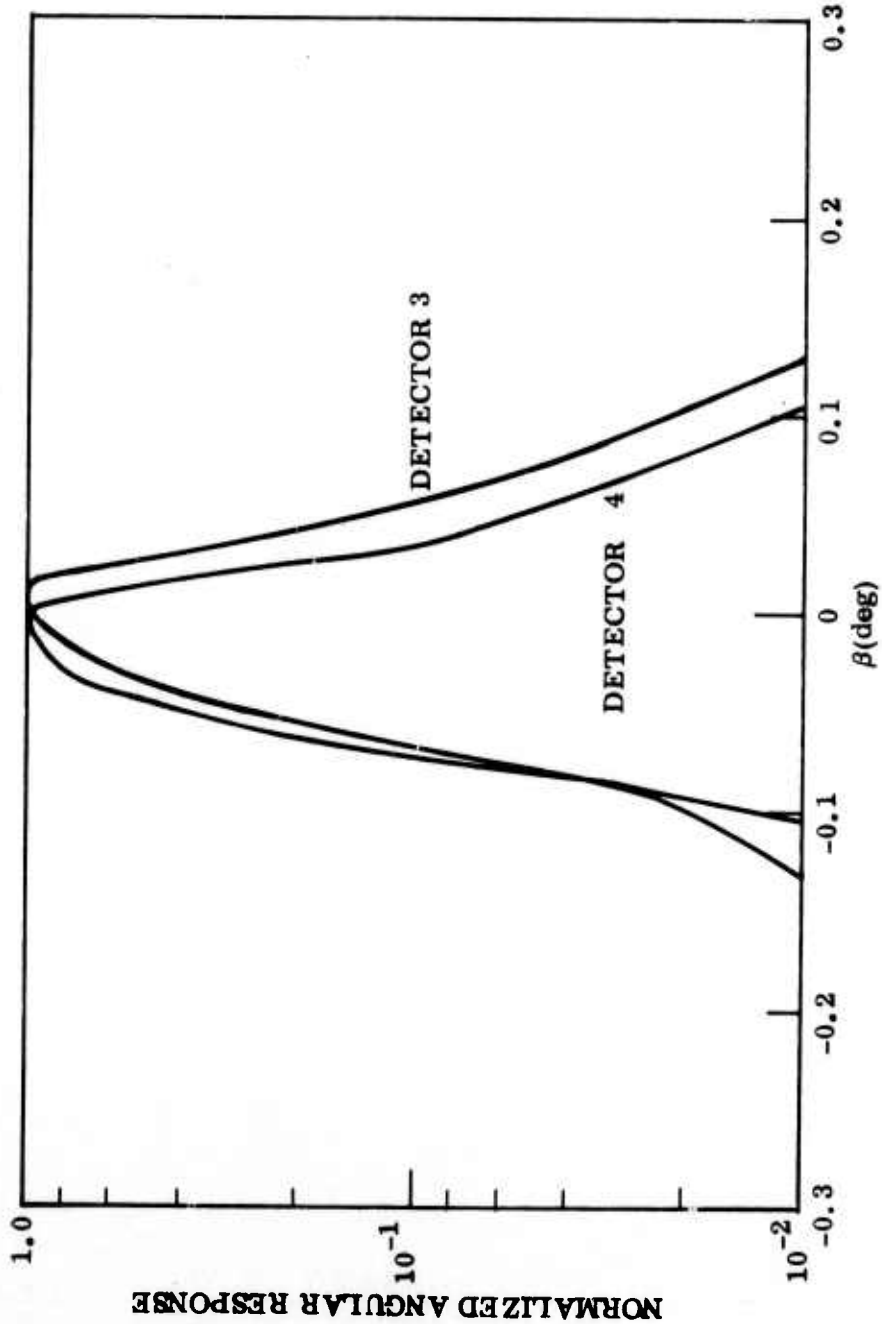

Fig. 3-9 Normalized Angular Response for Elevation Scan of Detectors 3 and 4

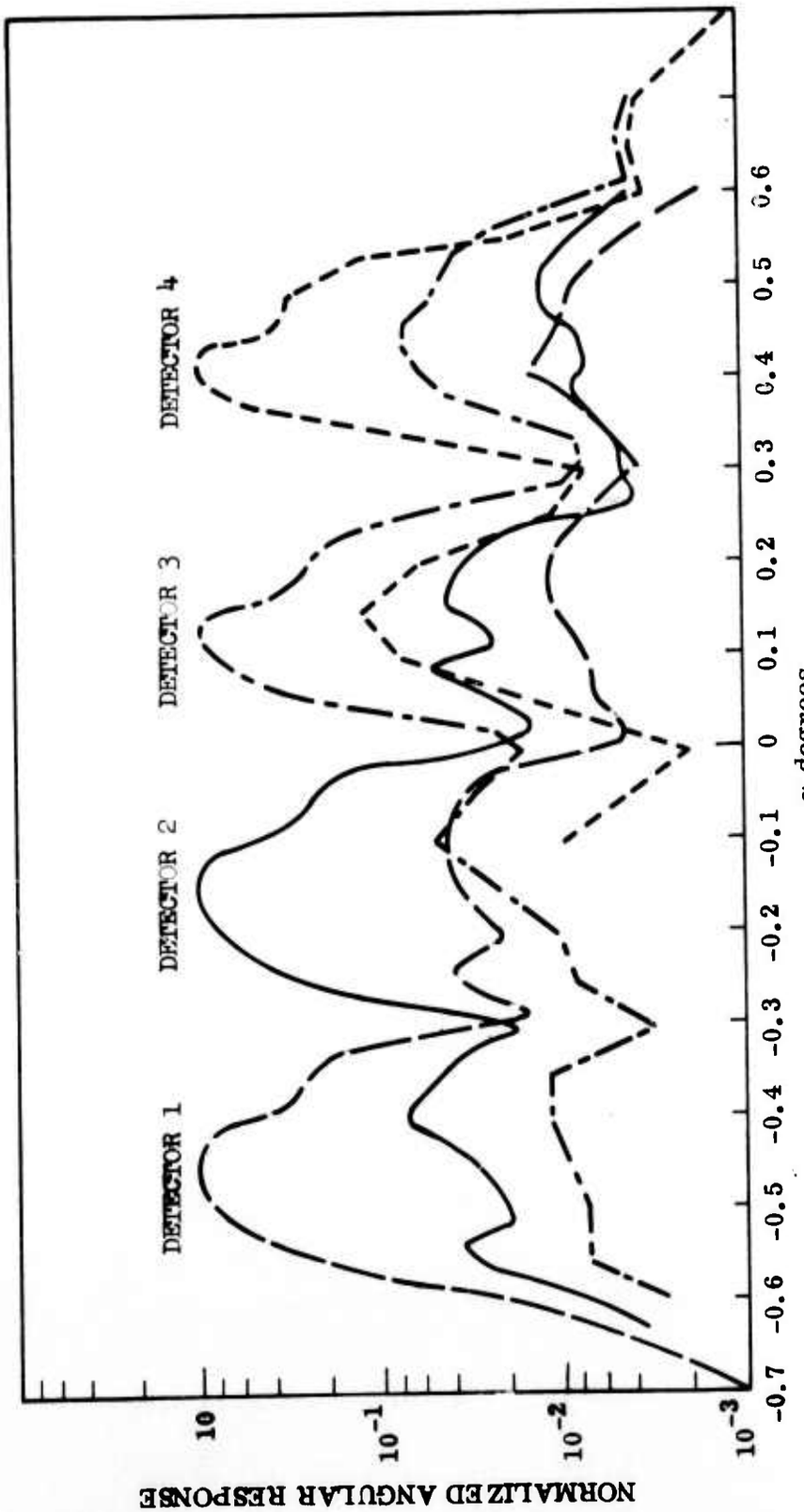

Fig. 3-10 Normalized Angular Response For Azimuth Scan for Each Detector

where

P = incident radiant power

V = output voltage

P_o = radiant power when output voltage is zero

then it is convenient to introduce a quantity $f(V)$ so that $P = \text{const} \times f(V)$ to provide a linear data reduction form. Curves of $f(V)$ normalized to a maximum 5-V output signal, which were used for reduction of the flight data, are plotted in Fig. 3-11. The data plotted in Fig. 3-11 were obtained subsequent to the second flight in June 1971,

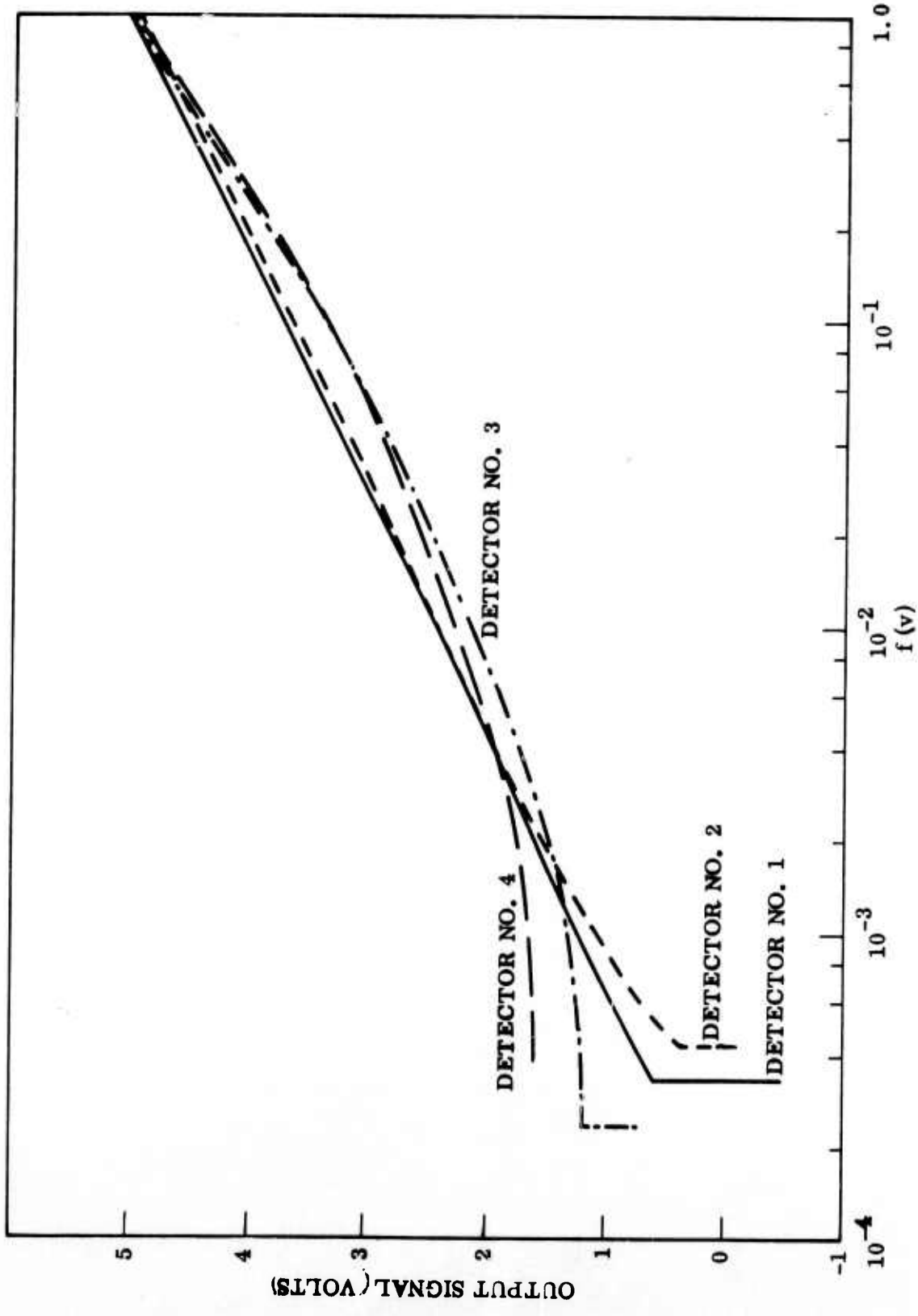

Fig. 3-11 Normalized Transfer Function f(V) Vs. Output Signal for Each Detector

Section 4
FLIGHT HISTORY

Two balloon-borne measurement tests were conducted at Holloman, New Mexico in February and June 1971. In the February flight, the instrument was flown with four spectral filters; however, new data were essentially not obtained because the tape recorder failed at launch and only partial telemetry coverage occurred.

Before the second flight, several minor modifications to the instrument were made, including locking the spectral filter wheel at one position, adding a back-up tape recorder, and including a P-band telemetry capability. A discussion of the second flight is presented in Ref. 3, and a summary of the data is provided in Section A. 3 of the Appendix. Radiance data were obtained between -5 and 15 deg from horizontal in the spectral band from 10.5 to 12.75 μm. The instrument performance was limited at the low and high end of the dynamic range by noise and saturation, and a more reliable positioning device for the filter wheels was indicated as a desirable modification before undertaking additional flight tests.

Following the second flight, the radiometer was returned to LMSC for recalibration.

Section 5
CONCLUSIONS AND RECOMMENDATIONS

A cryogenically cooled refractive radiometric instrument was constructed and evaluated in laboratory tests and flown on two flight tests at a 90,000-ft-altitude. Flight data were obtained on the second flight, but the electronic and electromechanical operation limited the sensitivity and spectral range. Optical performance was demonstrated to meet design expectations.

Evaluation of major system components, optical/detector alignment and system calibration all required state-of-the-art developments for this unique LWIR system. In particular, remote mapping and the precise location of the first and second images with the system cold in a vacuum environment was a time-consuming and tedious task for a near-diffraction-limited optical system. The additional requirement for the optical elements and associated enclosures to be free of frost and fog during prelaunch, ascent, and at floating altitude complicated and added considerable bulk to the inherently trouble-free solid cryogenic cooling system. However, the cryogenic system has operated successfully for 9 hr during flight and up to 16 hr in simulated tests.

Additional laboratory and field experience with the instrument is required to realize the ultimate capability of the device. The following additions, modifications, and investigations are therefore recommended:

- Addition of three additional sync generator circuits to permit phase adjustment for each detector
- Modification of the signal amplifier circuit to eliminate signal dropout and provide operation over the full five-decade dynamic range
- Modification of the filter wheel drives to ensure reliable drive and positioning
- Fabrication of an attachable calibration source with provision for spectral calibration at ambient pressure and atmosphere

- Increase of the dynamic range versatility by adding a 0.2-percent neutral density filter
- Performance of an analysis of integrated system preflight operation (with telemetry) to determine absolute system noise, accuracy, and sensitivy
- Performance of an analysis of flight data to optimize measurement parameters – spectral range and bandpass; dynamic range and elevation angle; signal spatial variations, chopping frequency, and FOV

Section 6
REFERENCES

1. T. Condron, J. Sullivan, G. Vliet, and A. Funai, Balloon-Borne Radiometer, No. 1 Calibration Book, 1 Oct 1970

2. Lockheed Missiles & Space Company, Inc., IR Radiometer Experiment, First Data Report for Balloon Flight on Feb. 25, 1971, by G. C. Vliet, LMSC TP-3242, Sunnyvale, Calif., 5 May 1971

3. -----, IR Radiometer Experiment, Second Data Report for Balloon Flight of 8 June 1971, by G. C. Vliet, G. A. Bell, and E. R. Streed, LMSC TP-3310, Sunnyvale, Calif., 15 Nov 1971

Appendix A
DETAILED DESCRIPTION OF ELECTRONICS

A.1 GENERAL

A brief description of each electronic subsystem and the detailed schematic are presented in this appendix. The electronic circuits are packaged as plug-in circuit boards which are mounted in the main electronics box.

A.1.1 Signal Electronics – Diagram BR69122 - (3 sheets)

There are four signal electronics boards, one for each detector. The circuit processes the low-level modulated detector signal from the detector MOS-FET amplifier output and supplies a 0- to 5-V demodulated logarithmic signal to the telemetry.

A.1.1.1 Preamplifier – Diagram BR69122-1, Sheet 1 (Fig. A-1)

The preamplifier utilizes an integrated operational amplifier. The gain is stabilized with feedback, and a potentiometer allows it to be varied from 2 to 12. The frequency response is approximately 10 to 1,000 Hz. The equivalent input noise is 0.02 $\mu V \sqrt{Hz}$ at the 200-Hz chopping frequency. The 10-kΩ source resistor for the MOS-FET is included in this circuit.

A.1.1.2 Band-Pass Amplifier, Demodulator, Low-Pass Filter – Diagram BR69122-1, Sheet 2 (Fig. A-2)

The bandpass amplifier has a frequency response of 150 to 250 Hz and a gain of 3. It has a third-order Butterworth characteristic. The demodulator synchronously rectifies the signal at the 200-Hz chopping frequency, using FET switches. The output is filtered by a 40-Hz, second-order, active, Butterworth low-pass filter to remove the higher harmonics and noise. The output from this circuit ranges from

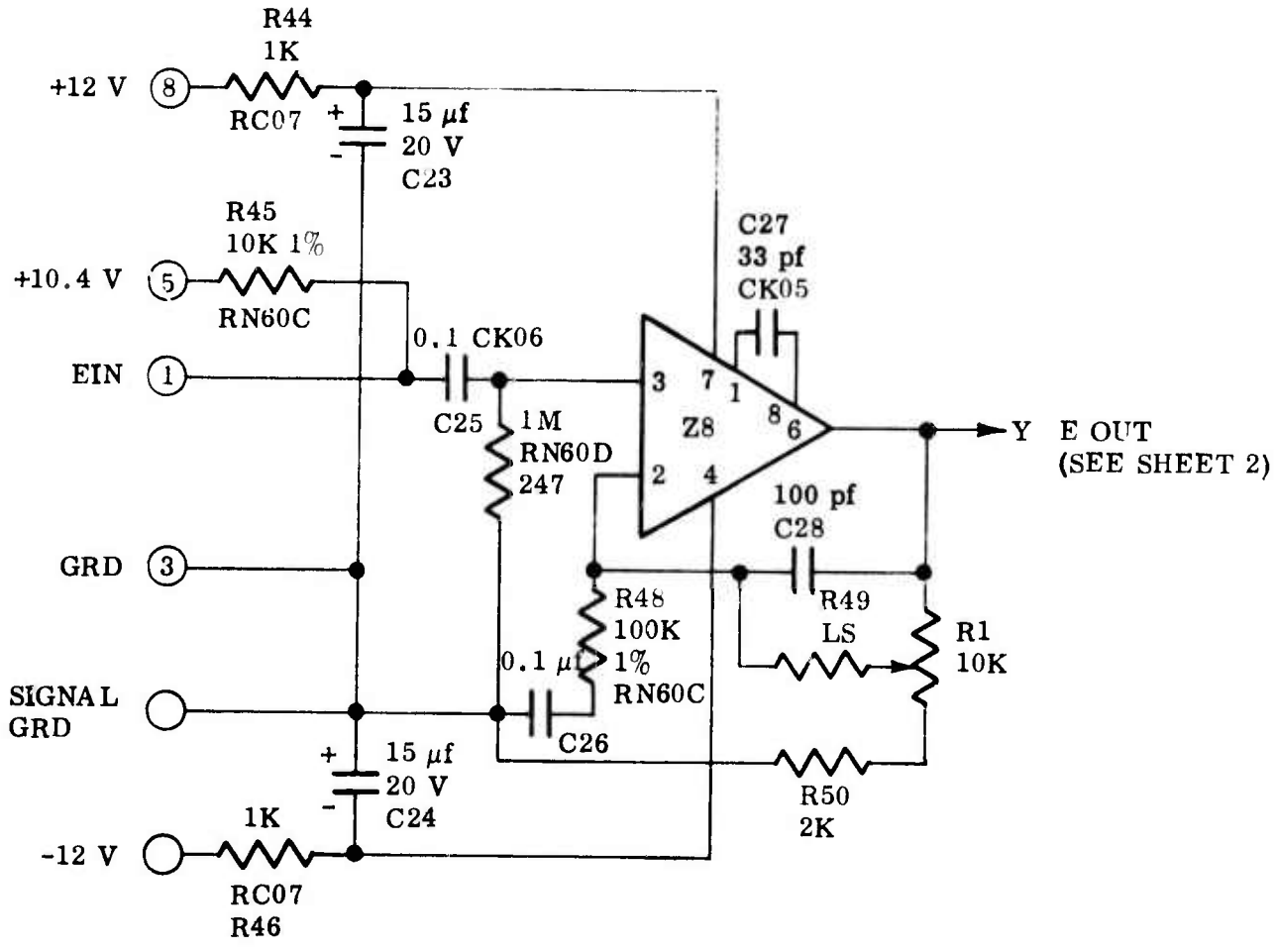

ADJUSTMENT PROCEDURE

1. WITH 60 μV P-P 200 Hz SQUARE WAVE AT PIN 1 ADJUST R20 FOR +50 μV DC AT POINT X (SHEET 2).
2. WITH 60 mV P-P 200 Hz SQUARE WAVE AT PIN 1 ADJUST R1 FOR +0.5 VDC AT POINT X (SHEET 2).

Fig. A-1 Preamplifier – Diagram BR69122-1. Sheet 1

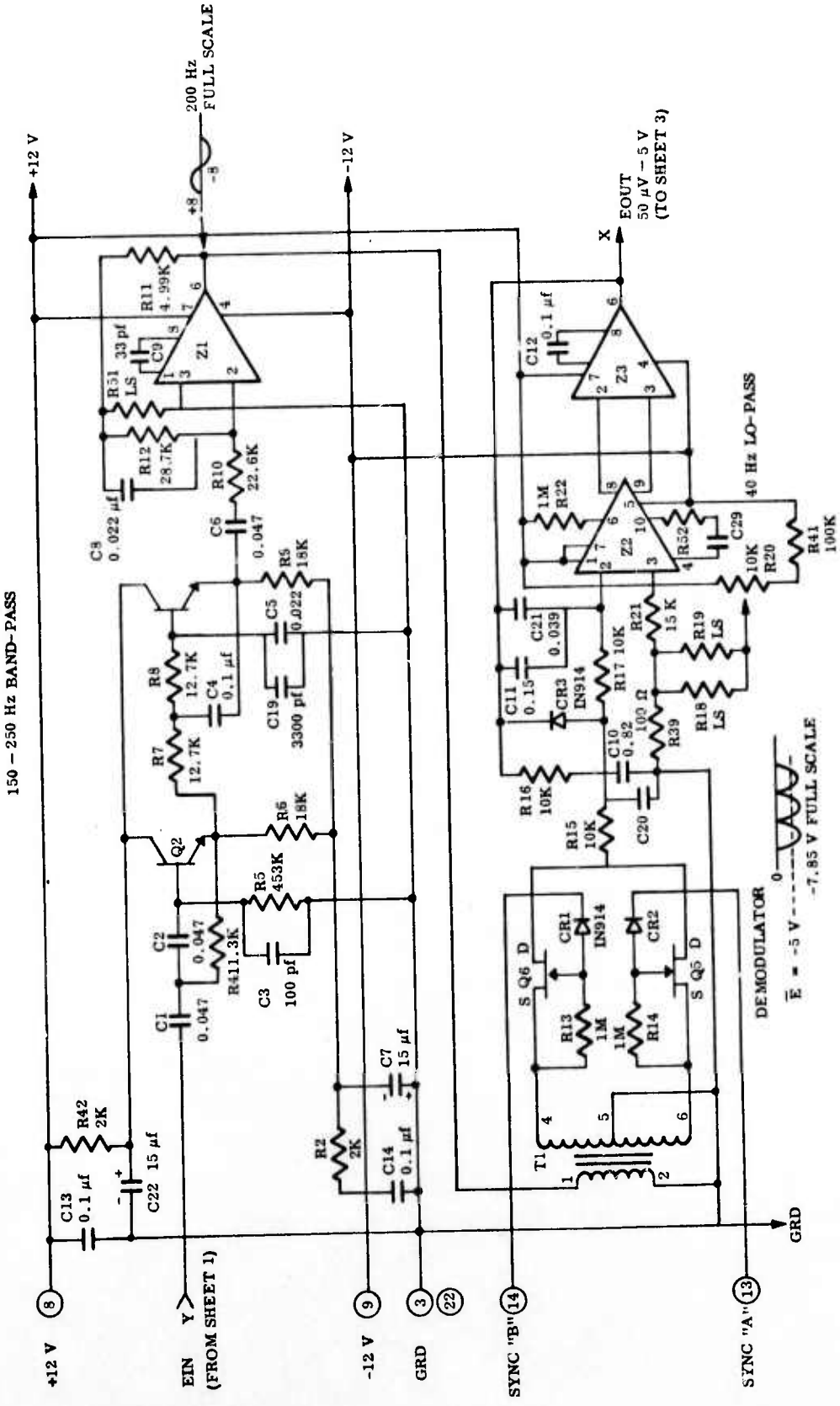

Fig. A-2 Bandpass Amplifier, Demodulator, Low-Pass Filter – Diagram BR69122-1, Sheet 2

50 μV to 5 V to cover the required five-order-of-magnitude dynamic range. The active filter utilizes a low-drift amplifier to allow stable operation at the least-signal level of 50 μV. This amplifier consists of two integrated circuit stages. The first stage is an LM727B preamplifier on a temperature-controlled silicon chip. It has a typical offset voltage drift of under 1 μV/°C and 5 μV/wk. The second stage is a standard LM201A operational amplifier.

A.1.1.3 Logarithmic Amplifier – Diagram BR69122-1, Sheet 3 (Fig. A-3)

The transfer characteristic of this circuit is: $E_{out} = \log (E_{Ti}/Er_{Ti})$ where Er_{Ti} = 50 μV. The logarithmic element is an npn transistor on a temperature-controlled silicon chip. It is used as the feedback element in a low-drift amplifier similar to that used in the 40-Hz low-pass filter. The output goes to a differential amplifier which utilizes a second npn transistor on the temperature-controlled chip for additional temperature compensation. The output has a slope of 1 V/decade over the 0- to 5-V range. A zener diode limits the output at 6.8 V.

A.1.2 Main Power Supply – Diagram BR69122-3 (Fig. A-4)

The 28-V input is regulated to 19 V. The 19 V input is used to drive a dc-dc converter which puts out ± 12 V. Three additional voltages are provided from the + 12 V line – passively filtered voltages of 5 V and 10 V, and an actively filtered voltage of 10.4 V.

A.1.3 Sync Generator – Diagram BR59122-4 (Fig. A-5)

This circuit provides two 180-deg out-of-phase square waves to switch the FET demodulators. The square waves are synchronized to the 200-Hz chopper. The circuit consists of an amplifier followed by two 1-shots. The first 1-shot has a pot adjustment for phase. The second 1-shot has an adjustment for symmetry.

PART NO	DESCRIPTION	SYMBOL
TRW663UW	CAPACITOR	C1 C2 C4 C5 C6 C8 C10 C11
C535	CAPACITOR	C17 C30 C9 C27 C28 C29
C536	CAPACITOR	C25 C26 C12 C13 C14 C15 C16 C18 C19 C20 C21
150D	CAPACITOR	C7 C22 C23 C24
RN60C	RESISTOR	R4 R5 R7 R8 R10 R11 R12 R15 R16 R17 R18 R19 R21 R23 R24 R25 R27 R28 R32 R33 R34 R35 R36 R37 R38 R41 R43 R45 R46 R48 R49 R50 R51
RC 07	RESISTOR	R2 R6 R9 R52 R53 R13 R14 R22 R29 R30 R31 R42 R44 R46, R52
RT24-C2-P-103	RES. VARIABLE	R1 R39
LM 727B	I.C.	Z2 Z5
LM 726C	I.C.	Z4
LM301A	I.C.	Z1 Z3 Z6 Z7 Z8
2N2484	TRANSISTOR	Q2 Q3
2N4393	TRANSISTOR	Q5 Q6
124-4C	TRANSFORMER	T1
1N 914	DIODE	CR1 CR2 CR3 CR4
1N 754A	DIODE	VR1
RN60D	RESISTOR	R26 R47

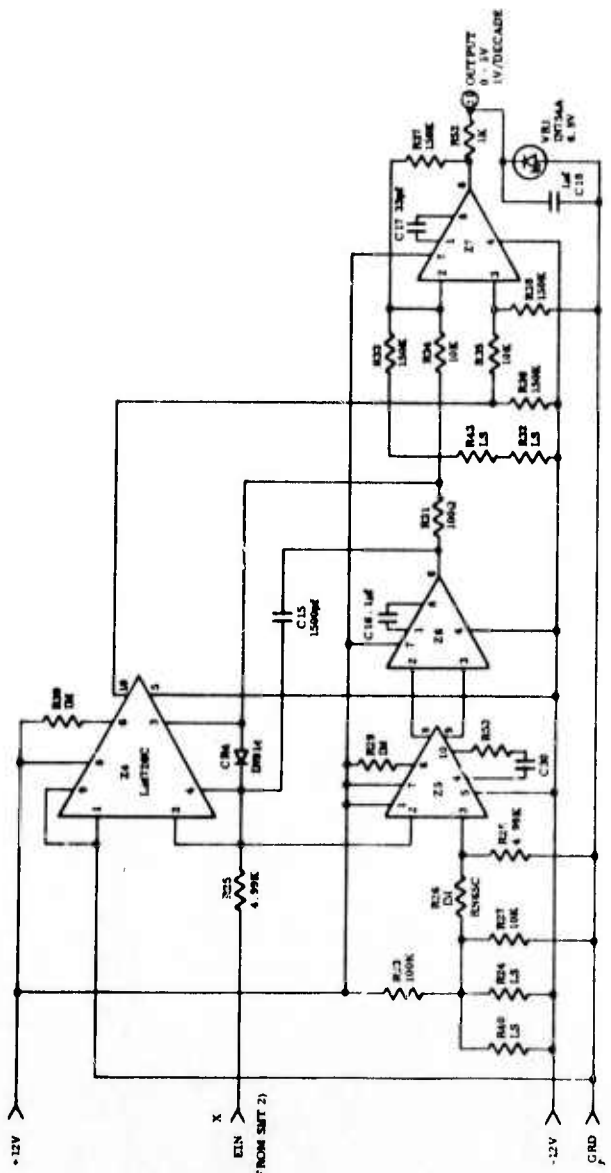

Fig. A-3 Logarithmic Amplifier – Diagram BR69122-1, Sheet 3

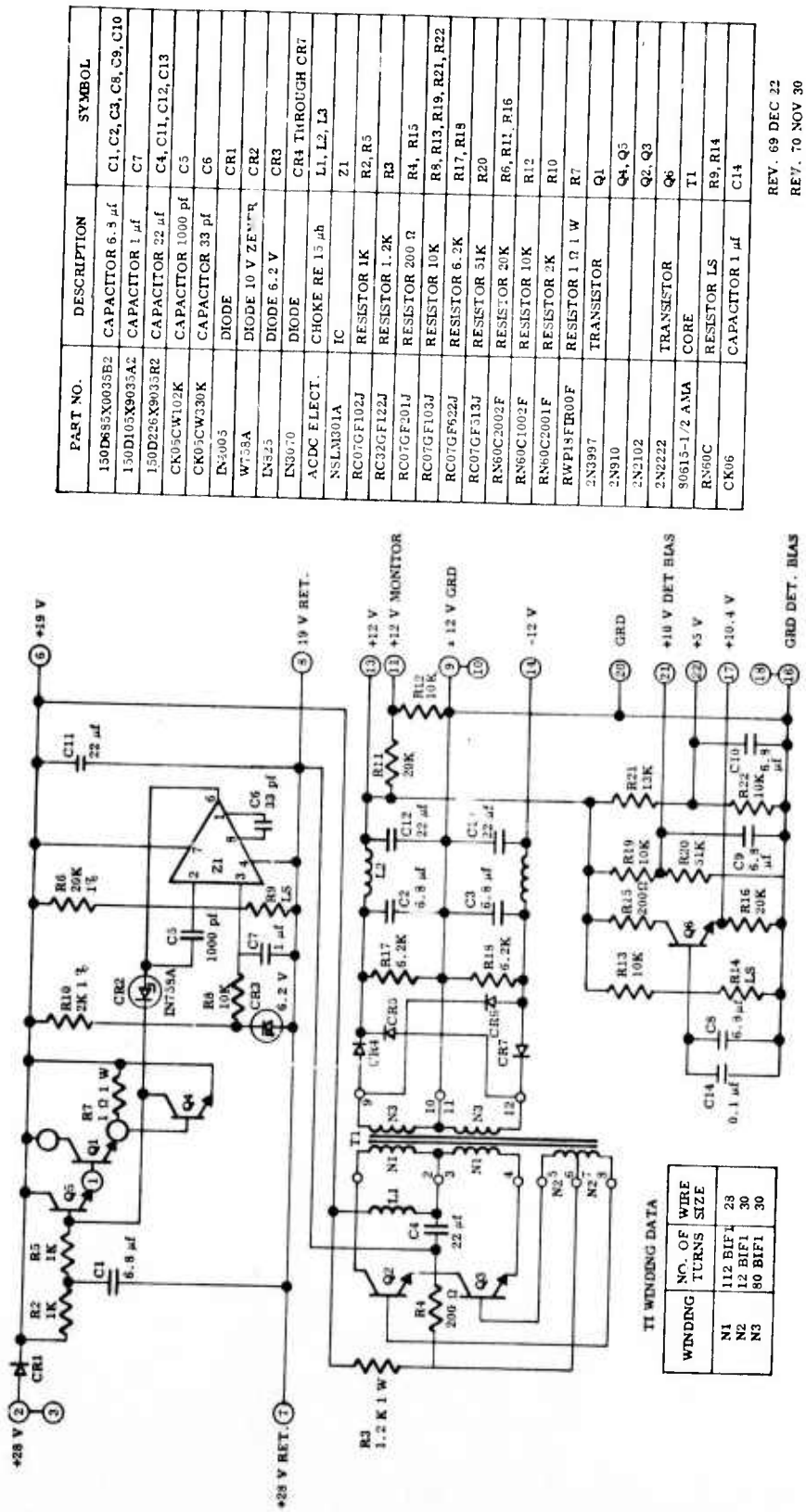

PART NO.	DESCRIPTION	SYMBOL
150D685X0035B2	CAPACITOR 6.8 μf	C1, C2, C3, C8, C9, C10
150D105X9035A2	CAPACITOR 1 μf	C7
150D226X9035R2	CAPACITOR 22 μf	C4, C11, C12, C13
CK05CW102K	CAPACITOR 1000 pf	C5
CK05CW330K	CAPACITOR 33 pf	C6
IN3005	DIODE	CR1
IN758A	DIODE 10 V ZENER	CR2
IN625	DIODE 6.2 V	CR3
IN3070	DIODE	CR4 THROUGH CR7
ACDC ELECT.	CHOKE RE 15 μh	L1, L2, L3
NSLM301A	IC	Z1
RC07GF102J	RESISTOR 1K	R2, R5
RC32GF122J	RESISTOR 1.2K	R3
RC07GF201J	RESISTOR 200 Ω	R4, R15
RC07GF103J	RESISTOR 10K	R8, R13, R19, R21, R22
RC07GF622J	RESISTOR 6.2K	R17, R18
RC07GF513J	RESISTOR 51K	R20
RN60C2002F	RESISTOR 20K	R6, R11, R16
RN60C1002F	RESISTOR 10K	R12
RN60C2001F	RESISTOR 2K	R10
RWP19FR00F	RESISTOR 1 Ω 1 W	R7
2N3997	TRANSISTOR	Q1
2N910		Q4, Q5
2N2102		Q2, Q3
2N2222	TRANSISTOR	Q6
90615-1/2 AMA	CORE	T1
RN60C	RESISTOR LS	R9, R14
CK06	CAPACITOR 1 μf	C14

REV. 69 DEC 22
REV. 70 NOV 30

T1 WINDING DATA		
WINDING	NO. OF TURNS	WIRE SIZE
N1	112 BIFI	23
N2	12 BIFI	30
N3	80 BIFI	30

Fig. A-4 Main Power Supply – Diagram BR69122-3

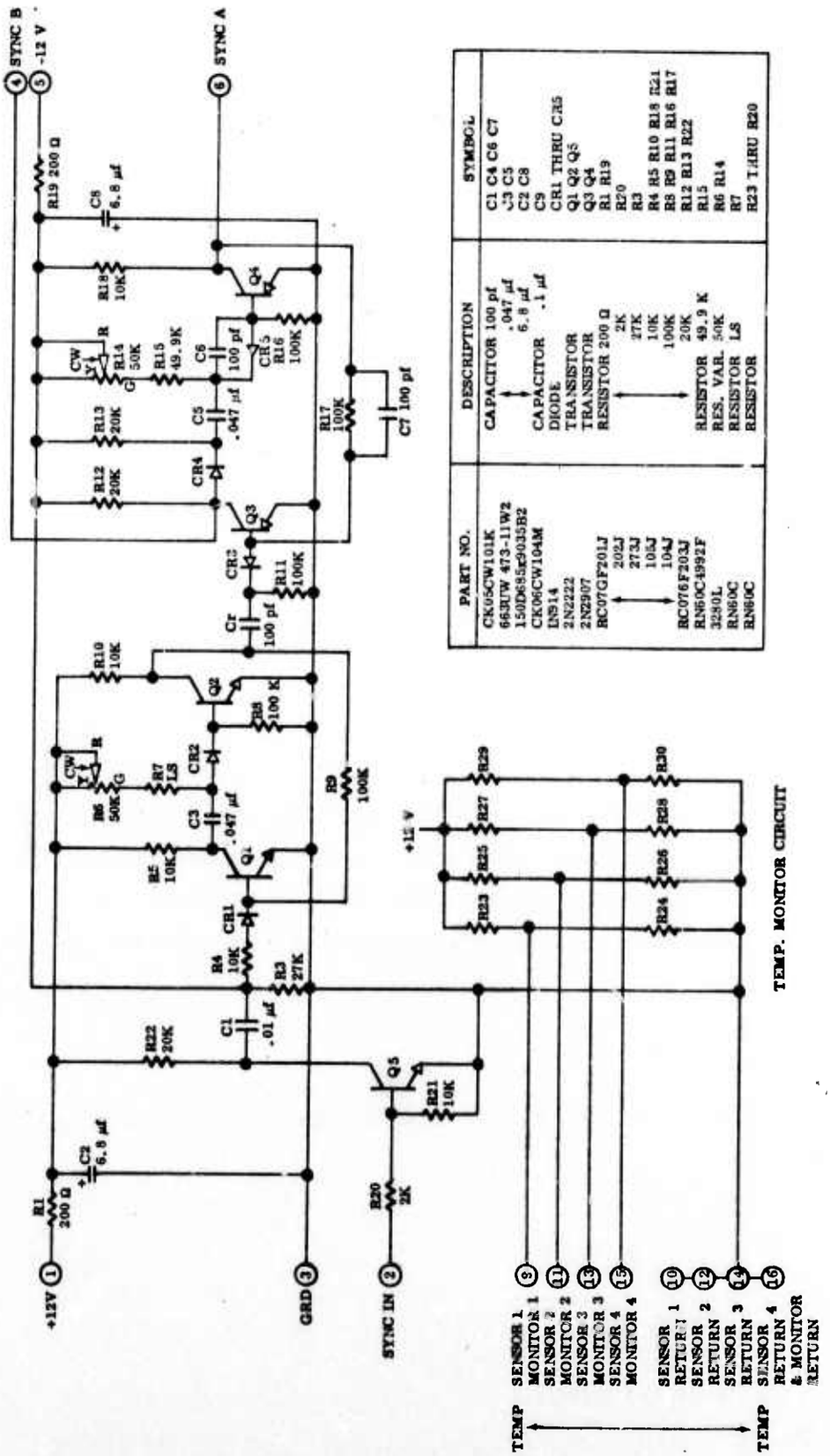

Fig. A-5 Sync Generator – Diagram BR69122-4

A.1.4 Neutral Density Filter Circuit – Diagram BR69122-5 (Fig. A-6)

This circuit actuates a two-position step motor to step a neutral density filter in or out of the optical path for increased dynamic range. The circuit works in two modes – automatic and by external command. In the automatic mode, the filter is stepped in if any of the four detector outputs exceeds 4 V. If all four outputs are under 0.5 V, the filter is stepped out. In addition, the filter can be externally commanded.

A.1.5 Spectral Filter Stepper Circuit – Diagram BR69122-6 (Fig. A-7)

This circuit drives a four-position 90-deg stepper motor. The motor has two center-tapped windings which are 90 deg out of phase. One-half winding is energized by external command for each of the four positions.

A.1.6 Chopper Driver – American Time, Type 4A Oscillator (Fig. A-8)

The chopper has a pickup coil to sense motion and a drive coil to provide for electrial power input. The chopper driver circuit is basically a two-transistor amplifier with input from the pickup coil and an output to the drive coil. Oscillation occurs through positive feedback. A small perturbation causes a voltage to be induced in the pickup coil which in turn causes a larger perturbation of the chopper and results in oscillation of the high Q chopper at its resonance frequency of 200 Hz. The chopper excursion is determined by the amplifier gain, electrical power to the drive coil, and mechanical losses of the chopper.

Tables A-1 through A-17 indicate various details regarding component location, cabling, and plug wiring.

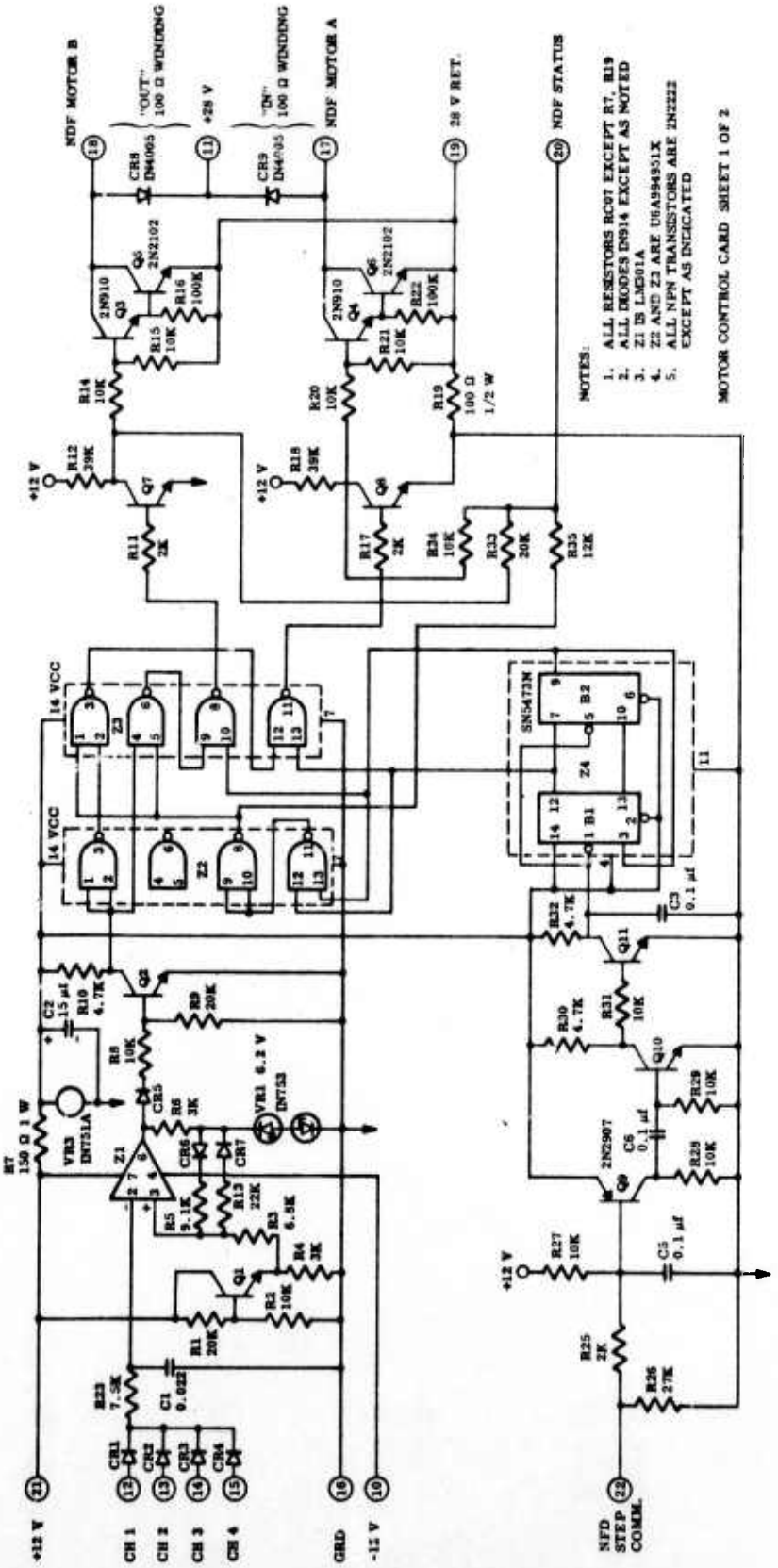

Fig. A-6 Neutral Density Filter Circuit – Diagram BR69122-5

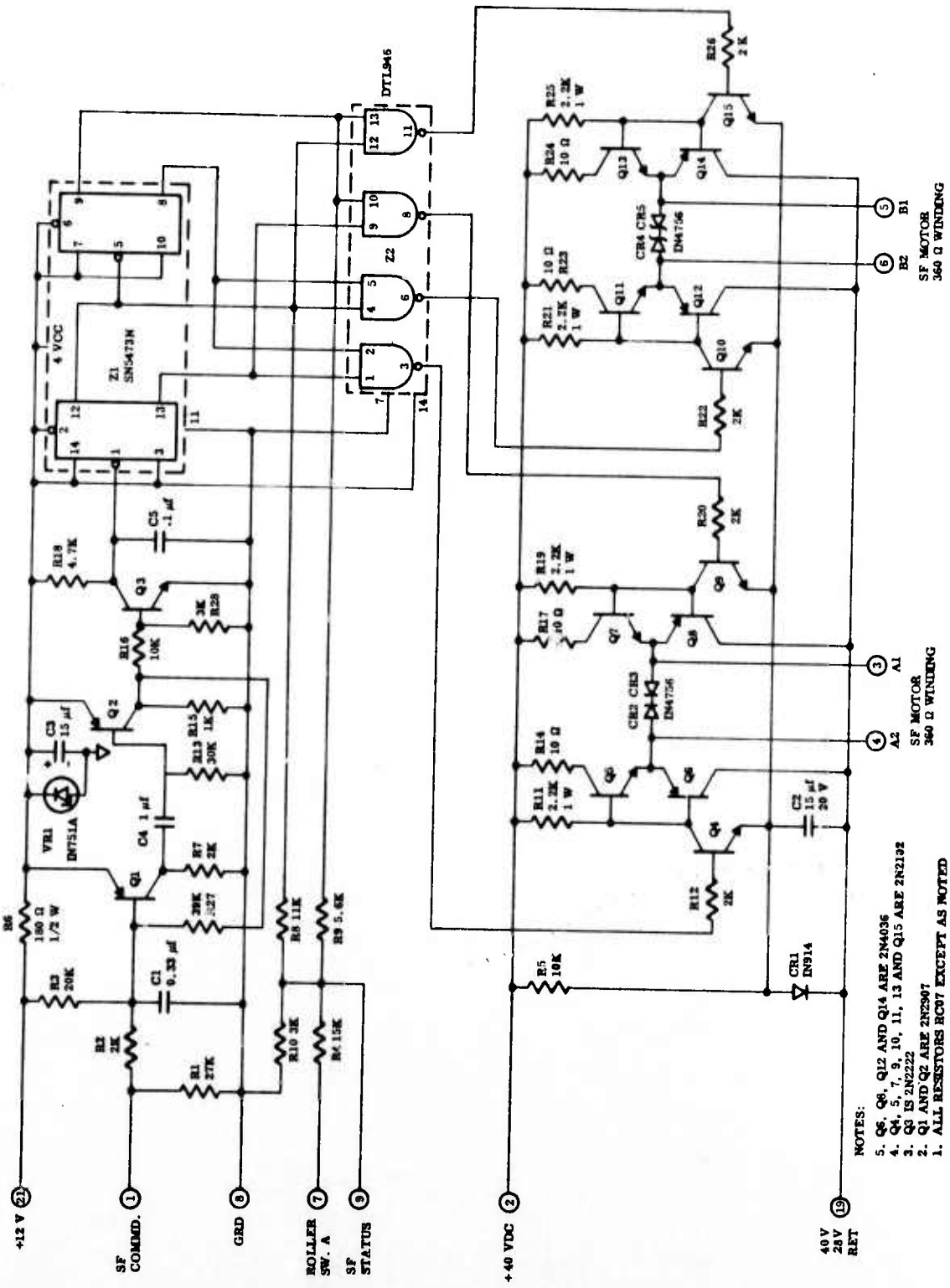

Fig. A-7 Spectral Filter Stepper Circuit – Diagram BR69122-6

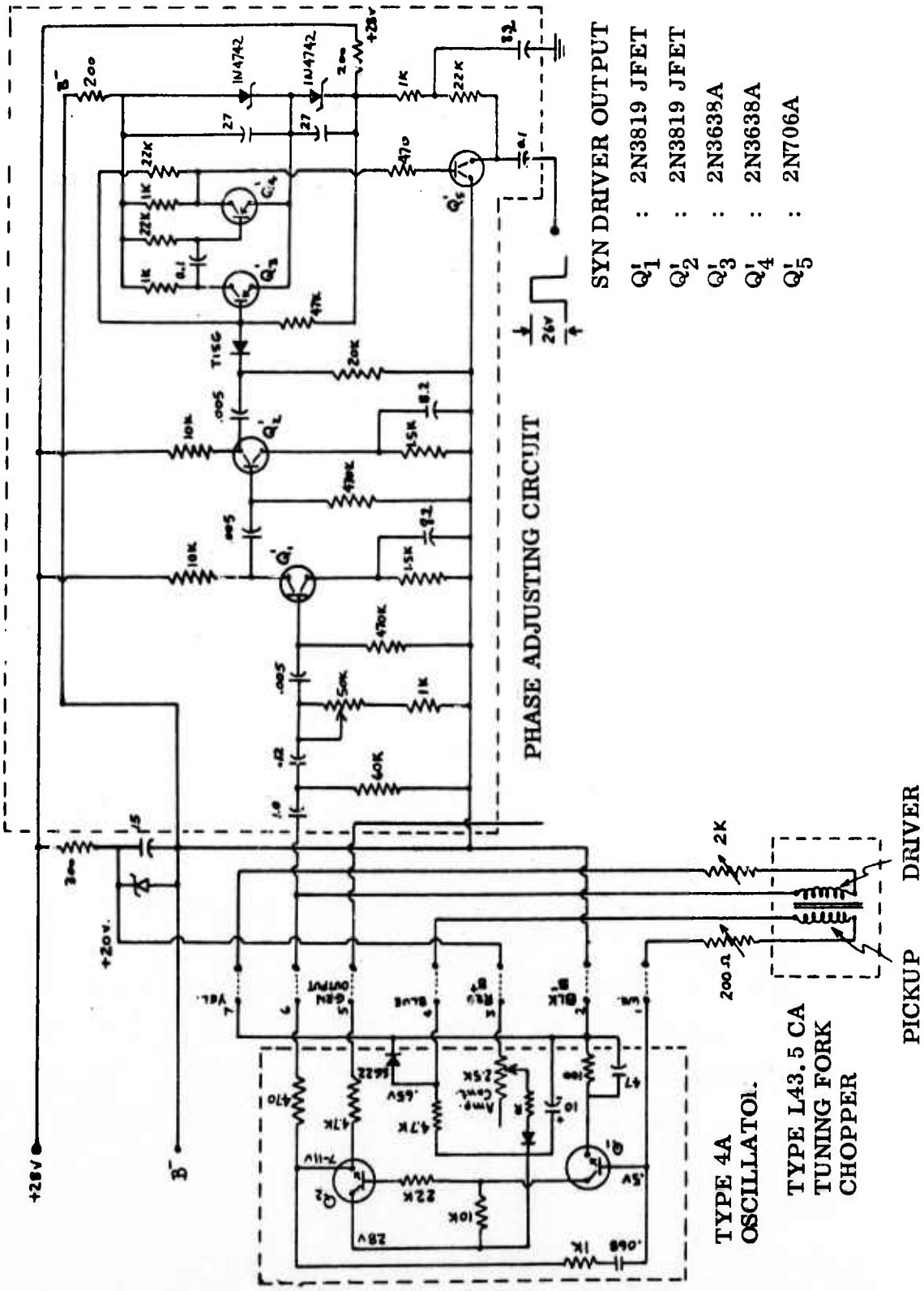

Fig. A-8 Chopper Driver – American Time

Table A-1

CONNECTOR AND TERMINAL LOCATIONS

Designation	Location	Type	Function
A	Dewar Cover Standoff	Amphenol 165-11	Detector
B	Dewar Cover Standoff	Amphenol 165-11	Filter Wheel Drives
C	Dewar Cover Standoff	Amphenol 165-11	Chopper
D	Dewar Cover Standoff	Amphenol 165-11	Radiometer PRT Sensors
E	Dewar Cover	Terminal Strip	Hatch Cover
F & G	Dewar Cover	No Connection	Hatch Cover and Flare PRT Sensors
J1	Electronic Box	L58721AR16-26PS	Telescope Interface
J2	Electronic Box	L58721AR16-26PS	Input-Output
J3	Electronic Box	LS8721AR18-11PS	Power
J4	Electronic Box	LS8721AR18-11PS	Channel 1 Preamp
J5	Electronic Box	LS8721AR18-11PS	Channel 2 Preamp
J6	Electronic Box	LS8721AR18-11PS	Channel 3 Preamp
J7	Electronic Box	LS8721AR18-11PS	Channel 4 Preamp
J8	Electronic Box	LS8721AR18-11PS	Spare
J9	Electronic Box	LS8721AR18-11PS	Spare
J10	Electronic Box	LS8721AR18-11PS	Chopper, 28 V
J11	Electronic Box	LS8721AR18-11PS	Chopper, Drive
J12	Electronic Box	LS8721AR18-11PS	Chopper, Sync Monitor
J13	Electronic Box	LS8721AR18-11PS	Chopper, Coil Monitor
J14	Temperature Circuit Box	LS8721AR18-11PS	Temperature Sensor Outputs

Table A-2

RADIOMETER AND ELECTRONIC INTERFACE CABLING
WIRING LIST – DETECTOR ARRAY, A1*

Pin No.	Function	Type Wire	Cable No.
A	Detector 1-2 Bias	Micro-Dot Low-Noise	1
B	Detector 3-4 Bias	Coaxial Cable	2
C	Detector Sub Bias	No. 250-3808	3
D	Detector 1 Large Outer	Micro-Dot Mini-Noise	4
E	Detector 2 Larger Center	Coaxial Cable	5
F	Detector 3 Small Center	No. 250-3820	6
H	Detector 4 Small Outer		7
J	Bias Return		
K	Open		
L	All Shields Command Ground		8
M		Resistor No. 24 Gauge Wire-Green	9
N		Resistor No. 24 Gauge Wire-Green	10

*Cable from electronic box has a female receptacle Amphenol No. 165-10-1000 connecting to No. 165-11 plug.

Table A-3

WIRING LIST – FILTER WHEEL DRIVE B1*

Pin No.	Function	Cable No. B
A	(N. D. F. Motor A.) (J1-B)	1
B	Dif. T.C. Ref. to Shade	2
C	(B-2 Elect Box) (J1-N)	3
D	(N. D. F. Motor B) (J1-A)	4
E	(+28 V Elect Box) (J1-J)	5
F	(A-1 Elect Box) (J1-R)	6
H	(A-2 Elect Box) (L1-S)	7
J	Roller Switch A	8
K	(B-1 Elect Box) (J1-P)	9
L	Hatch Cover Motor Dif. T. C.	10
N	F. W. Motor Dif. T. C.	11
M	Electronic Box Bnd.	12

*Cable from Electronic Box to Radiometer receptacle (Amphenol No. 165-10-1000), Plug (Amphenol No. 165-11)

Table A-4

WIRING LIST – CHOPPER, C1*

Pin No.	Function	Wire Code
A	Pickup	White Wire
E	Driver	Black Wire
F	Driver	Green Wire
K	Pickup	Red Wire
N L	Neon Tank Heaters, 28V	
C H	Hatch Cover Motor Heaters, 28 V	

Table A-5

WIRING LIST – PRT TEMPERATURE SENSORS NOS. 1, 2, AND 3*

Sensor No.	Sensor Location	Pin No.	Function	Wire Code
1	Neon Tank	A	Sensor Compensation	White
		B		Red
		C		Black
		D		Black
2	Rear Shade	E	Sensor Compensation	White
		F		Red
		H		Black
		J		Black
3	Front Shade	K	Sensor Compensation	White
		L		Red
		M		Black
		N		Black

*Cable D1 from Alphaline transmitters to radiometer flange with Amphenol receptacle No. 165-10-100 connecting to Plug Type 165-11.

Table A-6

HATCH COVER CABLES

Item	Function
Hatch Cover Motor Cables, E1	Connect 28-Vdc power to terminal strap mounted on dewar cover for the hatch cover motor
Hatch Cover and Warm Gas (Flare) PRT Sensor Cables, F1 and G1	Connect Alphaline transmitters directly under PRT's located on radiometer flange

Table A-7

POWER AND OUTPUT CABLING

Origin	Function	Termination
Radiometer Electronic Box ↓	Detector Output, Channel 1 Detector Output, Channel 2 Detector Output, Channel 3 Detector Output, Channel 4 Detector Output, Return Ground	Central Control Panel ↓
Control Panel ↓	SFW Input Command NDF Input Command Common Return Ground	Electronic Box ↓
Electronic Box ↓	Temperature Sensor 1 Temperature Sensor 2 Temperature Sensor 3 Temperature Sensor 4 Temperature Sensor 5 Temperature Sensor 6	Control Panel ↓
Control Panel ↓	Temperature Sensor, 28 Vdc Temperature Sensor, -28 Vdc 28-Vdc Power In* -28-Vdc Power In 40 Vdc to SFW Motor (Negative 40 Vdc is command to negative of 28 Vdc to electronic box) 28 V to Chopper -28 V to Chopper	Electronic Box ↓

*Red leads always positive; black leads always negative

Table A-8

ELECTRONIC CHASSIS WIRING LIST – TELESCOPE INTERFACE BALLOON RADIOMETER J1 CONNECTOR LS5721AR16-26PS

Pin No.	Signal or Function	Term	Remarks
J1-A	Chassis Ground		
J1-B	Temperature Sensor 2	A5-30	
J1-C	Sync Input Return	A5-12	From Chopper
J1-D	10 V Detector Bias	A7-40	Out
J1-E			
J1-F	10.4 V Preamp Bias	A7-40	Out
J1-G	5 V	A7-50	Out
J1-H		NC	
J1-J	NDF Motor C (23 Vdc)	A6-28	Out
J1-K	10-Vdc Detector Bias Return	A7-46	Out
J1-L	Temperature Sensor 1	A5-24	
J1-M	Temperature Sensor 1	A5-26	
J1-N	SF Motor B2	A6-18	Out
J1-P	SF Motor B1	A6-16	Out
J1-Q	SF Motor A1	A6-12	Out
J1-S	SF Motor A2	A6-14	Out
J1-T	Roller Switch A	A6-20	
J1-U	Roller Switch B	A6-44	
J1-V	28 Vdc Return	A7-22	Out
J1-W	10.4-V Preamp Bias Return	A7-38	
J1-X	5 Vdc Return	A7-42	Out
J1-Y	Temperature Sensor 2	A5-25	
J1-Z	Sync Input	A5-12	From Chopper
J1-a	NDF Motor B	A1-42	Out
J1-b	NDF Motor A	A6-40	Out
J1-c			

Table A-9

WIRING LIST – INPUT/OUTPUT CONNECTOR, BALLOON RADIOMETER J2, CONNECTOR LS3721AR16-36SS

Pin No.	Signal or Function	Term	Remarks
J2-A	Chassis Ground		
J2-B	19-Vdc Monitor	A7-18	
J2-C	19-Vdc Monitor Return	A7-22	
J2-D	12-Vdc Monitor	A7-28	
J2-E	10-Vdc Monitor	A7-47	
J2-F	Temperature Monitor 2	A5-37	
J2-G	Channel 1 Sync Detector Monitor	A1-	
J2-H	Temperature Monitor Return	A5-33	
J2-J	NDF Input Command Return	A6-37	In
J2-K	NDF Input Command	A6-50	In
J2-L		NC	
J2-M	SF Input Command Return	A6-38	In
J2-N	Output Return	A6-33	Out
J2-P	Output 4	A6-35	Out
J2-R	Output 3	A6-33	Out
J2-S	SF Input Command	A6-8	In
J2-T	SF Status Monitor	A6-24	Out
J2-U	12-Vdc Monitor Return	A7-26	
J2-V	10-Vdc Monitor Return	A7-45	
J2-W	Temperature Monitor 1	A5-23	
J2-X			
J2-Y	Temperature Monitor 4	A5-35	
J2-Z	Output 2	A6-31	Out
J2-a	Output 1	A6-29	Out
J2-b	NDF Status Monitor	A6-46	Out
J2-c			

Table A-10

WIRING LIST – POWER CONNECTOR, BALLOON RADIOMETER, J3
CONNECTOR LS3721AR16-11PS

Pin No.	Function	To
J3-A	Chassis Ground	
J3-B	28-V and 40-V Return	A7-20
J3-C		
J3-D		
J3-E		
J3-F		
J3-G		
J3-H		
J3-J		
J3-K	28 Vdc	A7-10
J3-L	40 Vdc	A6-10
J4	Channel 1 Preamp Input	A1-7
J5	Channel 2 Preamp Input	A2-7
J6	Channel 3 Preamp Input	A3-7
J7	Channel L4 Preamp Input	A4-7
J8	Spare	
J9	Spare	

Table A-11

WIRING LIST – SIGNAL ELECTRONICS CARD, A1

Connector Pin No.	Card Pin No.	Signal or Function	Term
A1-7	A1-1	Channel 1 Input	J4 Connector
A1-10	A1-2	Channel 1 Signal Ground	J4 Shield
A1-11	A1-3	PW 2 Ground	A2-11
	A1-4		NC
A1-15	A1-5	10.4 V	A2-15
	A1-6		NC
	A1-7		NC
A1-22	A1-8	12 Vdc	A2-22
A1-23	A1-9	-12 Vdc	A2-23
	A1-10		NC
	A1-11		NC
	A1-12		NC
A1-32	A1-13	Sync A	A2-32
A1-34	A1-14	Sync B	A2-34
	A1-15		NC
	A1-16	Detector Output Through Series 1K Resistor	
	A1-17		
	A1-18		
	A1-19		
	A1-20		NC
A1-47	A1-21	Channel 1 Output	A6-30
A1-49	A1-22	Power Ground	NC

Table A-12

WIRING LIST – SIGNAL ELECTRONICS CARD, A2

Connector Pin No.	Card Pin No.	Signal or Function	Term
A1-7	A2-1	Channel 2 Input	J5 Conductor
	A2-2	Channel 2 Signal Ground	J5 Shield
	A2-3	Power Ground	A3-11, A1-11
	A2-4		NC
A2-15	A2-5	10.4 Vdc	A3-15, A1-15
	A2-6		NC
	A2-7		NC
A2-22	A2-8	12 Vdc	A3-22, A1-22
A2-23	A2-9	-12 Vdc	A3-23, A1-23
	A2-10		NC
	A2-11		NC
	A2-12		NC
A2-32	A2-13	Sync A	A3-32, A1-32
A2-34	A2-14	Sync B	A3-34, A1-34
	A2-15		NC
	A2-16		NC
	A2-17		NC
	A2-18		NC
	A2-19		NC
	A2-20		NC
A2-47	A2-21	Channel 2 Output	A6-32
A2-49	A2-22	Power Ground	NC

Table A-13

WIRING LIST – SIGNAL ELECTRONICS CARD, A3

Connector Pin No.	Card Pin No.	Signal or Function	Term
A3-7	A3-1	Channel 3 Input	J6 Conductor
A3-10	A3-2	Channel 3 Signal Ground	J6 Shield
A3-11	A3-3	Power Ground	A4-11, A2-11
	A3-4		NC
A3-15	A3-5	10.4 Vdc	A4-15, A2-15
	A3-6		NC
	A3-7		NC
A3-22	A3-8	12 Vdc	A4-22, A2-22
A3-23	A3-9	-12 Vdc	A4-23, A2-23
	A3-10		NC
	A3-11		NC
	A3-12		NC
A3-32	A3-13	Sync A	A4-32, A2-32
A3-34	A3-14	Sync B	A4-34, A2-34
	A3 15		NC
	A3-16		
	A3-17		
	A3-18		
	A3-19		
	A3-20		NC
A3-47	A3-21	Channel 3 Output	A6-34
A3-49	A3-22	Power Ground	NC

Table A-14

WIRING LIST – SIGNAL ELECTRONICS CARD, A4

Connector Pin No.	Card Pin No.	Signal or Function	Term
A4-7	A4-1	Channel 4 Input	J7 Conductor
A4-10	A4-2	Channel 4 Signal Ground	J7 Shield
	A4-3	Power Ground	A5-12, A3-11
	A4-4		NC
A4-15	A4-5	10.4 Vdc	A7-40, A3-15
	A4-6		NC
	A4-7		NC
A4-22	A4-8	12 Vdc	A5-8, A3-22
A4-23	A4-9	-12 Vdc	A5-16, A3-23
	A4-10		NC
	A4-11		NC
	A4-12		NC
A4-32	A4-13	Sync A	A5-18, A3-32
A4-34	A4-14	Sync B	A5-14, A3-34
	A4-15		NC
	A4-16		
	A4-17		
	A4-18		
	A4-19		
	A4-20		NC
A4-47	A4-21	Channel 4 Output	A6-36
A4-49	A4-22	Power Ground	NC

Table A-15

WIRING LIST – SYNC GENERATOR CARD, A5

Connector Pin No.	Card Pin No.	Signal or Function	Term
A5-8	A5-1	12 Vdc	A6-48, A4-22
A5-10	A5-2	Sync Input	J1-Z
A5-11	A5-3	Sync Input Return (Ground)	J1-C
A5-12	A5-3	Ground	A6-11, A4-11
A5-14	A5-4	Sync B	A4-34
A5-16	A5-5	-12 Vdc	A6-26, A4-24
A5-18	A5-6	Sync A	A4-32
	A5-7		NC
	A5-8		NC
A5-23	A5-9	Temperature Monitor 1	J2-W
A5-24	A5-9	Temperature Sensor 1	J1-L
A5-26	A5-10	Temperature Sensor 1	J1-M
A5-27	A5-11	Temperature Monitor 2	J2-F
A5-28	A5-11	Temperature Sensor 2	J1-Y
A5-30	A5-12	Temperature Sensor 2	J1-B
A5-31	A5-13	Temperature Monitor 3	J2-L
A5-32	A5-13		
A5-34	A5-14		
A5-35	A5-15	Temperature Monitor 4	J2-Y
A5-36	A5-15	Temperature Sensor 4	*
A5-37	A5-16	Temperature Monitor Return	J2-H
A5-38	A5-16	Temperature Sensor 4	*
	A5-17		NC
	A5-18		
	A5-19		
	A5-20		
	A5-21		
A5-22	A5-22		NC

*Wire approximately 12 in. long to be connected to sensor mounted on chassis.

Table A-16

WIRING LIST – NEUTRAL DENSITY AND SPECTRAL FILTER CARD, A6
(MOTOR CONTROL CIRCUITS)

Connector Pin No.	Card Pin No.	Signal or Function	Term
A6-8	A6-1	S Input Command	J7-S
A6-10	A6-2	40 Vdc Unregistered	J3-L
A6-12	A6-3	SF Motor A1	J1-R
A6-14	A6-4	SF Motor A2	J1-S
A6-16	A6-5	SF Motor B1	J1-P
A6-18	A6-6	SF Motor B2	J1-N
A6-20	A6-7	Roller Microswitch A	J1-T
A6-22	A6-8	Ground	A7-24, A5-12
A6-24	A6-9	SF Status Monitor	J2-T
A6-26	A6-10	-12 Vdc	A7-34, A5-16
A6-28	A6-11	NDF Motor C (28 Vdc)	A7-12, J1-J
A6-29	A6-12	Channel 1 Output	J2-3
A6-30	A6-12	Channel 1 Output	A1-47
A6-31	A6-13	Channel 2 Output	J2-Z
A6-32	A6-13	Channel 2 Output	A1-47
A6-33	A6-14	Channel 3 Output	J2-R
A6-33	A6-14	Channel 3 Output	J2-R
A6-34	A6-14	Channel 3 Output	A3-47
A6-35	A6-15	Channel 4 Output	J2-P
A6-36	A6-15	Channel 4 Output	A4-47
A6-37	A6-16	Ground (NDF Input Command Return	J2-X
A6-38	A6-16	Ground	J2-M, J2-N
A6-40	A6-17	NDF Motor A	J1-b
A6-42	A6-18	NDF Motor B	J1-a
A6-44	A6-19	28 V Return	A7-19, J1-U
A6-46	A6-20	NDF Status Monitor	J2-b
A6-48	A6-21	12 Vdc	A7-32, A5-8
A6-50	A6-22	NDF Input Command	J2-K

Table A-17

WIRING LIST – POWER SUPPLY CARD, A7

Connector Pin No.	Card Pin No.	Signal or Function	Term
A7-8	A7-1	Q1 Base	A1-B
A7-10	A7-2	28 Vdc, Unregistered	J3-K
A7-12	A7-3	28 Vdc, Unregistered	A6-28
A7-14	A7-4	Q1 Collector	Q1-C
A7-16	A7-5	Q1 Emitter	Q1-E
A7-18	A7-6	19 Vdc Registered	J2-B
A7-20	A7-7	23-V and 19 V Return	J3B, Ag-44
A7-22	A7-8	28-V and 19 V Return	J2-C, J1-V
A7-24	A7-9	±12-Vdc Return (Ground)	A6-22
A7-26	A7-10	±12 Vdc Return (Ground)	J2-U
A7-28	A7-11	12-V Monitor	J2-D
	A7-12		NC
A7-32	A7-13	12 Vdc	A6-48
A7-34	A7-14	-12 Vdc	A6-26
	A7-15		NC
A7-38	A7-16	10.4-V Return	J1-W
A7-40	A7-17	10.4 Vdc	J1-F, A4-16
A7-42	A7-18	5 V-Return	J1-X
	A7-19		NC
A7-45	A7-20	10-V Return	J2-V
A7-46	A7-20	10-V Return	J1-E
A7-47	A7-21	10 Vdc	J2-E
A7-48	A7-21	10 Vdc	J1-D
A7-50	A7-22	5 Vdc	J1-G

A.1.7 Hatch Cover Electric Drive Control Circuit

Hatch cover operation is achieved by the use of a sequencing cam and switches operated in conjunction with ground command and in relation to hatch cover position. The circuit incorporates three switches and a two-position,double-throw, magnetic latch relay operating in the following sequence. The sequence begins when Switch S-1 is closed by a cam on the positioner. Power of 28 V is then applied to the normally closed side of Limit Switch S-2 and through the polarity relay to the motor. The hatch cover drive motor stops when the Limit Switch S-2 is actuated. When this switch is in the normally open position, the polarity is reversed to the drive motor for the following sequence by actuating the relay.

When the instrument positioner is commanded to the next stop, Microswitch S-1 rests at the normally open position and therefore applies 28 V to Switch S-3. This switch is closed to drive the motor until the Limit Switch S-2 is actuated to the normally open position. This also actuates the reversing relay again for the next sequence.

The circuit schematic is shown in Fig. A-9.

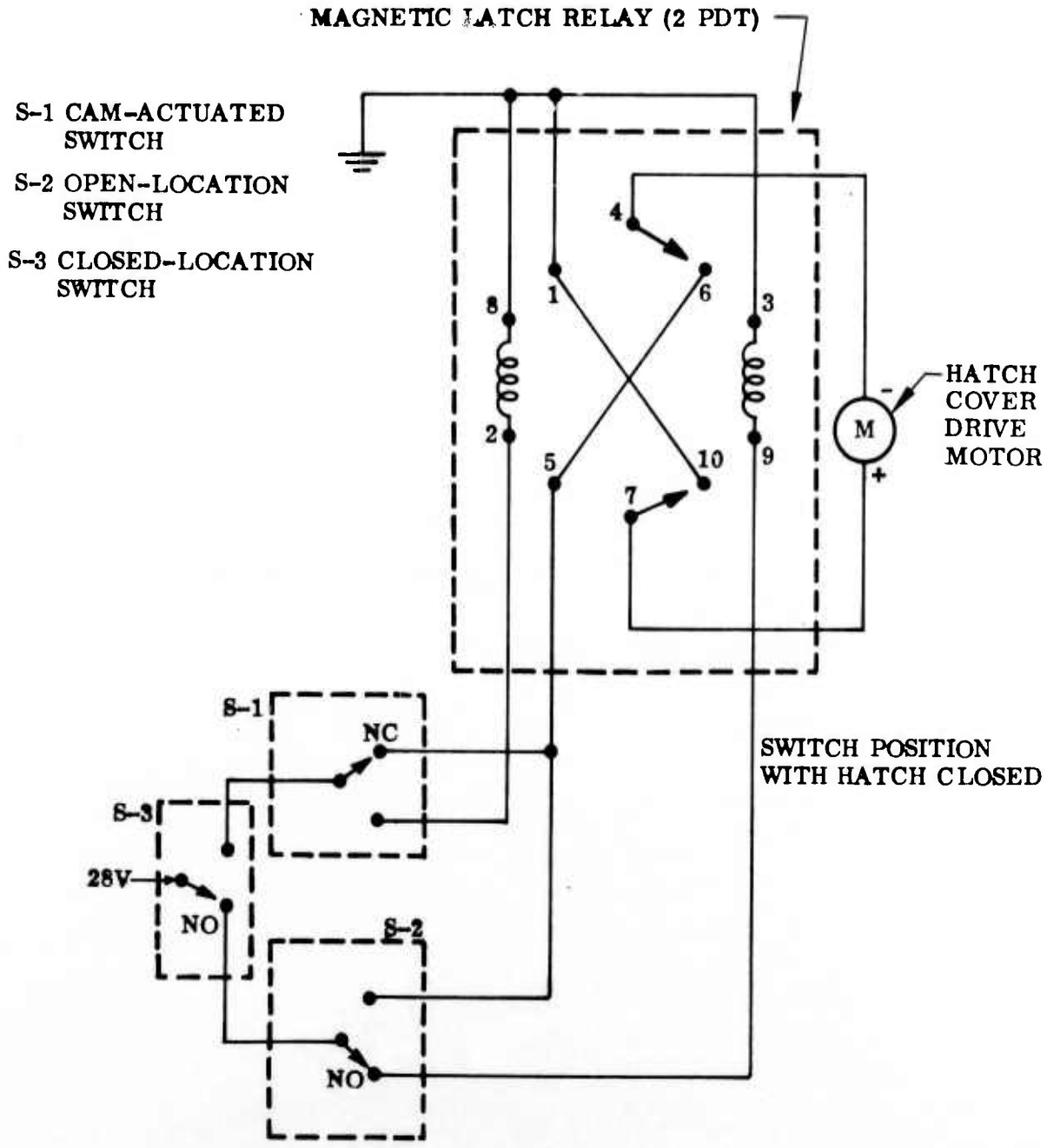

Fig. A-9 Hatch Cover Electronic Drive Control Circuit

Appendix B
RADIOMETER PREFLIGHT SERVICING

Radiometer flight package servicing before launch includes the following tasks:

- Filling and forming solid neon in the tank surrounding the optical train
- Filling and forming solid nitrogen in the dewar guard
- Filling the LN_2 storage vessel
- Filling and heating the water in the storage tank

Solid neon and nitrogen are used to eliminate the liquid venting and containment problem during the launch and ascent and to provide lower temperatures and extended cold time operation. A careful and complete purging of the optical system and the dewar interior is performed with gaseous helium prior to cooling to remove all condensable gases. Purging continues while cooling the radiometer to ensure against leakage of air or water vapor into the optical system. Cooldown is performed by first filling the dewar guard with LN_2. LHe is then transferred into the neon fill port to prechill the optical system to about 25°K. At this temperature, liquid neon is transferred into the neon tank until the liquid neon is discharged from the vent port. The LHe is then circulated through the cooling coils around the neon tank to freeze the neon. During the initial part of the transfer, the neon vent is open to ensure that the tank does not overpressurize due to the initial circulation of warm GHe. After the lines have cooled and the LHe is efficiently flowing, the main (external) neon vent is closed. The internal manual vent valve is then opened to allow GHe from the dewar interior to equalize the neon tank pressure with the dewar interior as the neon cools and its vapor pressure decreases. The cooling is continued until the neon is solidified (at 24.5° K) and finally subcooled to about 18°K as determined by the neon tank platinum resistance thermometer (PRT) bridge circuit.

The initial LHe cooldown takes about 3 hr and requires approximately 50 liters of LHe. After the radiometer has been moved to the launch area, an additional cooling (for ~ 0.5 hr) is performed before the neon filling. About 10 liters of liquid neon are required to fill the neon tank. The transfer takes about 40 min. The neon solidification with LHe is the last operation performed before launch.

The LN_2 storage tank filling and heating of the water are initiated about the same time as the radiometer cooling starts. After moving to the launch area, the water is heated to about 175°F and a mechanical vacuum pump (5 ft^3/min) is attached to the dewar guard reservoir to solidify the nitrogen. Just before launch, the pump is removed, and the storage tank is topped off with LN_2.

The water tank and LN_2 storage vessel valves are adjusted to provide the flow of warm nitrogen gas through the flare section as described in Section 2.6. A check of the internal manual neon valve is suggested just prior to launch to ensure that the enon gas is venting and purging the shade area.

A plumbing schematic of the cooling and frost-free systems is shown in Fig. B-1.

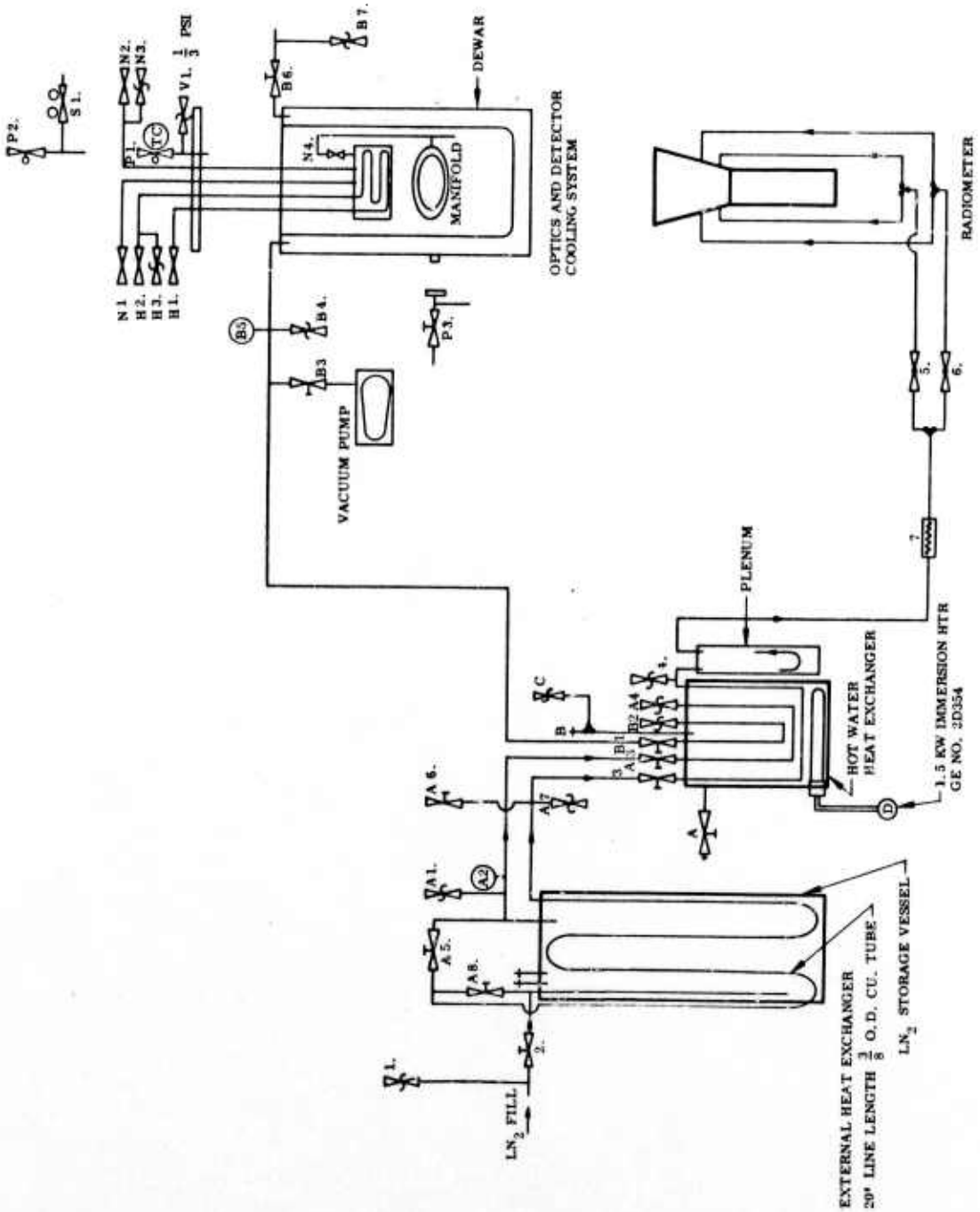

Fig. B-1 Radiometer Cooling and Frost-Free Plumbing System – Schematic

Appendix C
SUMMARY FLIGHT DATA REPORT

C.1 GENERAL

The second flight of the AFCRL-LMSC refractive optics radiometer occurred at Holloman Air Force Base, New Mexico, on June 8, 1971. The objective of the balloon flight program was to measure the atmospheric emittance in the 8- to 13-μ wavelength range. For this flight, measurements were made in the 10.5- to 12.75-μ band as a function of angle from the earth horizon while at floating altitude. A previous flight with this radiometer produced only limited data; consequently, several modifications were made to the radiometer. The radiometer calibration was rechecked after the flight to verify the performance and to obtain calibration curves for reduction of the flight data. Data reduction was performed by AFCRL personnel and the results were provided in tabular form for presentation in this report.

C.2 FLIGHT PREPARATION, LAUNCH, AND TERMINATION

The prelaunch servicing of the radiometer began with the LHe preliminary cooldown of the dewar at 1,615 hr, June 8, 1971. Cooling was terminated at 1830 hr; the package was taken to the launch area at 1930 hr. After a 1-hr hold for weather, Lhe cooling was resumed at 2040 hr. LNe transfer started at 2210 hr, and servicing was completed at 2240 hr. Just before launch, it was noted that the gondola tilted forward about 2 deg due to imblance.

Launch occurred at 2353 hr, and the float elevation of 91,700 ft was reached at 0244.5 hr. Package descent began at 0459 hr, and the flight was terminated at 0956 hr. Impact occurred near Socorro, New Mexico. The flight package was returned to Holloman Air Force Base on June 9, 1971. After a preliminary inspection, it appeared to be in good condition.

C.3 FLIGHT DATA

Six resistance thermometers provided temperature data for critical radiometer components as follows:

- T1 – detector/optics
- T2 – aft shade
- T3 – front shade
- T4 – hatch cover
- T5 – flare section
- T6 – electronic compartment

The temperature data as a function of time from launch to termination are listed in Table C-1. Temperature data for the front and back shades became erratic after 0120 hr and were not discernible from the noise. However, the detector temperature remained between 20° and 25°K during the entire flight, and initial data from the shades indicate that satisfactory cooling occurred. The hatch cover temperature was between 200° and 225°K during data acquisition and was used to provide an operational check on the system performance when the hatch was closed.

The chopper monitor provides an output voltage signal whose amplitude is related to frequency. A voltage above 4 Vdc signifies a suitable amplitude; this value was achieved at 0020 hr and remained satisfactory during the flight.

Data acquisition was initiated at 0235 hr Mountain Daylight Time (MDT). A summary of the instrument status and the telemetry status is shown in Table C-2. NDF refers to the position of the neutral density filter and β is the radiometer elevation angle from gondola horizontal. Initial data at all elevation angles (0235 to 0328 hr) were taken with the filter attached to assure that the detectors would not saturate. However, a signal was detected only on Detector 2 until the 0-deg position was reached. On the second pass, the NDF was out at β = 45 deg until β = 5 deg, and signals were recorded for Detectors 2, 3, and 4. Detector 1 responded only at 5 deg with the NDF out and at 0 deg and -5 deg with the NDF in.

Table C-1

RADIOMETER TEMPERATURE AND CHOPPER SIGNAL VERSUS TIME

Time (MDT) (hr)	T1 (°K)	T2 (°K)	T3 (°K)	T4 (°K)	T5 (°K)	T6 (°K)	Chopper Monitor (V)
2342	22.3	61.9	83.3	271.2	295.0	312.0	0.34
2400	23.1	61.0	83.7	269.4	292.8	311.4	1.93
0020	24.5	60.0	83.8	256.8	235.9	307.5	4.27*
0040	24.8	57.6	83.7	245.6	234.3	308.6	4.27*
0100	24.5	**	82.0	237.5	233.9	307.2	4.33*
0120	24.2	**	78.5	232.2	233.8	306.3	4.48*
0140	22.6	**	**	228.2	233.8	306.0	4.52*
0200	22.8	**	**	225.2	233.8	306.4	4.47*
0220	23.5	**	**	223.0	234.0	307.0	4.34*
0240	23.3	**	**	222.0	233.9	307.9	4.34*
0300	22.1	**	**	224.8	233.8	308.7	4.32*
0320	23.0	**	**	207.3	233.7	308.9	4.29*
0340	22.6	**	**	201.4	233.7	309.4	4.30*
0400	22.4	**	**	203.0	233.6	309.4	4.31*
0420	22.4	**	**	204.1	233.6	309.7	4.29*
0440	22.9	**	**	205.4	233.7	310.0	4.29*
0500	20.0	**	**	206.1	233.5	309.9	4.31*
0515	22.3	**	**	207.3	233.7	309.8	4.32*

*Chopper monitor voltage greater than desired 4 Vdc
**Erratic signals on these channels

Table C-2

SUMMARY OF JUNE 1971 BALLOON FLIGHT VERSUS TIME

Time (hr/min)	NDF	β (deg)	Signals
A. Data Summary			
023444.9	IN	45	Below thresholds for all detectors
024542.5	IN	15	Signal on detector 2 only
025005.5	IN	10	Signal on detector 2 only
025512.3	IN	5	Signal on detector 2 only
030019.2	IN	0	Signals on all detectors
030504.1	IN	-5	Signals on all detectors
031054.8	IN	-5	Radiometer cover ON
031328.3	IN	90	Radiometer cover ON
032447.7	IN	45	Radiometer cover ON
032910.7	OUT	45	Cover off; signal below threshold for all detectors
034008.3	OUT	30	Signal below threshold for all detectors
040013.8	OUT	15	Signals on detectors 2, 3, 4; Detector 1 inoperative
040859.8	OUT	10	Signala on detectors 2, 3, 4; Detector 1 still inoperative
041807.8	OUT	5	Signals on all detectors
042653.8	IN	5	Signal on Detector 2 only
042927.3	IN	0	Signals on all detectors
043412.2	IN	-5	Signals on all detectors
044531.7	IN	–	Radiometer rotated to $\beta = 90°$ preparatory to balloon descent
B. Summary of Telemetry Status During Flight			
033311.8	TM	Off	
033756.8	TM	On	
034325.6	TM	Off	
034748.6	TM	On	
040225.3	TM	Off	
040754.1	TM	On	
041217.1	TM	Off	
041640.1	TM	On	
042125.1	TM	Off	
043857.1	TM	On	

During the data acquisition period, the telemetry was turned off and on periodically (Table A-18 B) to determine the extent of transmission noise on the signal. Data were continuously recorded by the onboard tape recorders. It was subsequently considered that the telemetry did not contribute significant electrial noise.

Table C-3 indicates the threshold radiance and voltage levels for each channel. The value designated f(V) is a radiance value normalized to a 5-V output signal and used in data reduction. The values were determined primarily from a postflight calibration at LMSC on 22 July 1971 and adjusted for the inflight calibration.

The gondola motion has a period of about 6 min with amplitudes of approximately 240 deg and a maximum rotation rate of 40 to 50 mr/sec. Damping of the oscillations resulted in decreased gondola rotation rates during certain periods, i.e., when the coupling between the gondola and balloon (double-pendulum action) occurred.

Data are presented primarily for Detector 2 to illustrate the variations recorded with azimuth angle, position of the neutral density filter, and for the first or second pass. The variation in radiance with elevation angle for the first and second passes with Detector 2 has been shown in Fig. C-1. Variations in the data for the -5-deg elevation may be due to the radiometer intermittently viewing the earth's limb because of the 2-deg tilt of the gondola and the rocking motion. At 90,000 ft, the angle to the earth's limb is about 6 deg below the gondola horizontal.

Table C-3

DETECTOR RADIANCE AND VOLTAGE THRESHOLD LEVELS

Detector No.	Radiance ($w/cm^2\mu$ - sr)		Voltage	Normalized Threshold Radiance f(V) ($w/cm^2\mu$ - sr)
	NDF OUT	NDF IN		
1	5.10 - 08	3.83 - 06	0.7	3.95 - 04
2	1.46 - 08	1.10 - 06	0.7	5.90 - 04
3	3.16 - 08	2.37 - 06	1.5	2.05 - 03
4	8.80 - 08	6.60 - 06	1.8	2.55 - 03

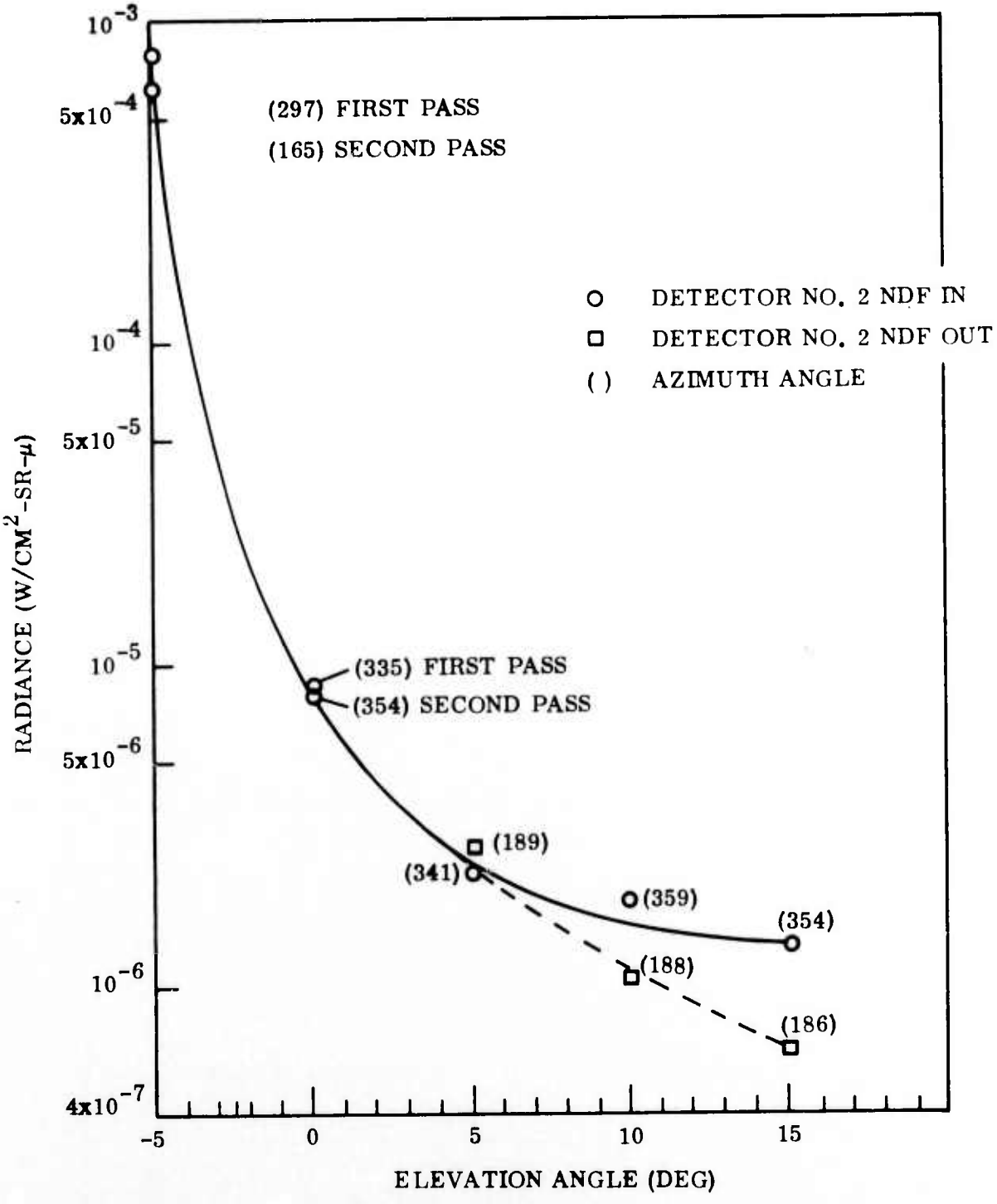

Fig. C-1 Radiance as a Function of Elevation Angle With Neutral Density Filter In and Out

Unclassified

Security Classification

DOCUMENT CONTROL DATA - R & D

(Security classification of title, body of abstract and indexing annotation must be entered when the overall report is classified)

1. ORIGINATING ACTIVITY *(Corporate author)*
Lockheed Missiles & Space Company, Inc.
Lockheed Research Laboratories
3251 Hanover Street, Palo Alto, California 94304

2a. REPORT SECURITY CLASSIFICATION
UNCLASSIFIED

2b. GROUP

3. REPORT TITLE
INFRARED RADIOMETER EXPERIMENT

4. DESCRIPTIVE NOTES *(Type of report and inclusive dates)*
Scientific Final. 1 August 1969 – 9 March 1972 (Approved, 18 August 1972)

5. AUTHOR(S) *(First name, middle initial, last name)*
Gary C. Vliet

6. REPORT DATE	7a. TOTAL NO. OF PAGES	7b. NO. OF REFS
9 March 1972		3

8a. CONTRACT OR GRANT NO.	9a. ORIGINATOR'S REPORT NUMBER(S)
F19628-70-C-0012; ARPA Order No. 1366	LMSC-D246510
b. PROJECT NO. 5130 – N/A - N/A	
c. 62301D	9b. OTHER REPORT NO(S) *(Any other numbers that may be assigned this report)* AFCRL-72-0053
d. N/A	

10. DISTRIBUTION STATEMENT
B – Distribution limited to U.S. Government agencies only; Test and Evaluation; 18 August 1972. Other requests for this document must be referred to AFCRL (OPS), L. G. Hanscom Field, Bedford, Massachusetts 01730

11. SUPPLEMENTARY NOTES	12. SPONSORING MILITARY ACTIVITY
This research was supported by the Defense Advanced Research Projects Agency.	Air Force Cambridge Research Laboratories (OP) L. G. Hanscom Field Bedford, Massachusetts 01730

13. ABSTRACT

The design, fabrication, calibration, and flight of a double-focused refractive optical system employing a solid cryogen for operation at 22° K on a balloon-supported platform are described. The inherent out-of-field energy rejection and the diffraction limited characteristics of a refractive system have been combined with a four-element Hg:Ge detector array for an optimized radiometric measuring system for the 8- to 13-μm wavelength range. Additional features include an eight-position spectral filter wheel, a two-position neutral density filter, a four-decade logarithmic amplifier, and a frost-prevention system. The system was developed to measure the atmospheric emittance as a function of elevation angle near the earth's horizon while at a nominal floating altitude of 90,000 ft.

The results of laboratory evaluation of the individual optical, detector and electronic components, as well as the system performance for responsivity, optical resolution, out-of-field energy rejection and field-of-view, are presented. Simulated flight tests in an evacuated chamber were performed to verify the cryogenic and electro-optical design. Finally, the results of a successful balloon flight in June 1971 are summarized in the Appendixes.

A follow-on contract, No. F19628-72-C-0033, is in progress to fabricate an attachable calibration source, modify some of the electronic and mechanism components, and perform a complete calibration, and to support two additional balloon flights in 1972.

DD FORM 1 NOV 65 1473 (A)

Unclassified

Security Classification

14 KEY WORDS	LINK A		LINK B		LINK C	
	ROLE	WT	ROLE	WT	ROLE	WT
Infrared Radiometer, Double-Focus Optics, Hg:Ge Detector System, Cryogenic Optical System, Balloon Measurements, Horizon Infrared Radiance						